

FZR - 180
May 1997

Annual Report 1996

Institute of Radiochemistry

Editor: Prof. Dr. H. Nitsche

Editorial staff: Dr. H.-J. Engelmann
PD Dr. G. Bernhard

Foreword

The overall goal of the institute is to contribute through basic and applied research to the better understanding of radionuclide transport in the environment. This goes beyond mere phenomenological observation of the processes involved. We have set out to understand the individual transport-controlling processes on a molecular level and then use this knowledge to synthesize a more comprehensive view of radionuclide transport.

We have made progress in elucidating some of the molecular processes such as the speciation of uranium in solution and the binding of uranium to inorganic and natural organic materials. We have shown that our synthetic humic acids can effectively model the functionality of natural humic acids and therefore constitute a stable standard for inter-laboratory comparison of the thermodynamic properties describing metal-humic acid interaction. First steps were made to incorporate our knowledge of the chemistry involved in radionuclide transport into existing risk assessment software that did not consider the detailed chemistry along the environmental transport path.

One of our many tools to understand the coordination of radionuclides in solution, in inorganic and organic materials, and on surfaces is X-ray Absorption Spectroscopy (XAS). The construction of the Rossendorf Beam Line (ROBL) at the European Synchrotron Radiation Facility (ESRF) in Grenoble, France, is rapidly moving forward. ROBL will provide the ability to investigate radioactive elements beyond uranium. Due to the hard work of the team which is jointly staffed by members of the Institute of Ion-Beam Physics and Materials Research, the Institute of Radiochemistry, and the Department of Experimental Facilities and Information Technology, the project is on time and within budget. The experimental hutches were already tested for their tightness against radiation by using the white beam of the ESRF light source. Currently, the optical components are being installed and first tests using monochromatic radiation from 5 to 35 keV are planned for the fall of 1997.

The commissioning of our new radiochemistry building, however, is less successful. Although the construction was completed in the beginning of 1996 and the building was inaugurated in March of 1996, we still have not obtained our license to handle radioactive materials. The licensing process is extremely involved and slow. The FZR has spent close to half a million DM alone for obtaining the mandated independent expertise on the suitability of the building and its installations to handle the projected levels of radioactivity. Currently, a second independent evaluation with a projected cost to the FZR of 60.000 DM has been requested by the authorities. Despite all these obstacles, we are still hopeful that the Sächsische Staatsministerium für Umwelt und Landesentwicklung will grant us the unrestricted operating license for handling radioactive material including non-fissionable actinides in the second half of 1997. This would enable us to expand our research beyond uranium and address the issues of environmental contaminations that were caused world-wide by the production of nuclear weapons and by accidents from careless operation of nuclear facilities.

During 1996, we embarked on several new projects that are not reflected in this report. We began to characterize the biosorption of radioactive contaminants by microorganisms which are isolated from a uranium mill tailing pile that we selected as a project for interdisciplinary and application-oriented research. We are currently characterizing the mineralogy, hydrology, chemistry and radiochemistry, and biochemistry and microbiology of the uranium mine tailing pile "Haberlandhalde" in Johanngeorgenstadt in Saxony. This is done as a collaboration among our Departments of Radioecology and Nuclear Waste Disposal and Organic Tracer Chemistry, the Institute of Geology and Hydrology of the Technische Universität Bergakademie Freiberg, the Umweltforschungszentrum Leipzig and our newly-founded group of Microbiology and Genetics, for which two modern molecular-biological and genetic laboratories were established. Once our current exploratory studies are successfully completed, we envision a large collaboration on an international level. Another project that was begun is the investigation of the transfer factors of uranium between soil and plants as a function of its chemical form in the environment. This is done in collaboration with the Verein für Kernverfahrenstechnik und Analytik e.V. (VKTA),

Rosendorf, and the Institute of Plant and Wood Chemistry of the Technische Universität Dresden.

Although, the research on the chemistry of the heaviest elements is not in the mainstream of the institute, I would like to mention that several members of the institute and of my radiochemistry group at the Technische Universität Dresden were involved in the international collaboration that successfully carried out the first chemistry experiments with element 106, Seaborgium. It was shown that Seaborgium chemically behaves like its lighter homologues, molybdenum, Mo, and tungsten, W.

I would also like to report that the institute's first graduate student, Dr. A. Vahle, obtained her degree with *summa cum laude* from the Technische Universität Dresden in 1996.

We would like to thank the many visitors, German and international, for their interest in our research and for their participation in the institute's seminars. We would like to also thank our scientific collaborators and the visiting scientists for coming to Rosendorf during 1996 to share their knowledge and experience with us. We continue to strongly encourage the collaborations and visits by scientists in the future.

Rosendorf, May 1997

Prof. Dr. Heino Nitsche

CONTENTS

I. SCIENTIFIC CONTRIBUTIONS

1. SPECIATION AND MIGRATION OF RADIONUCLIDES

Titration of a Uranium Mill Tailing Water from Helmsdorf - Species Determination by Time-Resolved Laser-Induced Fluorescence Spectroscopy (TRLFS) G. Geipel, V. Brendler, G. Bernhard, H. Nitsche	1
Quenching Effect of Chloride Ion on Uranyl-Sulfate Complex Fluorescence S. Nagasaki, G. Geipel, G. Bernhard, H. Nitsche	2
Identification of a Uranium Surface Species Sorbed on a Ferrihydrite Surface Using Time-Resolved Laser-Induced Fluorescence Spectroscopy (TRLFS) T. Arnold, G. Geipel, G. Bernhard, H. Nitsche	4
Sorption of Uranium(VI) onto Phyllite T. Zorn, T. Arnold, G. Bernhard, H. Nitsche	5
Sorption of Uranium(VI) on Polypropylene Surfaces T. Arnold, T. Zorn, G. Bernhard, H. Nitsche	7
Interaction of Uranium(VI) with Silicon Species in Aqueous Solutions H. Moll, G. Geipel, V. Brendler, G. Bernhard, H. Nitsche	10
Redox Behavior and Speciation of Hexavalent Uranium in Non-Complexing Media A. Abraham, L. Baraniak, H. Nitsche	11
Software to Compute Fluorescence Lifetimes from Time-Resolved Laser-Induced Fluorescence Spectroscopy (TRLFS) Studies, Exploiting the Full Spectrum V. Brendler, A. Brachmann, G. Geipel	13
Coupling of Chemical Speciation Modeling with Risk Assessment Software: Code Development with Emphasis on Parameter Sensitivity Analysis V. Brendler, G. Bernhard, H. Nitsche	14
Preparation of Thin-Layer Sources for the Direct Measurement of Actinides in Concrete C. Nebelung, G. Bernhard, H. Nitsche	16
Determination of Actinides in Fish Samples from the River Irtysh and the Koienovskoie Lake C. Nebelung, A.A. Bessonov, H. Nitsche, I. Ryabov	17
Preliminary Results of the Application of SIMS for the Local Determination of Radium in Radioactivity-Containing Rocks of the Königstein Uranium Mine M. Thieme, F.J. Stadermann, L. Baraniak, G. Bernhard, H. Nitsche, K. Nindel, J. Schreyer	19

2. ORGANIC MATTER AND ITS INTERACTION WITH RADIONUCLIDES

Isolation and Characterization of Humic Acid from a Floodplain of the Rhein River M. Bubner, S. Pompe, A. Otto, K.H. Heise	21
Synthesis of Uranium(VI) and Calcium Complexes with Carboxylic and Humic Acids M. Bubner, S. Pompe, M. Meyer, R. Jander, G. Schuster, K.H. Heise	22
Thermoanalysis of a Synthetic and a Natural Humic Acid and their Calcium- and Uranyl Compounds G. Schuster, M. Bubner, S. Pompe, K.H. Heise, H. Nitsche	24
Complexation Behavior of a Synthetic Humic Acid with Uranyl Ions in Comparison to a Natural Humic Acid by Time-Resolved Laser-Induced Fluorescence Spectroscopy S. Pompe, A. Brachmann, G. Geipel, K.H. Heise, H. Nitsche	25

Interaction of Pb(II) and Bi(III) with Humic Acid Studied by Time-Resolved Laser-Induced Fluorescence Spectroscopy (TRLFS) A. Brachmann, G. Geipel, G. Bernhard, H. Nitsche	27
Complex Formation of Hexavalent Uranium with Lignin Degradation Products L. Baraniak, M. Schmidt, G. Bernhard, H. Nitsche	28
Interaction of U(VI) with Wood Degradation Products - A Potentiometric Study M. Schmidt, L. Baraniak, G. Bernhard, H. Nitsche	30
Interaction of Hexavalent Uranium with Gluconic Acid and Glucuronic Acid L. Baraniak, M. Schmidt, G. Bernhard, H. Nitsche	31
Determination of Lignin-Reducing Capacity by Alkaline Ferricyanide Titration B. Mack, L. Baraniak, G. Bernhard, H. Nitsche	32
Analysis of Carbohydrates Dissolved from Pitwood under Mine Flooding Conditions K. Jelen, R. Schiene, H. Koch, K. Fischer, L. Baraniak, H. Nitsche	33
Experiments for the Disposal of Carbon-14 Labeled Organic Material: 1. Mineralization of Organic Model Compounds by Ammonium Peroxydisulfate E. Förster, H. Petzold, M. Rösseler, K. Wolf, K.H. Heise, H. Nitsche	35
Experiments for the Disposal of Carbon-14 Labeled Organic Material: 2. Mineralization of Organic Model Substances Using Hydrogen Peroxide and a Mixture of Transition Metal Salts E. Förster, H. Petzold, M. Rösseler, K.H. Heise, H. Nitsche	36
3. APPLICATION OF X-RAY ABSORPTION SPECTROSCOPY	
Arsenite and Arsenate Concentration Ratios in Aqueous Mixtures by XANES M.A. Denecke, T. Reich, H. Friedrich, G. Bernhard, T. Knieß, D. Rettig, T. Zorn, H. Nitsche	39
Differentiation Between Monodentate and Bidentate Carboxylate Ligands Coordinated to Uranyl Ions Using EXAFS M.A. Denecke, T. Reich, M. Bubner, S. Pompe, K.H. Heise, H. Nitsche, P.G. Allen, J.J. Bucher, N.M. Edelstein, D.K. Shuh	40
Structural Analysis of Uranium(VI) Complexes with Simple Carboxylic Acids in Aqueous Solution Using EXAFS T. Reich, V. Brendler, M.A. Denecke, P.G. Allen, J.J. Bucher, N.M. Edelstein, D.K. Shuh, H. Nitsche	42
Structural Investigations of the Technetium and Rhenium Complexes by EXAFS. 2. Studies of Tc and Re Oligoglycine Complexes R. Jankowsky, B. Noll, H. Spies, B. Johannsen, T. Reich, H. Nitsche	43
X-Ray Absorption Spectroscopic and Mössbauer Studies of Redox and Cation-ordering Processes in Manganese Ferrite G. Bonsdorf, M.A. Denecke, K. Schäfer, S. Christen, H. Langbein, W. Gunßer	45
Polarized X-Ray-Absorption Spectroscopy of the Uranyl Ion: Comparison of Experiment and Theory E.A. Hudson, P.G. Allen, L.J. Terminello, M.A. Denecke, T. Reich	45
4. BEHAVIOR OF COLLOIDS AND AEROSOLS	
Comparison of Methods for Colloid Particle Sizing: Filtration, Centrifugation, Photon Correlation Spectroscopy (PCS), and Scanning Electron Microscopy (SEM) H. Zänker, G. Hüttig, H. Moll, H. Nitsche	47
Determination of the Particle Diameter of Industrial TiO ₂ in Aqueous Suspension in the Presence of a Detergent W. Richter, H. Zänker, E. Förster	49

Detection of Aerosol Losses in Glass Vessels D. Rettig, P. Merker, H. Nitsche	51
Transport of Radon Daughters by Salt Aerosols P. Merker, D. Rettig	52
Different Shapes of Aerosols Generated by Atomization D. Rettig, P. Merker, R. Müller	53
5. CHEMISTRY OF THE HEAVIEST ELEMENTS	
Reaction Gas Chromatography of Oxide and Hydroxide Species of Molybdenum - Simulation and Experiment A. Vahle, S. Hübener, R. Dressler, B. Eichler, A. Türler	55
On-Line Isothermal Gas Chromatography with Short-Lived Molybdenum and Technetium Isotopes in the O ₂ -H ₂ O _(g) /SiO _{2(s)} - System A. Vahle, M. Böttger, M. Grantz, S. Hübener	56
Thermochromatography of Heavy Actinides - Determination of the Sublimation Enthalpy of Es S. Taut, S. Hübener, B. Eichler, H.W. Gäggeler, M. Schädel, I. Zvara	58
Thermochromatography of No-259 S. Taut, S. Hübener, B. Eichler, A. Türler, H.W. Gäggeler, S.N. Timokhin, I. Zvara	59
Calculation of Rate Constants of the Basic Reactions of Reaction Gas Chromato- graphy - Trace Amount Components in Laminar Gas Flow M. Grantz	61
Olga Experiments with ²⁶¹ 104 Under Chlorinating and Brominating Conditions H.W. Gäggeler, B. Eichler, D.T. Jost, D. Piguet, A. Türler, G.V. Buklanov, V.Ya. Lebedev, S.N. Timokhin, M.V. Vedeneev, A.B. Yakushev, I. Zvara, S. Hübener	62
First Thermochemical Property of Seaborgium Determined S. Hübener, M. Grantz, St. Taut, A. Vahle for a collaboration	64
II. PUBLICATIONS, PATENTS, LECTURES AND POSTERS	67
III. SEMINARS	77
IV. PERSONNEL	81
V. ACKNOWLEDGMENTS	83

I. SCIENTIFIC CONTRIBUTIONS

Speciation and Migration of Radionuclides

TITRATION OF A URANIUM MILL TAILING WATER FROM HELMSDORF - SPECIES DETERMINATION BY TIME-RESOLVED LASER-INDUCED FLUORESCENCE SPECTROSCOPY (TRLFS)

G. Geipel, V. Brendler, G. Bernhard, H. Nitsche
 Forschungszentrum Rossendorf e.V., Institute of Radiochemistry

The distribution of U(VI) species in different tailing water samples of an uranium mining area was calculated with the speciation modeling software EQ 3/6 NR /1/ using the NEA data base /2/. To validate this calculation, a series of TRLFS measurements was carried out. The pH of the original tailing water from the tailing site Helmsdorf was changed by addition of perchloric acid. At pH values lower than pH six, fluorescence spectra found that are typical for uranylphosphate and uranylsulfate solution species.

Experimental and Results

Tab. 1 lists the main chemical components of the Helmsdorf tailing water. From these data, we calculated the species distribution in this solution as a function of pH using the modeling software package EQ3/6NR /1/. The speciation diagram is shown in Fig. 1.

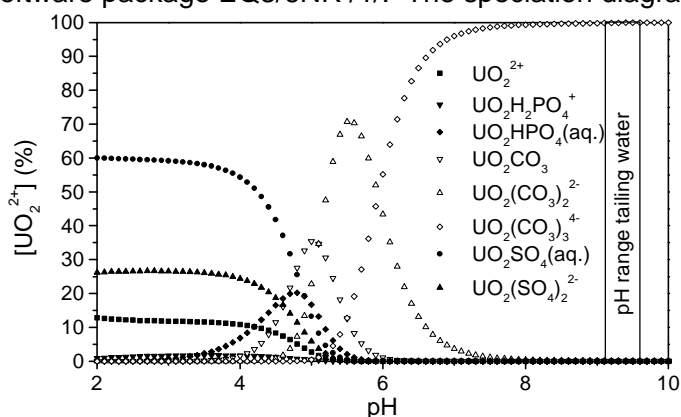


Fig. 1: Species distribution as function of pH in the tailing water (concentrations see Tab. 1)

	Concentration [mmol]
Ca	0.3
Mg	0.9
U	0.025
As	0.52
SO ₄ ²⁻	35.6
PO ₄ ³⁻	0.29
CO ₃ ²⁻ (total)	10.3
Cl ⁻	25.8
TOC [mg/L]	132
pH	9.76

Tab. 1: Chemical analysis of Helmsdorf tailing water

This system has a low calcium concentration and therefore the $\text{Ca}_2\text{UO}_2(\text{CO}_3)_3(\text{aq})$ species will not be formed in a measurable concentration. At pH values higher than six only carbonate species exist. These species do not show any fluorescence signals. Therefore it is impossible to determine these species by TRLFS. At lower pH values, complexes form between the uranyl ions and phosphate. At a pH lower than 4.5, the uranylsulfate speciation becomes dominant. We obtained spectroscopic information on the tailing water using time-resolved laser-induced fluorescence spectroscopy (TRLFS). The TRLFS method and our experimental setup are described in /3,4/. The excitation wavelength used was 266 nm. The TRLFS of the original tailing water shows a spectrum that is typical for organic compounds in natural systems. No uranium fluorescence could be obtained. We increased the calcium concentration by adding a $\text{Ca}(\text{ClO}_4)_2$ solution with the same pH and obtained the spectrum of the $\text{Ca UO}_2(\text{CO}_3)_3(\text{aq})$ species. Fig. 2 shows the comparison of this spectrum with a spectrum that was obtained from

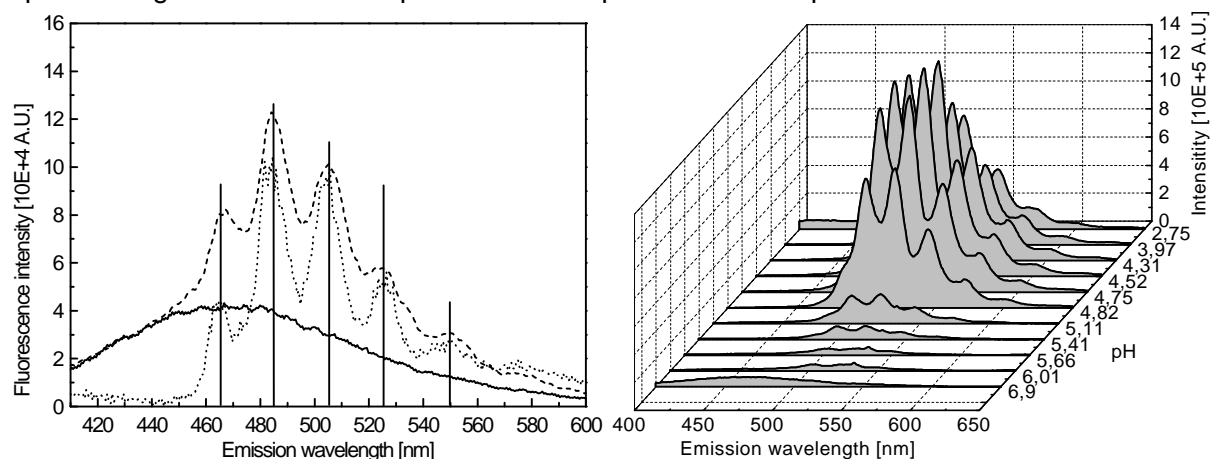


Fig. 2 (left): Fluorescence spectra of original tailing water (solid); synthetic solution with $1 \times 10^{-2} \text{ M Ca}^{2+}$; $2 \times 10^{-5} \text{ M UO}_2^{2+}$ and $2 \times 10^{-3} \text{ M HCO}_3^-/\text{CO}_3^{2-}$ (dot) and tailing water after addition of $1.25 \times 10^{-2} \text{ M Ca}^{2+}$ (dash)

Fig. 3 (right): Fluorescence spectra of the tailing water as a function of pH

a synthetic solution containing 1×10^{-2} M Ca^{2+} ; 2×10^{-5} M UO_2^{2+} and 2×10^{-3} M $\text{HCO}_3^-/\text{CO}_3^{2-}$ at pH 8.0. This shows that the Ca concentration in the tailing water is too low to form the $\text{Ca}_2\text{UO}_2(\text{CO}_3)_3(\text{aq})$ species.

In a second series of measurements, we titrated the original tailing water with perchloric acid by keeping a constant ratio (90%) of the original tailing water to the added perchloric acid. With decreasing pH, we found fluorescence spectra. Fig. 2 shows spectra which were measured at constant delay times. With decreasing pH, the spectral shape changes strongly. Starting at about pH 6, the fluorescence intensity increases and reaches a maximum at about pH 4. Analysis of the emission wavelength of the band maxima showed that these spectra can be ascribed to the formation of phosphate complexes. If the pH is lowered to below three, the spectra become typical to those for sulfate complexation of uranium(VI). This agrees with the speciation calculations. At pH values below six complex formation begins between uranium(VI) and phosphate. Because the fluorescence intensity of the phosphate complexes is very strong, we can determine them concurrently to the sulfate complexes. The formation of uranyl sulfate and phosphate complexes begins for both approximately below pH 6. The maximum concentration for the phosphate complexes was determined at pH 4.9 deconvoluting the different species using the lifetime function. At lower pH values, the more than two times higher concentration of the second sulfate complex gives an additional fluorescence signal, which results in an increase of the integral fluorescence intensity up to pH 4.3. At pH values lower than 4.3, we found fluorescence spectra of uranyl sulfate species.

The TRLFS measurements of the Helmsdorf uranium tailing water in the pH range from two to nine confirmed the speciation calculations for free uranyl, uranyl phosphate and uranyl sulfate species. This validates the thermodynamic data for these systems. This work is currently being extended to the basic pH range in order to detect the formation of uranyl hydroxo complexes such as $\text{UO}_2(\text{OH})_4^{2-}$.

References

- 1/ Wolery, T.J.: *EQ3/6 A software package for the geochemical modeling of aqueous systems*. Report UCRL-MA-110662 Part 1, Lawrence Livermore National Laboratory, California, USA, 1992
- 2/ Grenthe, I., Fuger, J. et. al.: *Chemical Thermodynamics of Uranium*. North Holland, Amsterdam, 1992
- 3/ Brendler, V., Geipel, G., Bernhard, G., Nitsche H.: Complexation in the System $\text{UO}_2^{2+}/\text{PO}_4^{3-}/\text{OH}^-$ (aq): Potentiometric and Spectroscopic Investigations at very low Ionic Strength. *Radiochimica Acta* **74**, 75-80 (1996)
- 4/ Geipel, G., Brachmann, A., Brendler, V., Bernhard, G., Nitsche, H.: Uranium(VI)-Sulfate Complexation Studied by Time-Resolved Laser-Induced Fluorescence Spectroscopy (TRLFS). *Radiochimica Acta* **75**, 199 (1996)

QUENCHING EFFECT OF CHLORIDE ION ON URANYL-SULFATE COMPLEX FLUORESCENCE

S. Nagasaki¹, G. Geipel, G. Bernhard, H. Nitsche

Forschungszentrum Rossendorf e.V., Institute of Radiochemistry

¹ University of Tokyo, Department of Quantum Engineering, Tokyo

In uranium mining related waters chloride ions can quench the fluorescence of uranyl species. Uranyl sulfate complexes are the main species on acidic uranium solutions containing sulfate ions. Therefore the quenching effect of chloride ions on the fluorescence of U(VI)-sulfate complexes was investigated in aqueous U(VI)-sulfate solutions ($[\text{U(VI)}] = 1 \times 10^{-5}$ M, $[\text{SO}_4^{2-}] = 2 \times 10^{-2}$ - 2×10^{-1} M, $[\text{Cl}^-] = 1 \times 10^{-3}$ - 5×10^{-2} M, pH = 2, ionic strength = 1 M). Time-resolved laser-induced fluorescence spectroscopy measurements were carried out to evaluate the fluorescence decay constants and the quenching coefficients for UO_2^{2+} , UO_2SO_4 and $\text{UO}_2(\text{SO}_4)_2^{2-}$. The quenching coefficients of UO_2^{2+} , UO_2SO_4 and $\text{UO}_2(\text{SO}_4)_2^{2-}$ range from 4.04×10^8 to 6.27×10^8 $\text{M}^{-1}\text{s}^{-1}$, from 1.23×10^8 to 1.42×10^8 $\text{M}^{-1}\text{s}^{-1}$, and from 2.48×10^7 to 3.58×10^7 $\text{M}^{-1}\text{s}^{-1}$, respectively.

Results and Discussion

Fig. 1 shows the influence of sulfate concentration on the fluorescence spectra of U(VI). The time delay was set to 100 ns, and the chloride concentration was 1×10^{-3} M. No marked difference in the shape of spectra was observed in the sulfate concentration range from 2×10^{-2} to 2×10^{-1} M. The four strong fluorescence emission peaks are located at 494, 515, 539 and 564 nm. Because the corresponding fluorescence emission peaks of the free UO_2^{2+} without sulfate and chloride ions present are located at 485, 509, 532 and 558 nm, the peaks of the U(VI)-sulfate system are shifted to longer wavelengths.

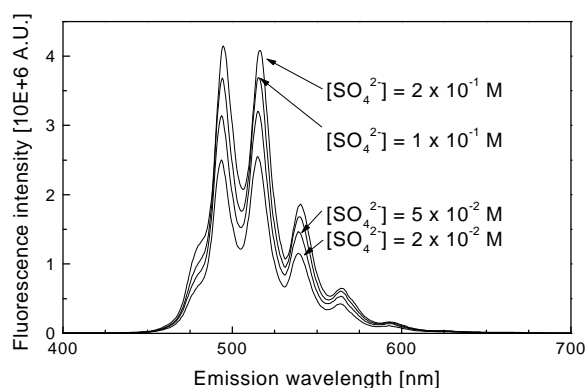


Fig. 1: Fluorescence spectra of uranyl ions in sulfate media at different sulfate concentration.

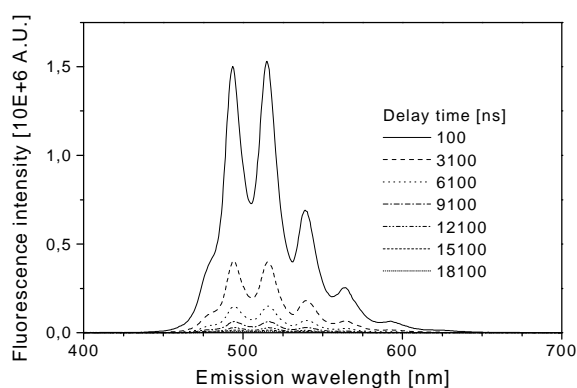


Fig. 2: Time resolved spectrum of U(VI) at 2×10^{-2} M sulfate and 1×10^{-3} M chloride

Fig. 2 shows the time-resolved fluorescence spectra of U(VI) at sulfate and chloride concentrations of 2×10^{-2} M and 1×10^{-3} M, respectively. Assuming a short laser pulse relative to the apparent excited state lifetime, the fluorescence decay curves can be described as follows:

$$A(t) = A_i \times c_i \times \exp(-t/t_i)$$

where A_i are the initial specific fluorescence intensities of the species i at $t = 0$, c_i the species concentration and t_i fluorescence decay constants of the fluorescent species. By fitting the time-resolved fluorescence spectra with parameters according to the above equation, we obtain the number of fluorescent species in the sample solution, and the fluorescence decay constant of each species. The initial fluorescence are mainly dependent on the absorbance of the U(VI) complexes and on the prefilter effect /1/. The evaluated fluorescence decay constant depends on the quenching of coexisting species, namely chloride ions in the present work. From the fit we derive that the fluorescence spectrum shown in Fig. 3 is a superposition of the spectra of three species.

The dominant U(VI) species under these conditions are UO_2^{2+} , UO_2SO_4 and $\text{UO}_2(\text{SO}_4)_2^{2-}$ with the respective fluorescence decay constants of 892 ± 42 , 2476 ± 137 and 5769 ± 504 ns. The fluorescence decay constant decreases with increasing chloride concentration. We also found that the initial fluorescence decreases with increasing chloride concentration at constant sulfate concentration. As the sulfate concentration increases at the constant chloride concentration, the initial fluorescence of UO_2^{2+} decreases, but those of UO_2SO_4 and $\text{UO}_2(\text{SO}_4)_2^{2-}$ increase, indicating the formation of uranyl-sulfate complexes in the solutions of higher sulfate concentration.

From the fluorescence decay constants obtained in the present work, the quenching coefficient, k_q , of chloride ion can be calculated according to the Stern-Volmer equation /2/. Fig. 3 shows the dependence of the fluorescence decay constant of UO_2SO_4 on the chloride concentration at a constant sulfate concentration of 5×10^{-2} M. The k_q can be calculated from the slope of the line, and the fluorescence decay constant without chloride ion, t_0 , can be obtained from the intersection at zero chloride concentration. The obtained k_q values are summarized in Tab. 1. We relate for the first time k_q to the species UO_2^{2+} , UO_2SO_4 and $\text{UO}_2(\text{SO}_4)_2^{2-}$.

References

- /1/ Berthoud, T., Decambox, P., Kirsch, B., Mauchien, P., Moulin, C.: Direct Uranium Trace Analysis in Plutonium Solutions by Time-Resolved Laser-Induced Spectrofluorometry. *Anal. Chem.* **60**, 1296-1299 (1988)
 /2/ W. Schmidt: *Optische Spektroskopie*. Verlag Chemie Weinheim, 1994, S. 230

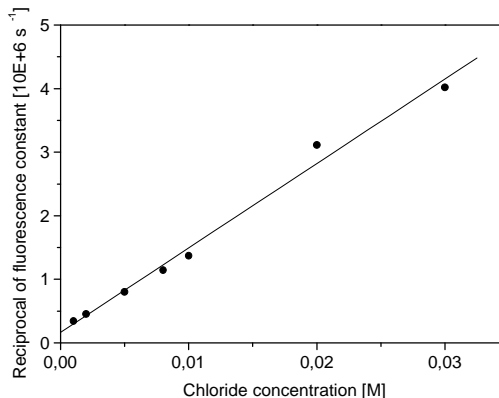


Fig. 3: Reciprocal fluorescence decay constant at the sulfate concentration of 5×10^{-2} M as function of the chloride concentration

Species	k_q ($\text{M}^{-1}\text{s}^{-1}$)	t_0 (μs)
UO_2^{2+}	$(4.9 \pm 1.0) \times 10^8$	1.7 ± 0.4
UO_2SO_4	$(1.3 \pm 0.1) \times 10^8$	5.0 ± 1.8
$\text{UO}_2(\text{SO}_4)_2^{2-}$	$(2.9 \pm 0.4) \times 10^7$	8.4 ± 1.7

Tab.1: Quenching coefficients, k_q , for UO_2^{2+} , UO_2SO_4 and $\text{UO}_2(\text{SO}_4)_2^{2-}$, and fluorescence decay constants, t_0 , without chloride

IDENTIFICATION OF A URANIUM SURFACE SPECIES SORBED ON A FERRIHYDRITE SURFACE USING TIME-RESOLVED LASER-INDUCED FLUORESCENCE SPECTROSCOPY (TRLFS)

T. Arnold, G. Geipel, G. Bernhard, H. Nitsche
 Forschungszentrum Rossendorf e.V., Institute of Radiochemistry

A surface species of uranium sorbed on a ferrihydrite surface at pH 5.8 was identified by Time-Resolved Laser-Induced Fluorescence Spectroscopy (TRLFS). The fluorescence maximum of this uranium surface species occurs between 600 and 700 nm. It is easily distinguishable from the fluorescence maximum at 480 to 550 nm of uranium in solution.

Results and discussion

The sorption of uranium on the iron mineral ferrihydrite was studied in the pH range of 3.5 - 9.5 in a system open to the atmosphere. The batch experiments were carried out under the following experimental conditions: total U(VI) concentration of $1 \cdot 10^{-5}$ M, ferrihydrite concentration of $1 \cdot 10^{-3}$ M (as Fe), ionic strength of 0.1 M adjusted with NaNO_3 , and a contact time of 50 hours between the solid phase and uranium solution. The experiments showed that uranium sorbs to the ferrihydrite surface in the pH range of 4.0 to 8.5 and reaches its sorption maximum between pH 5.5 and 7.5. Similar results were found by Waite and coworkers /1/. Fig. 1 shows that at pH 5.8 95 ± 5 % of the uranium sorbs to a 1 mM suspension of the iron mineral ferrihydrite.

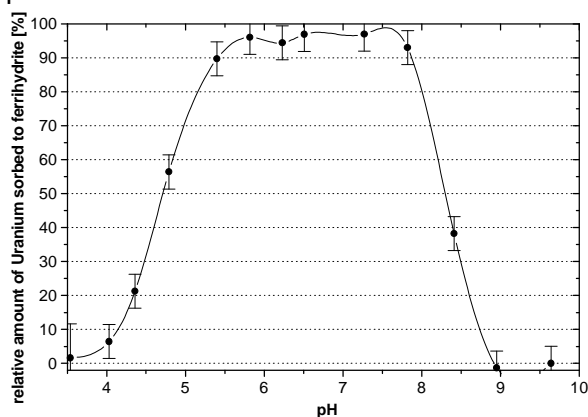


Fig. 1: Sorption of uranium(VI) ($1 \cdot 10^{-5}$ M) on ferrihydrite (as 1 mM Fe) as a function of pH in 0.1 M NaNO_3 system open to the atmosphere

Waite and coworkers /1/ tried to investigate the nature of the uranium sorbed to ferrihydrite surface and conducted EXAFS measurements on samples representing sorption conditions of pH 5.0 and 5.5. They found an average U to Fe distance of 3.37 Å and concluded that the major uranium species at the ferrihydrite surface is a inner-sphere mononuclear bidentate complex.

We carried out TRLFS measurement on above described batch samples at pH 5.8 to obtain more information about the uranium surface species that are bound to the ferrihydrite. The first series of TRLFS measurements were performed with solutions containing $1 \cdot 10^{-5}$ M of uranium(VI) and no iron(III). Time-resolved

fluorescence spectra between 480 and 550 nm are shown in Fig. 2. This fluorescence signal was also observed by Meinrath et al. /2/. At this pH mainly the uranium hydrolysis products are present in solution, in particular $\text{UO}_2(\text{OH})_2^0$, $(\text{UO}_2)_3(\text{OH})_5^+$ and $\text{UO}_2(\text{OH})^+$. The second series of TRLFS measurements were conducted with solutions containing 1 mM of ferrihydrite and no uranium. No fluorescence signal could be detected in these suspensions. However, in solutions containing both 1 mM Fe as ferrihydrite and $1 \cdot 10^{-5}$ M of uranium(VI) that were mixed for 50

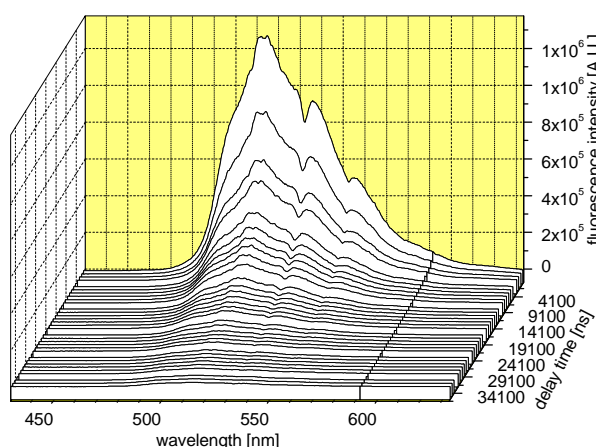
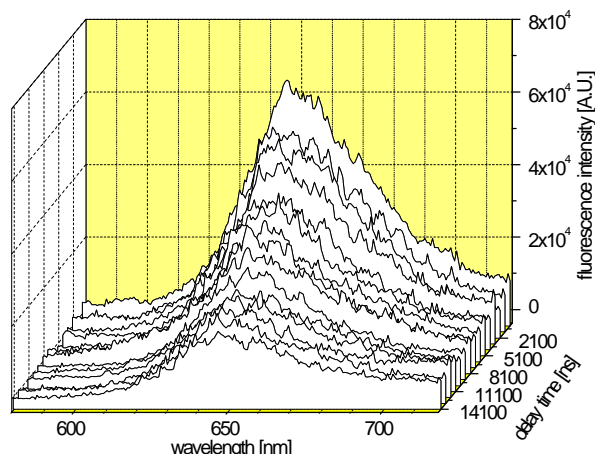


Fig. 2: TRLFS spectra of uranium hydroxide species pH 5.8



at Fig. 3: TRLFS spectra of an uranium surface species sorbed to ferrihydrite at pH 5.8

hours, it was clearly showed that the characteristic fluorescence signal of uranium in the wavelengths 480-550 nm disappeared as a function of time in the presence of ferrihydrite and a new species appeared with a fluorescence signal at wavelengths between 600 and 700 nm. The fluorescence spectrum of this new species is depicted in Fig. 3. Based on previously conducted sorption experiments /1/, this new fluorescence signal can be assigned to a uranium surface species forming on a ferrihydrite surface at pH 5.8. Using speciation calculations, this uranium surface species on the ferrihydrite surface could be due to a specific surface complex forming on the ferrihydrite surface or to surface precipitation of the solid uranium hydroxide phase schoepite, $UO_2(OH)_2 \cdot H_2O$.

TRLFS seems to be a promising surface-sensitive technique to detect surface species in complex aqueous solutions. The results of this study could be especially helpful for identifying surface species in natural waters containing uranium and iron at weakly acidic to neutral pH.

Acknowledgment

We thank Dr. Wiesner for ICP-MS measurements.

References

- /1/ Waite, T.D., J.A: Davis, T.E. Payne, G.A. Waychunas, Xu, N.: Uranium(VI) adsorption to ferrihydrite: Application of a surface complexation model. *Geochimica et Cosmochimica Acta* **58** (24), 5465-5478 (1994)
- /2/ Meinrath, G., Kato, Y., Yoshida, Z.: Spectroscopic Study of the uranyl hydrolysis species $(UO_2)_2(OH)_2^{2+}$. *J. Radioanal. Nucl. Chem.* **174**, 299-314 (1993)

SORPTION OF URANIUM(VI) ONTO PHYLLITE

T. Zorn, T. Arnold, G. Bernhard, H. Nitsche

Forschungszentrum Rossendorf e.V., Institute of Radiochemistry

The adsorption of U(VI) onto phyllite and onto several of individual minerals was studied in batch experiments under ambient conditions. The pH range of 3.5 - 9.5 was studied with an uranium concentration of $1 \cdot 10^{-5}$ M and a solid to solution ratio of 1 g/20 mL, using the 63 to 200 μ m size fraction. Maximum sorption of uranium onto the various mineral surfaces occurred between pH 6.0 and 7.3. Based on the calculated uranium speciation, the sorption of uranium was attributed to a combination of precipitation of the solid uranium phase schoepite and to surface complex formation between $UO_2(OH)_2$ and the individual mineral surfaces.

Experimental

The phyllite was obtained from the uranium mining site "Schlema-Alberoda" near Aue in Western Saxony. It was collected 540 m underground and represents /1/ a fairly typical light-colored phyllite of this mining site. The phyllite was crushed, ground and separated into different size fractions by sieving. The 63 to 200 μ m fraction was used in batch sorption experiments. The feldspar minerals oligoclase, labradorite, orthoclase and the glimmer minerals muscovite and biotite were purchased and treated identical to the phyllite.

The quartz used in these experiments was a commercially available fine-grained quartz, 0.2 - 0.8 mm, which was already washed and calcined. One gram of the solid material of the 63 to 200 μ m fraction was added to 20 mL of distilled water in polypropylene centrifuge tubes. Then the pH was adjusted to the desired pH value using the appropriate amounts of HNO_3 and NaOH. In samples with a pH higher than 7, a calculated amount of $NaHCO_3$ was added to accelerate the equilibration process with atmospheric CO_2 . Twenty-four hours later, uranium was added to obtain a concentration of $1 \cdot 10^{-5}$ M, and the pH was readjusted. The samples were shaken for about 50 hours and the final pH values were measured. The samples were centrifuged at 3000 rpm for 7 min. The supernatant was transferred to a polypropylene sample container, acidified to a pH of about 1.5, and analyzed for uranium with ICP-MS. The difference of the analyzed supernatant solution to the added $1 \cdot 10^{-5}$ M uranium was attributed to sorption. Furthermore, values for the specific surface area (BET) were determined for various feldspar minerals (0,3 - 0,7 m^2/g), quartz (0,2 m^2/g), muscovite (1,4 m^2/g), biotite (1,3 m^2/g), and phyllite (4,0 m^2/g).

Results and Discussion

The results of the batch sorption experiments are depicted in Fig. 1. The sorption maxima of

uranium onto the various minerals and phyllite surfaces takes place in the near neutral pH range of about 6.0 to 7.3, and seems to be independent of the individual surfaces.

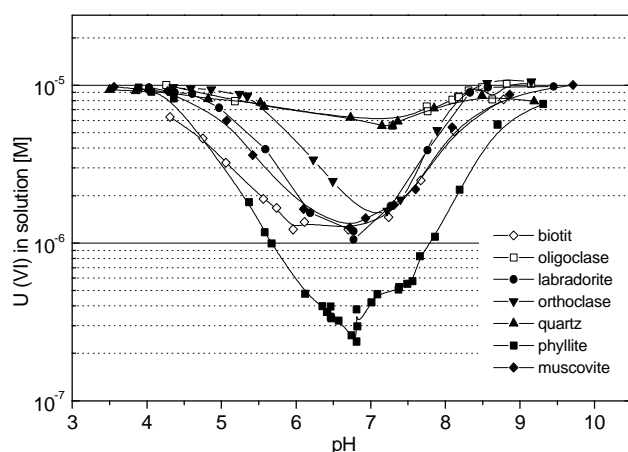


Fig.1: Adsorption of uranium(VI) onto oligoclase, orthoclase, labradorite, muscovite, biotite, quartz and phyllite

However, there is a difference in the amount of the sorbed uranium. Quartz and oligoclase sorb less uranium (approximately 45 %) compared to orthoclase and labradorite and the glimmer minerals biotite and muscovite which sorb up to 80-90 %. Phyllite sorbed nearly 96 % of uranium in the pH range of 6.5 to 7.0. This is a surprising result considering the composition of the phyllite which consists of about 30-60 % quartz, 20-50 % glimmer, 0-20 % chlorite and 0-20 % feldspar. It was expected that the uranium sorption of the phyllite would be lower because the sorption onto the individual minerals is significantly lower. The maximum amount of uranium sorbed onto the phyllite should

not be larger than the amount that is sorbed onto its strongest sorbing individual mineral. However, there may be two possible explanations for these high sorption values. First, chlorite was not yet included in this study and it may be possible that this mineral sorbs more uranium than the other minerals. Secondly, a thin film of brownish-reddish color was observed at the end of the phyllite sorption experiments. This film may possibly be the result of various dissolution and reprecipitation reactions at the phyllite surface. Because the phyllite contains about 2 % of iron, this newly formed secondary surface precipitation phase may contain more iron than the initial phyllite surface. Small amounts of iron minerals are sufficient to adsorb large quantities of uranium from solution. Various studies /2, 3/ have shown that at neutral pH, 20 mL of an 1 mM iron-suspension was responsible for sorbing almost 100 % of uranium in a 1×10^{-5} M uranium solution. Furthermore, Bruno et al. /4/ showed that uranium can also be removed from solution by co-precipitation with a newly formed solid phase. The reasons why the amount of the uranium sorbed onto the various minerals studied is still under investigation. It is very likely related to the different number of surface sites of each mineral, to a different affinity of these sites for uranium, and to different specific surface areas.

Conclusions

Sorption was strongest in the pH range 6.0 - 7.3 and this pH dependency applies to all the minerals studied. By comparing speciation calculations with the results from the sorption experiments, one can conclude that the sorption of uranium is possibly a combination of surface precipitation of the solid uranium hydroxide schoepite $UO_2(OH)_2 \cdot nH_2O$ and adsorption of the neutral charged complex $[UO_2(OH)_2]^0$ onto the mineral and phyllite surface forming surface complexes.

Acknowledgment

The authors would like to thank Dr. Wildner from the WISMUT GmbH for providing phyllite samples and Dr. Wiesner for conducting ICP-MS measurements.

References

- /1/ Wilner, M., Wismut GmbH, personal communication, 1996
- /2/ Waite, T.D., Davis, J.A., Payne, T.E., Waychunas, G.A., Xu, N.: Uranium(VI) adsorption to ferrihydrite: Application of a surface complexation model. *Geochimica et Cosmochimica Acta* **58** (24), 5465-5478 (1994)
- /3/ Arnold, T., Kohler, M., Bernhard, G., Nitsche, H.: Using a surface complexation model to simulate the adsorption of U(VI) on Ferrihydrite. In: Report FZR-95, Institute of Radiochemistry, Annual Report 1995, p.17 (1996)
- /4/ Bruno, J., De Pablo, J., Duro, L., Figuerola, E.: Experimental study and modeling of the U(VI)-Fe(OH)₃ surface precipitation/coprecipitation equilibria. *Geochimica et cosmochimica Acta* **59** (20), 4113-4123 (1995)

SORPTION OF URANIUM (VI) ON POLYPROPYLENE SURFACES

T. Arnold, T. Zorn, G. Bernhard, H. Nitsche
Forschungszentrum Rossendorf e.V., Institute of Radiochemistry

The sorption of uranium (VI) on polypropylene centrifuge tubes was studied as a function of pH and various uranium(VI) concentrations in a system open to the atmosphere. The sorption of uranium to polypropylene had its sorption maximum in the pH range of about 6.0 to 7.3 and reached values of up to 50 % of uranium sorbed to the centrifuge tubes when using an initial U(VI) concentration of $1 \times 10^{-7} \text{ M}$. At a starting concentration of $1 \times 10^{-6} \text{ M}$ sorption was still significant. Approximately 10-20 % of the uranium in the pH range of 6.0 to 7.3 sorbed to the polypropylene.

Results and discussion

Polypropylene is a commonly used container material in batch experiments. Several authors (e.g. /1,2/) claim that the loss is negligible of uranium (VI) from solution onto polypropylene container walls during sorption experiments of uranium on various geomaterials. However, these authors do not specify pH and uranium concentration. In batch experiments, the amount of dissolved species sorbed to a solid surface is usually determined by subtracting the concentration of the dissolved element at the end of the sorption experiment from the initially added element concentration. The amount of the sorbed element could then be used to determine K_d values or surface complex formation constants with the solid surface. However, when a considerable amount of uranium is sorbed to the polypropylene these constants will be invalid. To obtain more information about the sorption process of uranium to solid phases, the speciation of uranium in a $1 \times 10^{-5} \text{ M}$ uranium solution open to the atmosphere ($p_{\text{CO}_2} = -3.47$) was calculated with HYDRAQL /3/ using formation constants from Grenthe et al. /4/. In the first calculation shown in Fig. 1 the formation of solid uranium phases is allowed and in the second one, displayed in Fig. 2, their formation is excluded.

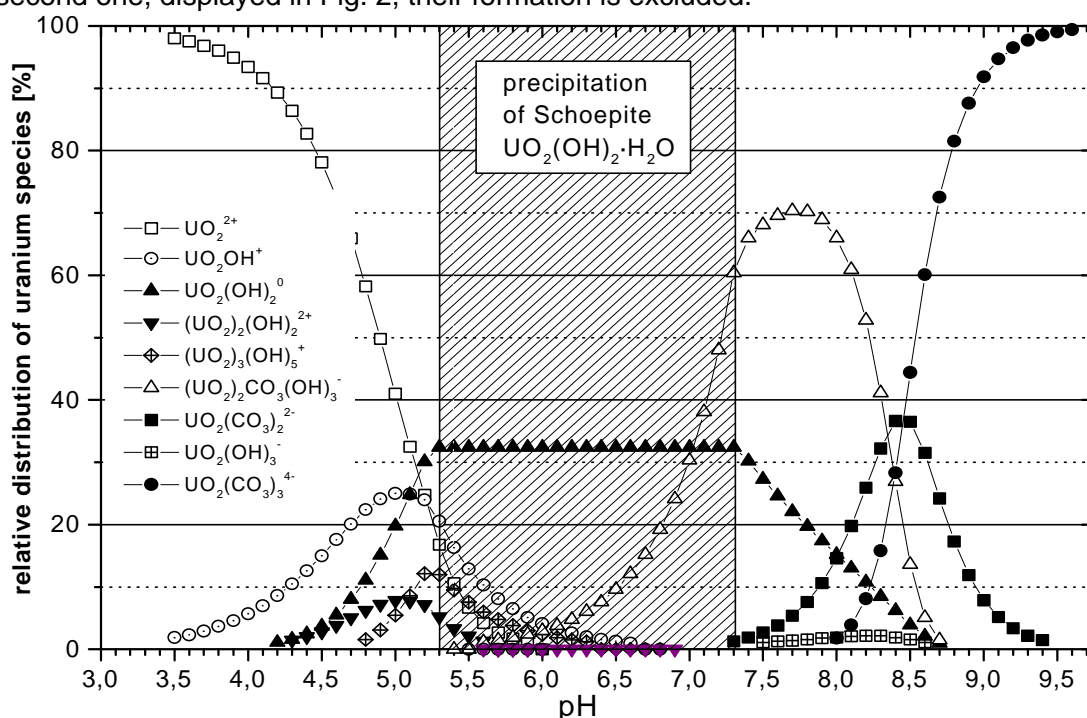


Fig. 1: Speciation calculation of uranium ($1 \times 10^{-5} \text{ M}$) conducted with HYDRAQL in a system open to the atmosphere. Solid species are included in the calculation.

Fig. 1 shows that, assuming equilibrium conditions, the solid uranium phase schoepite, $\text{UO}_2(\text{OH})_2 \cdot \text{H}_2\text{O}$, precipitates in the pH range of 5.3 to 7.3 and thereby reduces the concentration of dissolved uranium in this pH regime. However, using an initial uranium(VI) concentration of $1 \times 10^{-6} \text{ M}$ and also including the formation of all solid uranium phases no precipitation of dissolved uranium is predicted. In Fig. 2, the formation of solid uranium phases is excluded, because this should represent the scenario were the formation of solid uranium phases is kinetically hindered or where equilibrium conditions are not established. These speciation calculations are compared with the results from batch experiments in which the sorption of

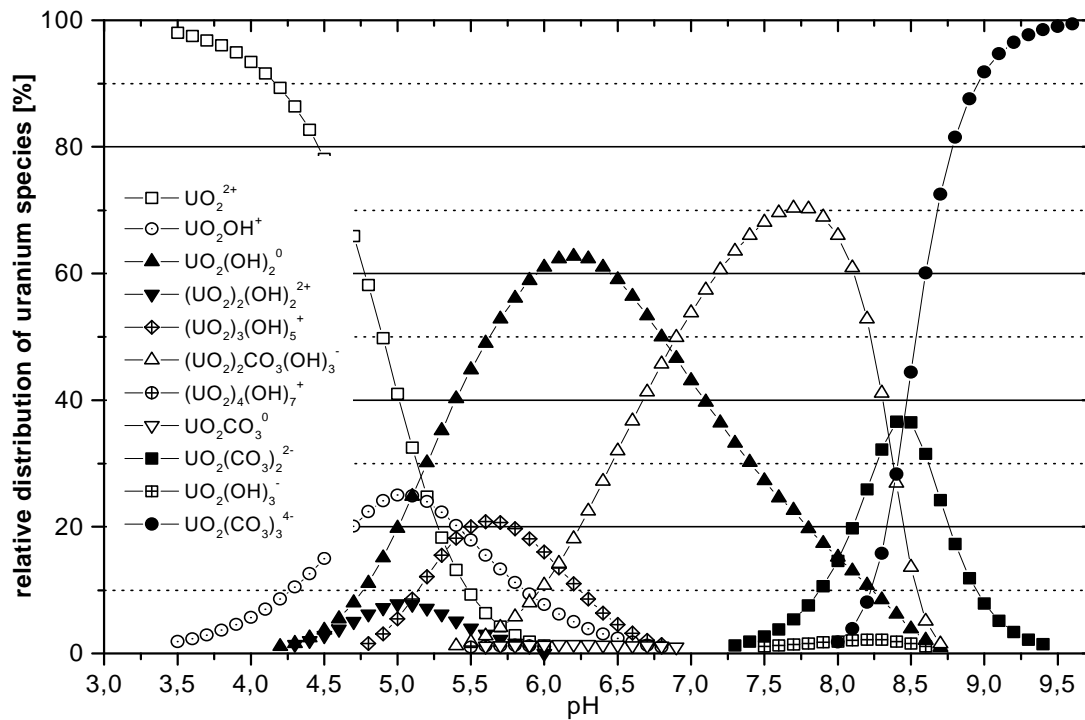


Fig. 2: Speciation calculation of uranium (1×10^{-5} M) conducted with HYDRAQL in a system open to the atmosphere. Solid species were not included in the calculation.

uranium (VI) to centrifuge tubes made of polypropylene using three different uranium concentrations (1×10^{-5} M, 1×10^{-6} M, and 1×10^{-7} M) was studied in the pH range from 3.5 to 9.5 in a system open to the atmosphere. The contact time between the dissolved uranium and the solid phase polypropylene was 50 hours. It was found for an initial uranium concentration of 1×10^{-5} M that the sorption of uranium to the centrifuge tubes takes place in the pH range of 6.2 to 8.0. The amount of uranium sorbed to the centrifuge tubes was highest at a pH of about 7.0, with a maximum of 5 - 10 %.

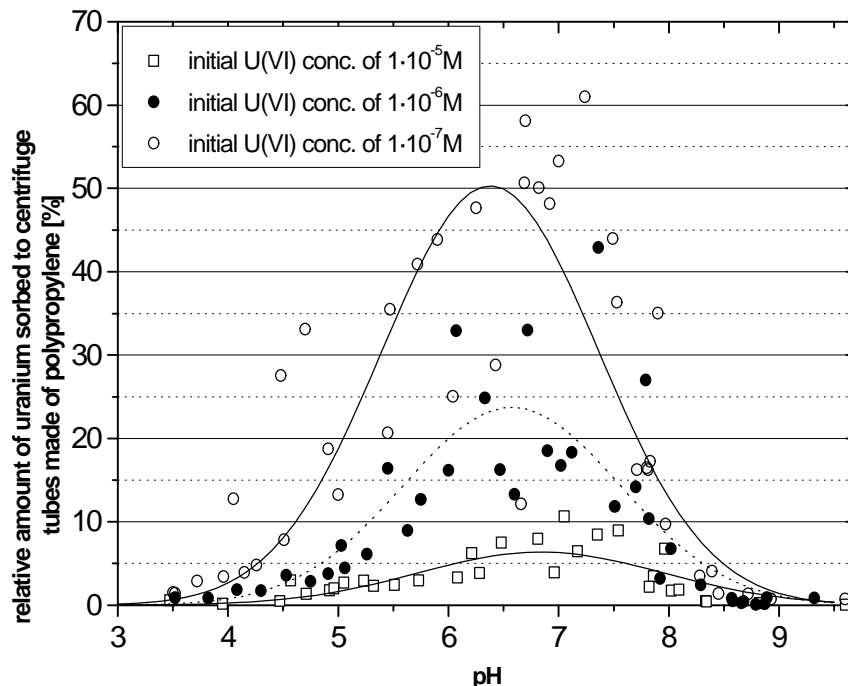


Fig. 3: Relative amount of U(VI) sorbed to centrifuge tubes made of polypropylene as a function of pH.

Using an initial uranium concentration of 1×10^{-6} M, it was shown that the sorption starts at slightly lower pH values and the maximum amount of U(VI) sorbed to the polypropylene is higher. Sorption occurs from pH 5.0 to 8.0 whereby the sorption maximum is observed between pH 6.0 to 7.3 with a maximum of about 15-20 %. The highest relative amount of uranium sorbed to the polypropylene was obtained for an initial uranium concentration of 1×10^{-7} M. Sorption was observed between pH 4.4 to 8.0 and reached its maximum in the pH range of 6.0 to 7.3 with up to 50 % of the U(VI) sorbed to the polypropylene. Results of these batch experiments are displayed in Fig. 3 and show that some data points are widely scattered around the fitted curves indicating that centrifuge tubes might show different sorption characteristics based on individual surface roughness. This study clearly shows that sorption of uranium to centrifuge tubes made out of polypropylene in the near neutral pH range can be

significant and therefore should be routinely checked. Furthermore, it appears obvious by comparing these results with results obtained from sorption experiments conducted with minerals and rocks /5,6/ that the area in which sorption takes place seems to be fairly independent of the solid surface. Moreover, sorption seems not to be affected by the charge of the surface. Feldspar minerals, for example, have a point of zero charge at about pH 2 indicating that the surface in the pH region where sorption is strongest is negatively charged, whereas ferrihydrite has a point of zero charge of about 7.8 meaning that its surface is positively charged in the region of maximum sorption. Comparing these results with the information obtained from the speciation calculations shown in Fig. 1 it can be seen that the pH area in which sorption takes place is quite similar to the area where schoepite precipitates. Conclusively, the reduction of uranium out of solution could be attributed to surface precipitation. However, previous sorption experiments with uranium sorbing to ferrihydrite /6/ and the results of the present study showed that sorption is even stronger and the sorption area wider when using an starting uranium concentration of 1×10^{-6} M and 1×10^{-7} M, both uranium concentrations where, based on known formation constants no precipitation of a solid uranium phase occurs. If surface precipitation is the only process responsible for the reduction of uranium in solution, the same amount of uranium should precipitate on each mineral. However, this was not the case. Referring to the speciation calculation depicted in Fig. 2, it can be seen that there is one aqueous uranium complex, $\text{UO}_2(\text{OH})_2$, dominating in the pH range with maximum sorption. The same complex is also dominating in speciation calculations using a maximum uranium concentration of 1×10^{-6} M and 1×10^{-7} M. At higher pH values uranium carbonate species become the dominant species and the sorption of uranium to the various mineral surfaces is reduced. It could be possible that this neutral charged aqueous uranium complex forms surface complexes with the solid mineral or rock particle surface.

Conclusions

At U(VI) concentrations of 1×10^{-6} M and 1×10^{-7} M neither schoepite nor another solid uranium phase should precipitate. However, there is a remarkable coincidence between the solubility minimum of schoepite and the pH range where the sorption of U(VI) onto the centrifuge tubes is maximum. This may indicate that at U(VI) concentrations of 1×10^{-6} M or below the formation of a solid uranium phase, similar to schoepite, may occur on the polypropylene material. Furthermore, the formation of surface complexes between the neutral charged $\text{UO}_2(\text{OH})_2$ and the solid surface may contribute to the decrease of the uranium in solution. Based on the results from batch experiments and speciation calculations of uranium it was concluded that the sorption of uranium is controlled by a combination of surface precipitation of the uranium hydroxide phase schoepite and/or an additional similar solid uranium phase and the formation of surface complexes between the neutral charged uranium species $\text{UO}_2(\text{OH})_2$ and the solid surface.

Acknowledgment

The authors would like to thank Dr. Wiesener for ICP-MS measurements.

References

- /1/ Aksoyoglu, S.: Sorption of U(VI) on Granite. *Journal of Radioanalytical and Nuclear Chemistry, Articles* **134** (2), 393-403 (1989)
- /2/ Idemitsu, K., Obata, K., Furuya, H., Inagaki, Y.: Sorption behaviour of uranium (VI) on a biotite mineral. In: *Mater. Res. Soc. Symp. Proc.*, **353** (Scientific Basis for Nuclear Waste Management XVIII, Pt. 2), 981-988 (1995).
- /3/ Papelis, C., Hayes, K.F., Leckie, J.O.: *HYDRAQL: A Program for the Computation of Aqueous Batch Systems Including Surface Complexation Modeling of Ion Adsorption at the Oxide/Solution Interface*. Tech. Rep. 306, Dep. of Civil Eng., Stanford University (1988)
- /4/ Grenthe, I., Fuger, J., Lemire, R.J., Muller, A.B., Nguyen-Trung, C., Wanner, H.: *Chemical Thermodynamics of Uranium*, 1st ed., Elsevier Science, Amsterdam, (1992)
- /5/ Zorn, T., Arnold, T., Bernhard, G., Nitsche, H.: Sorption of uranium (VI) onto phyllite. In: *This Report*, Institute of Radiochemistry, Annual Report 1996, (1997), p. 5
- /6/ Waite, T.D., J.A. Davis, T.E. Payne, G.A. Waychunas, Xu, N.: Uranium(VI) adsorption to ferrihydrite: Application of a surface complexation model. *Geochimica et Cosmochimica Acta* **58** (24), 5465-5478 (1994)

INTERACTION OF URANIUM(VI) WITH SILICON SPECIES IN AQUEOUS SOLUTIONS

H. Moll, G. Geipel, V. Brendler, G. Bernhard, H. Nitsche
Forschungszentrum Rossendorf e.V., Institute of Radiochemistry

The interaction between soluble species of uranium(VI) with silicic acid was studied in 0.3 M NaClO₄ solution using Time-resolved Laser-induced Fluorescence Spectroscopy (TRLFS). The stability constant of the complex UO₂OSi(OH)₃⁺ was determined at pH 3.9, an uranyl concentration of 2.1·10⁻⁵ M, and monosilicic acid concentrations up to 3.0·10⁻³ M. Fluorescence lifetimes were obtained for the free uranyl cation, the 1:1 complex and for particles which are probably the result from interactions of polymeric silicic acid with uranyl ions.

Results and discussion

The TRLFS spectra were measured with delay times ranging from 0.1 μs to 135 μs, with increments of 0.5 μs. The excitation wavelength was 266 nm.

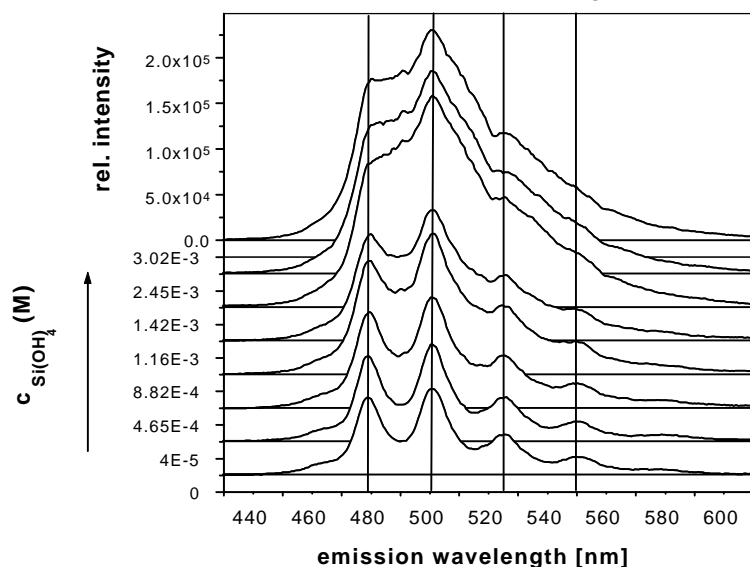


Fig. 1: TRLFS-spectra as a function of monosilicic acid concentration (delay time: 2.1 μs, pH = 3.9)

Fig. 1 depicts the influence of the ligand on the UO₂²⁺-fluorescence. The measured spectra showed an increase of the fluorescence intensity with increasing ligand concentration. It exists a linear relation between the log [fluorescence intensity] vs. log [Si]_{total}. The slope of about 0.9 indicates a predominantly 1:1 complex formation with monomeric silicic acid. The slope of smaller than one could be attributed to a second silicato-uranyl complex which may form between uranyl ions with polymeric silicic acid.

The fluorescence decay of solutions containing silicic acid is much slower than in pure uranyl solutions. The fluorescence life-

times were determined by evaluation the time-resolved fluorescence spectra (Tab. 1).

We assume that three species are present in solutions containing 2.1·10⁻⁵ M UO₂²⁺ and silicic acid concentrations from 4.0·10⁻⁵ M to 3.0·10⁻³ M at a pH of 3.9. There are no lifetimes available in the literature for the uranyl-silicate system. One species was determined with a lifetime of 1.4 ± 0.16 μs which is typical for the free uranyl ion /1/. For the 1:1 complex we determined a lifetime of 34 ± 3 μs. A third fluorescence lifetime between 90 and 200 μs suggests an interaction of uranium(VI) with polymeric silicic acid particles. About 80 % of the total silicon concentration were detected using the β -silicomolybdate method which shows that the solutions contained polymeric silicic acid.

Species	Lifetime [μs]	Fluorescence signal (rel. to UO ₂ ²⁺)
UO ₂ ²⁺	1.4 ± 0.16	1
UO ₂ OSi(OH) ₃ ⁺	34 ± 3	1.4
UO ₂ ²⁺ polymeric silicic acid adducts; [UO ₂ (SiO _{2-0.5x} OH _x) _n] ²⁺	95 - 200	3

Tab. 1: Lifetimes and fluorescence signals relative to UO₂²⁺ at an ionic strength of 0.3 M and a total silicic acid concentration of 3.0·10⁻³ M

We assume that these particles form during the preparation of the silicic acid solution (quick neutralization of sodium metasilicate solution).

Using peak deconvolution to evaluate TRLFS spectra, it was possible to calculate the spectra of the three individual species (Fig. 2). The integrated fluorescence signal from 450 nm to 650 nm measured at different silicic acid concentrations was fitted to a sum of exponential decay functions /2/. This lifetime fitting process yielded the concentrations of the involved species, UO₂²⁺_{free}, UO₂OSi(OH)₃⁺ and [UO₂(SiO_{2-0.5x}OH_x)_n]²⁺. The interaction of uranyl ions with monosilicic acid can be described by the following reaction /3/:



We determined a stability constant $\log\beta^\circ = -(1.60 \pm 0.36)$ for this reaction. The stability constant was extrapolated to infinite dilution using the Davies-Equation.

Conclusions

The results of this study shows that the TRLFS technique was able to investigate the complexation of U(VI) with silicic acid at low concentrations ($c_{\text{Si, total}} < 0.01 \text{ M}$). Our determined stability constant $\log\beta^\circ = -(1.60 \pm 0.36)$ suggests a stronger complexation of U(VI) with silicic acid compared to the stability constant $\log\beta^\circ = -(2.25 \pm 0.13)$ obtained by Porter and Weber /3/ as well as $\log\beta^\circ = -(2.70 \pm 0.34)$ reported by Satoh and Choppin /4/. First TRLFS measurements were performed using tetramethylorthosilicate (TMOS) as source of silicic acid in order to minimize the formation of polymeric silicon species.

The fluorescence lifetime between 90 and 200 μs was not detected. Therefore, the assumption was confirmed that this fluorescence lifetime is related to the interaction of uranyl ions with adducts of polymeric silicic acid.

Acknowledgments

The authors would like to thank Dr. W. Wiesener, Department of Analytics, Forschungszentrum Rossendorf e.V., for the ICP-MS measurements.

References

- /1/ Eliet, V., Bidoglio, G., Omenetto, N., Parma, L., Grenthe, I.: Characterisation of hydroxide complexes of uranium(VI) by Time-resolved Fluorescence Spectroscopy. *J. Chem. Soc., Faraday Trans.* **91**, 2275 (1995).
- /2/ Geipel, G., Brachmann, A., Brendler, V., Bernhard, G., Nitsche H.: Uranium(VI) sulfate complexation studied by Time-Resolved Laser-Induced Fluorescence Spectroscopy (TRLFS). *Radiochim. Acta* **75**, 199 (1996).
- /3/ Porter, R.A., Weber, W.J.: The interaction of silicic acid with iron(III) and uranyl ions in dilute aqueous solution. *J. Inorg. Nucl. Chem.* **33**, 2443 (1971).
- /4/ Satoh, I., Choppin, G.R.: Interaction of uranyl(VI) with silicic acid. *Radiochim. Acta* **56**, 85 (1992).

REDOX BEHAVIOR AND SPECIATION OF HEXAVALENT URANIUM IN NON-COMPLEXING MEDIA

A. Abraham¹, L. Baraniak, H. Nitsche

Forschungszentrum Rossendorf e.V., Institute of Radiochemistry

¹ Technische Universität Dresden, Institute of Analytical Chemistry, Radiochemical Group

The redox behavior of U(VI) in environmental relevant concentrations was studied over the pH range 4-12 by voltammetric methods. The reduction waves were correlated with speciation calculations.

Environmental radionuclide and heavy metal transport via the aquatic pathway depends mainly on the chemical species of the elements that form in natural waters and on their specific interaction with the contacting solid phases (rocks, sediments and soils).

Experimental methods, results and modeling

The U(VI) reduction in non-complexing solution was studied over a wide pH range by square-wave and cyclic voltammetry. The reduction waves were compared with species distributions which were calculated by the multi-equilibria program RAMESES (variant VIII) /1/ using U(VI) hydrolysis constants /2/ adjusted to $I(c) = 0.1 \text{ M}$. The voltammetric measurements were carried out using the AUTOLAB Potentiostat (Eco Chemie) combined with the Metrohm polarographic cell.

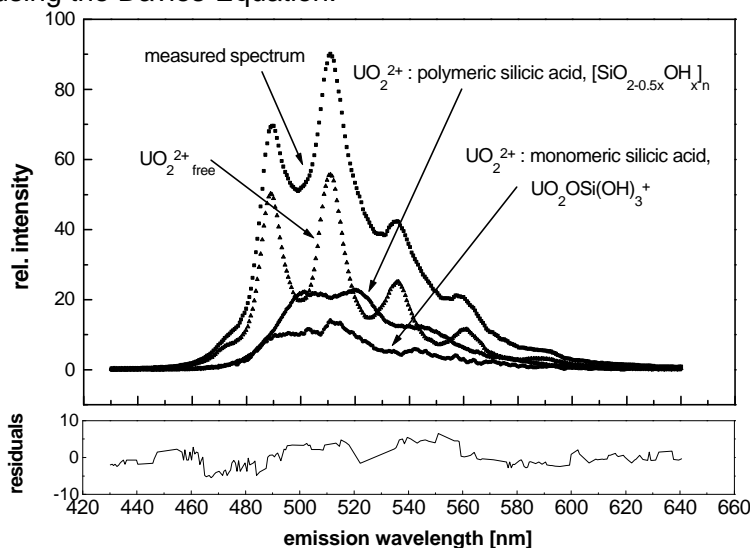


Fig. 2: TRLFS spectra of the postulated species for a solution containing $2.10 \cdot 10^{-5} \text{ M UO}_2^{2+}$ and $1.42 \cdot 10^{-3} \text{ M}$ silicic acid at $\text{pH} = 3.9$, delay time $0.1 \mu\text{s}$

The voltammetric waves of $5 \cdot 10^{-4}$ M U(VI) in 0.1 M NaClO_4 solution were recorded in the range of +0.2 V to -1.2 V using a static mercury drop electrode (SMDE) versus a Ag/AgCl, KCl/3M (SE) reference electrode. The pH was kept constant by addition of corresponding amounts of diluted HClO_4 and carbonate-free NaOH before the measurement which was carried out under nitrogen.

In addition to the well-known reversible U(VI)/U(V) reduction in mineral-acid solution at -180 mV vs. SE /3/ there are two ranges with characteristic reduction behavior.

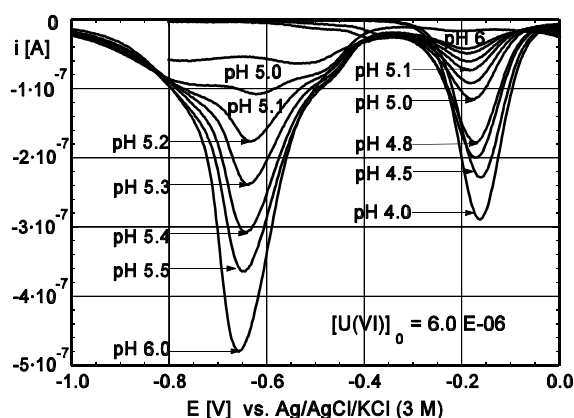


Fig. 1a: Square-wave voltammogram of U(VI) in the pH range 4-6

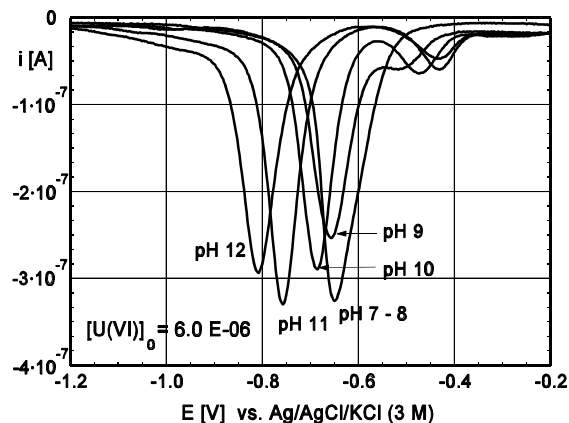


Fig. 1b: Square-wave voltammogram of U(VI) in the pH range 7-12

i) pH 4-8: The voltammograms show the decrease of the cathodic wave at -180 mV vs. SE at the pH is increased from 4 to 6 and the simultaneous appearance of a wave at -650 mV vs. SE (Fig. 1a). This change is caused by the hydrolysis of the uranyl(VI) ion where coordinated water molecules are replaced by hydroxyl groups /4/.

ii) pH 8.5-12: Between pH 8 and pH 10 we find the transition of the uranyl(VI)-dihydroxo complex to the trihydroxo complex which is the only species in the pH range 10-12. Above pH 8 the voltammograms shift to more negative potentials (Fig. 1b), just at the pH where the trihydroxo complex is formed. In contrast to the second peak group we do not find a uniform wave family for the reduction of the pure U(VI)-trihydroxo complex in the pH section 10-12.

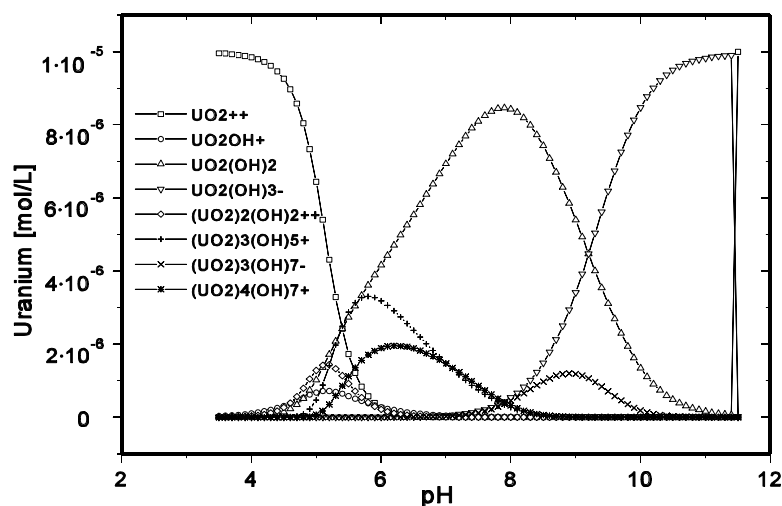


Fig. 2: Distribution of U(VI) species in dependence on the pH

The speciation diagram (Fig. 2) shows that the concentration of the free uranyl(VI) ion decreases to zero and different hydrolyzed species are formed with increasing pH:

- $[\text{UO}_2(\text{OH})_2]$ in the pH range 5-10 and $[\text{UO}_2(\text{OH})_3]^-$ above 8,
- $[\text{UO}_2(\text{OH})]^+$ and $[(\text{UO}_2)_2(\text{OH})_2]^{2+}$ at pH 4.5-6,
- $[(\text{UO}_2)_3(\text{OH})_5]^+$ and $[(\text{UO}_2)_4(\text{OH})_7]^+$ at pH 5-8 and,
- $[(\text{UO}_2)_3(\text{OH})_7]^-$ at pH 7.5-10.

Acknowledgments

This study was supported by the Sächsisches Ministerium für Wissenschaft und Kunst under contract no. 4-7541.83-FZR/512.

References

- Darvell, B.W., Leung, V.W.H.: *Talanta* **37**, 425 (1990)
- Baes, Jr., C.F., Mesmer, R.E.: *The Hydrolysis of Cations*. Krieger Publ. Comp., Malabar, Florida, 1986, p. 176
- Diogic, R., Sipos, L., Branica, M.: *Limnol. Oceanogr.* **31**, 1122 (1986)
- Diogic, R., Branica, M.: *Electroanalysis* **4**, 151 (1992)

SOFTWARE TO COMPUTE FLUORESCENCE LIFETIMES FROM TIME-RESOLVED LASER-INDUCED FLUORESCENCE SPECTROSCOPY (TRLFS) STUDIES, EXPLOITING THE FULL SPECTRUM

V. Brendler, A. Brachmann, G. Geipel
Forschungszentrum Rossendorf e.V., Institute of Radiochemistry

Nearly all published speciation data that is based on TRLFS experiments is derived from only a part of the primary spectroscopic information. The software "POLYLIFE" was developed to improve this situation. To obtain fluorescence lifetimes, it applies a robust multi-level minimization strategy to the whole wavelength range.

Methodology

With time-resolved laser-induced fluorescence spectroscopy (TRLFS) it is possible to discriminate between species that show nearly identical fluorescence spectra, especially in environmental samples. Here the component of interest, e.g., uranium(VI), is usually present only in very small amounts, and nevertheless with a complicated speciation pattern. To obtain fluorescence lifetimes, the fluorescence is fitted as a function of time to a sum of exponential decay functions. Up to now, only a limited number of wavelengths (most often the main peaks) or the integral of the whole spectrum (or part of it) is used for the fit, see e.g. /1/.

We use the full information of the 2D-TRLFS-spectrum. The spectrum is analyzed separately and sequentially for each wavelength. Fluorescence lifetimes and signal amplitudes are obtained for all the distinguishable species together with their respective standard deviations. Then the fluorescence lifetimes are averaged over all wavelengths with their standard deviations as weighing factors. This gives a total fluorescence lifetime for each species and the standard deviation of the mean. The nonlinear fitting procedure to find the best parameter set has three steps. First, user-specified parameter guesses (or in absence of them, a guess from the program) are used to start a random search algorithm. The second minimization level feeds the results of step one into a derivative-free optimization method that is based on the simplex method. And third, these results in turn initialize a Levenberg-Marquardt search. For step one and three, modules from /2/ have been adapted, whereas step two is based on /3/.

Results

C was chosen as the programming language. The program, called POLYLIFE, runs under various UNIX operating systems; a port to MS Windows is planned. The user can analyze the whole spectrum or just a part of it by defining a wavelength and/or a time window. To smooth the signal it is possible to integrate over a fixed number of wavelength (pooling). The input for the program has to be supplied by the user either interactively or in a batch file (with each item on a separate line). Its structure is listed below and gives also an overview about the main software features available at the moment:

- Name of input file with 2-D spectrum
- Name of output file
- Number of distinguishable species
- Estimation values of the fluorescence lifetime in nanoseconds (ns) for each species. Each such value can be followed by space and any letter to indicate that this lifetime should be considered as fixed throughout the minimization procedure.
- "j" or "n" for whether or not extensive runtime output should be generated
- Start of the wavelength window in nm
- End of the wavelength window in nm
- Number of wavelengths to be pooled for internal averaging
- Start of the decay time window in ns
- End of the decay time window in ns

The program is limited to a maximum of up to four species, 500 wavelengths and 30 time steps. The spectrum to be analyzed must be in a format where the first line consists of a keyword and all the time steps (in ns). Each following line starts with the wavelength (in nm) and contains the signal for each time step. All entries in the input file have to be separated by at least one space or tab. The program output has the following column structure:

- 1st column: wavelength in nm
- 2nd column: lifetime in ns for 1st species
- 3rd column: error of lifetime in ns for 1st species
- 4th column: signal amplitude for 1st species
- :
- { same blocks of 4 columns for 2nd, 3rd, ... species }
- :
- last column: sum of squared deviations between measured and calculated fluorescence signal

Discussion and Conclusions

There are several advantages of the new software. The exploitation of the full spectral information allows for the detection of species contributing only to a small part of the spectrum. It is based on a very robust fitting procedure and gives more reliable parameter uncertainties. The data processing is flexible and the software can be used in batch mode for background operation. It has already been applied successfully to a variety of TRLFS spectra in systems containing uranyl complexes, e.g., in /4/.

References

- /1/ Meinrath, G., Kato, Y., Yoshida, Z.: Spectroscopic study of the uranyl hydrolysis species $(\text{UO}_2)_2(\text{OH})_2^{2+}$. J. Radioanal. Nucl. Chem. (Art.) **174**, 299 (1993)
- /2/ Vetterling, W.T., Teukolsky, S.A., Press, W.H., Flannery, B.P.: *Numerical Recipes in C*, 2nd ed., Cambridge Univ. Press, Cambridge (1992)
- /3/ Phillips, G.R., Eyring, E.M.: Error estimation using the sequential simplex method in nonlinear least squares data analysis. Anal. Chem. **60**, 738 (1988)
- /4/ Brendler, V., Geipel, G., Bernhard, G., Nitsche, H.: Complexation in the system $\text{UO}_2^{2+}/\text{PO}_4^{3-}/\text{OH}^-(\text{aq})$: Investigations at very low ionic strengths. Radiochimica Acta **74**, 75 (1996)

COUPLING OF CHEMICAL SPECIATION MODELING WITH RISK ASSESSMENT SOFTWARE: CODE DEVELOPMENT WITH EMPHASIS ON PARAMETER SENSITIVITY ANALYSIS

V. Brendler, G. Bernhard, H. Nitsche
Forschungszentrum Rossendorf e.V., Institute of Radiochemistry

An already approved risk assessment software package (PRISM / BIOPATH) has been extended with chemical speciation code modules. This enables a better description of the physico-chemical state of environmental systems by unfolding the K_d value, which presently is the only parameter beside concentrations and pH to characterize the chemistry in PRISM / BIOPATH applications. Up to now the chemical speciation is calculated by the EQ3/6 software. It is planned to incorporate other chemical speciation codes.

Modelling Approach and Results

PRISM /1/ is a suite of three programs used for parameter sensitivity analysis. The BIOPATH /2/ code provides the risk assessment model predictions. Its mathematical method is based on compartment theory. Presently, BIOPATH utilizes the K_d concept of distribution coefficients, i.e., ratios of the sorbed (fixed, immobilized) and unsorbed (free) fraction of a component. This is, however, a consolidation of many physico-chemical processes into one parameter, creating a severe weakness of the K_d principle /3/. A much better strategy is to decompose the K_d value into its main defining processes. Thus the parameters affecting the K_d the strongest can be identified and extra measurements be designed to reduce their uncertainties.

We make K_d values available to the risk assessment code via on-line calls of external speciation programs. This will slow down the computing, but makes the model development efficacious and fast, and provides a much higher accuracy of the results. The EQ3/6 /4/ package was chosen from the variety of available speciation programs. It is available as source code, has been used for many years and was checked by a number of international validation programs. EQ3/6 covers all chemical reactions in homogeneous aqueous solutions, including redox reactions, and handles precipitation and dissolution equilibria using kinetic rate laws. A drawback is the lack of an implementation of surface complexation models. But due to the flexible software interfaces that we designed between speciation and risk assessment codes, it needs

a comparatively small effort to later substitute the present speciation modules by another, better program. The following strategy proved to be successful, with all the non-chemical set-up steps left out for the sake of clarity:

Step: Action (the term box is used as a synonym for compartment):

- 1 Define the compartment structure and create a file MODEL.BOX
- 2 Define the chemical model for each box, collect all the necessary chemical data and create a file MODEL.CHEM.
- 3 Scan MODEL.CHEM with a separate preprocessor executable **CHEM2EQ** and build from it in parallel (to guarantee consistency between all files):
 - an **EQ3NR** input template EQ3.TEMPLATE
 - a **PRISM1** input file MODEL.PRISM
 - a further input file DIM.CHEM containing just the dimensions of the problem: number of boxes and number of components for each box
- 4 Run of **PRISM1**: generation of all parameter set variations
- 5 Run of **PRISM2**: loop over all parameter sets, for each vector a subroutine *user.for()* is called:
 - 5.1 Build an **EQ3NR** input file for each box and concatenate them to one large input file PRISM.3i (also including the constant parameters)
 - 5.2 Run **EQ3NR** to get for all boxes: the speciation of the aqueous phase and the saturation indices for the minerals
 - 5.3 Check for mineral oversaturation, call in such cases **EQ6**
 - 5.4 Calculate K_d values for all boxes, using the results from the **EQ3NR** output file PRISM.3o (and the **EQ6** output file PRISM.6o if necessary)
 - 5.5 Build the input vector for **BIOPATH**
 - 5.6 Run **BIOPATH**
 - 5.7 Update all concentrations for the next time step and go back to step 5.1 until the end of the time scale is reached
 - 5.8 Collect the final response sets together with the respective input parameter sets and write an output file
- 6 Run of **PRISM3**: Sensitivity analysis of the output file
- 7 Create graphs and reports

The file MODEL.CHEM has to be written by the user, following a well defined, line-oriented structure. After some general information for documentation purposes, detailed chemical data for each compartment are specified. This includes pH and redox state information, all components and their concentration value. To keep the chemical model as simple as possible (and thereby speeding up the computation), the set of chemical components can differ from box to box. Reaction constants k can be modified depending on the actual components for each compartment. Such reactions may include complexation, precipitation / dissolution and sorption. Another option allows to suppress certain reactions totally. Finally, every line starting with a double-cross # is a comment, inserted to guide the user when checking the input file, and is consequently skipped by the program.

In EQ3.TEMPLATE, for each parameter that is varied by **PRISM**, an appropriate tag of the form **#@#PARAiii##** is inserted, with **iii** standing for the respective three-digits number of the parameter (= position in the vector obtained from **PRISM**). All constant parameters (of the chemical model) are not forwarded to **PRISM** but rather incorporated into the **EQ3NR** template to make the model and thus the computing lean and fast.

References

- /1/ Bergström, U., Edlund, O., Evans, S., Rödger, B.: *BIOPATH - A computer code for calculation of the turnover of nuclides in the biosphere and the resulting doses to man.* Report NW-82/261, Studsvik Energiteknik AB, Nyköping (1982)
- /2/ Gardner, R.H., Rödger, B., Bergström, U.: *PRISM - A systematic method for determining the effect of parameter uncertainties on model predictions.* Report NW-83/555, Studsvik Energiteknik AB, Nyköping (1983)
- /3/ Read, D.: *Chemval-2 project. Report on stage 1: status of six technical areas.* Report EUR 15161, CEC Nuclear Science and Technology, Luxembourg (1994)
- /4/ Wolery, T.J.: *EQ3/6, A software package for the geochemical modeling of aqueous systems.* Report UCRL-MA-110662 Part I, Lawrence Livermore National Laboratory (1992)

PREPARATION OF THIN-LAYER SOURCES FOR THE DIRECT MEASUREMENT OF ACTINIDES IN CONCRETE

C. Nebelung, G. Bernhard, H. Nitsche
Forschungszentrum Rossendorf e.V., Institute of Radiochemistry

The determination of alpha-active nuclides in the “clearance-level” region is essential during the decommissioning of nuclear plants. The direct measurement of thin layer sources is an easy method to determine actinides in concrete without chemical separation.

For the direct measurements of actinides in concrete extremely thin and large area sources are required because the alpha-radiation has only a short range and it is absorbed in the concrete layers. Previously we prepared layers $5 \mu\text{m}$ with a particle size of $2 \mu\text{m}$ /1/. Using a two step crushing process, particle sizes with a mean diameter of $0.6 \mu\text{m}$ were obtained. The first step involves breaking the concrete into particles with diameters between 0.02 mm (fragmentation with pulsed electrical discharge /2/) and 0.2 mm (with a jaw breaker). In the second step, the concrete is milled with special wolfram carbide milling spheres having a diameter of $1.5 \mu\text{m}$. To prevent particle agglomeration in the suspension during the preparation of the sources this process should be carried out at a pH which is very different from the pH of the zeta potential. The zeta potential was determined by adjusting the pH of our solution accordingly we obtained layers of about $1 \mu\text{m}$ thickness.

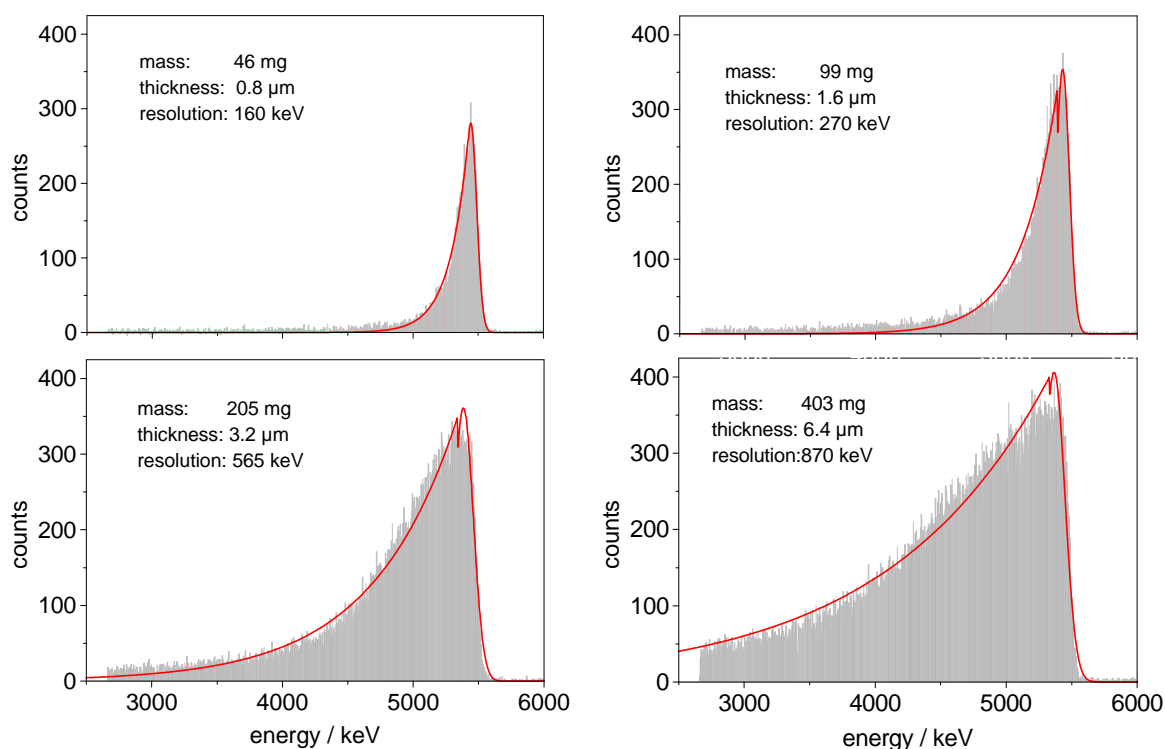


Fig. 1: GIC-spectra and peak fitting functions of concrete with $10.1 \text{ Bq/g } ^{241}\text{Am}$. 20 h measuring time, background spectrum subtracted.

Fig.1 shows the alpha-spectra and the peak fitting functions of a concrete with an added ^{241}Am tracer at various thickness. The spectra were measured with a grid ionization chamber (GIC). The diameter of the source was 200 mm .

The peak width of the signal is directly proportional to the layer thickness at a near-constant peak height. The peaks from the $1 \mu\text{m}$ -sources are comparable to the ones of ideal “massless” spectra. We are fitting the spectra of reference and unknown samples and compare the peak shape. By fitting and deconvoluting the unknown sample spectra, it is possible to determine different actinides and their concentration in a single sample. This direct measurement can be done within one day and does neither require thermal chemical treatment of the concrete nor chemical separation and electrochemical deposition.

Fig. 2 shows the spectra of the same concrete sample using a large-area passivated ion-implanted planar silicon detector (PIPS). The diameter of the source was 80 mm .

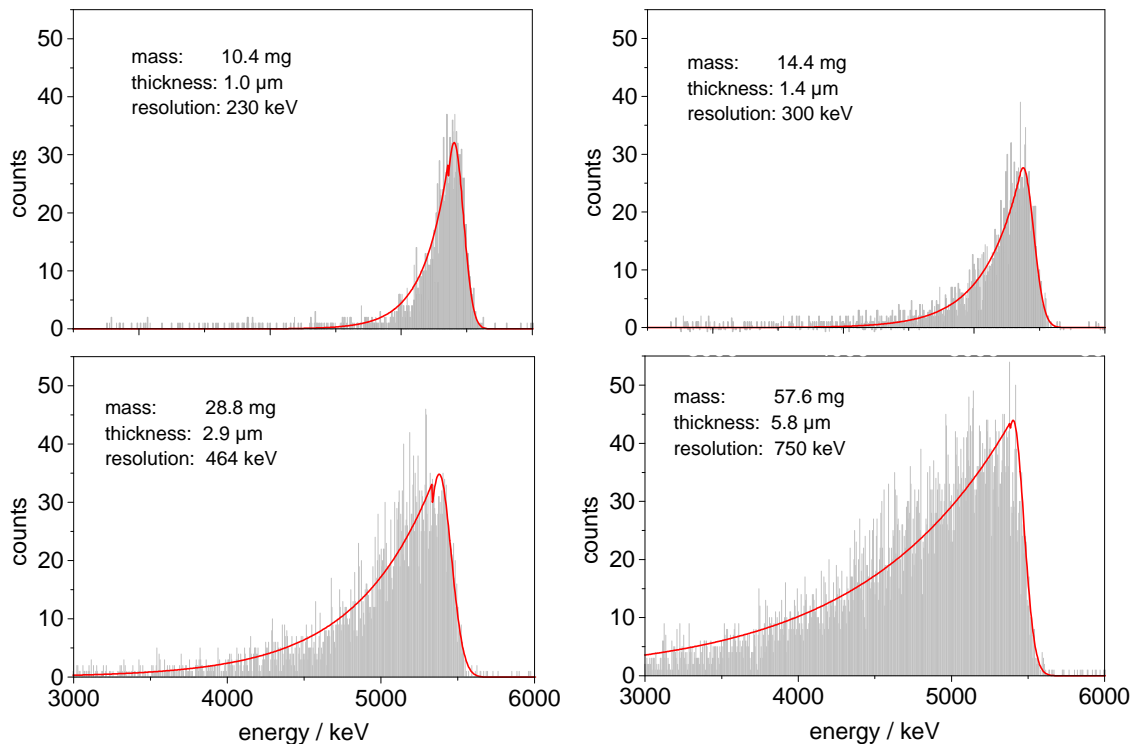


Fig. 2: PIPS-spectra and peak fitting functions of concrete with $10.1 \text{ Bq/g } ^{241}\text{Am}$. 20 h measuring time, background spectrum subtracted

Acknowledgments

This study was supported by the Bundesminister für Bildung und Forschung of the Federal Republic of Germany under the contract number 02 S 7655A8

We gratefully acknowledge the collaboration of Dr. I. Haase, TU Dresden for particle size analysis, Dr. H. Friedrich, IKTS Fraunhofer Gesellschaft for the Zeta potential measurement and B. Barz for the source preparation.

References

- /1/ Nebelung, C., Hübener, S., Bernhard, G.: *Methodenentwicklung zur Freimessung von Bauschutt auf alpha-aktive Nuklide (Th, U, Np, Pu, Am)*. Schlußbericht BMBF-Fördervorhaben 02 S 7442 2, FZ Rossendorf, 1996
- /2/ Schultheiss, C., Hübner, R.: *Fragmentierung von Feststoffen durch gepulste elektrische Entladung*. 5. Sitzung des Arbeitskreises "Freimessung von Anlageteilen und Bauschutt aus dem Abbau kerntechnischer Anlagen des Brennstoffkreislaufes", TU München, 15.3.96

DETERMINATION OF ACTINIDES IN FISH SAMPLES FROM THE RIVER IRTYSH AND THE KOIENOVSKOIE LAKE

C. Nebelung, A.A. Bessonov¹, H. Nitsche, I.N. Ryabov²

Forschungszentrum Rossendorf e. V., Institute of Radiochemistry

¹ Russian Academy of Science, Institute of Physical Chemistry, Moscow, Russia

² Russian Academy of Science, A.N. Svrtsov Institute of Ecology and Evolution, Moscow, Russia

The fish samples from two areas which may be contaminated by irradiated nuclear fuel were measured for transuranium elements. In all samples only very low concentrations of ^{237}Np were found.

The direct determination of the actinides in solid samples is practically impossible due to their minuscule quantities and the short range of the α -radiation. Therefore, the transuranics were separated from the bulk mass of the samples and then separated from each other.

First the samples were incinerated at 600 to 700°C in order to completely destroy all organic material present. After the incineration, masses between 0.85 and 4.54 % of the initial wet mass were obtained. The samples were leached treated with H_2O_2 to obtain tetravalent pluto-

samples	¹³⁷ Cs Bq/g	fraction 1 Bq/g	¹³⁷ Np Bq/g	fraction 2 Bq/g
Samples from the Koienovskoie Lake				
441(Y)	14.25	3.26 $\times 10^{-3}$	2.29 $\times 10^{-3}$	1.90 $\times 10^{-4}$
444	12.34	2.44 $\times 10^{-3}$	1.15 $\times 10^{-3}$	3.10 $\times 10^{-4}$
62	39.32	1.68 $\times 10^{-3}$	9.10 $\times 10^{-4}$	3.30 $\times 10^{-4}$
65	43.32	3.85 $\times 10^{-3}$	2.11 $\times 10^{-3}$	7.50 $\times 10^{-4}$
625	43.20	8.47 $\times 10^{-4}$	2.20 $\times 10^{-4}$	1.22 $\times 10^{-3}$
638	27.47	3.68 $\times 10^{-4}$	8.0 $\times 10^{-5}$	1.60 $\times 10^{-4}$
Samples from the River Irtysch				
N1-2	0.020	2.90 $\times 10^{-4}$	1.60 $\times 10^{-4}$	7.0 $\times 10^{-5}$
N3-5	0.065	2.4 $\times 10^{-4}$	8.0 $\times 10^{-5}$	6.0 $\times 10^{-5}$
N6-13	0.065	8.0 $\times 10^{-5}$	2.0 $\times 10^{-5}$	2.0 $\times 10^{-5}$
441(B)	0.075	1.40 $\times 10^{-4}$	3.0 $\times 10^{-5}$	1.0 $\times 10^{-5}$
442	<0.005	1.80 $\times 10^{-4}$	2.0 $\times 10^{-5}$	1.0 $\times 10^{-5}$
11-1	<0.005	1.6 $\times 10^{-4}$	3.0 $\times 10^{-5}$	0

Tab.1: The measured total α -activity of fractions 1 and 2 in comparison to the ¹³⁷Cs content

shown in Tab. 1.

The cesium activity and the total α -activity of both fractions are higher in the Koienovskoie Lake samples than in the Irtysch River samples. The ²³⁷Np-peak is measurable in fraction 1 of all samples. The measured α -activity is from about 4×10^{-3} to 1×10^4 Bq/g. The annual exposure limit in Germany for the ingestion of ²³⁷Np is 1×10^4 Bq per person. This would be equivalent to a consumption of 2500 kg fish per person and year using the values from the most contaminated sample No. 65.

The α -spectra of the fraction 1 and fraction 2 of two samples (one sample of each region) are shown in Fig. 1 and Fig. 2, respectively.

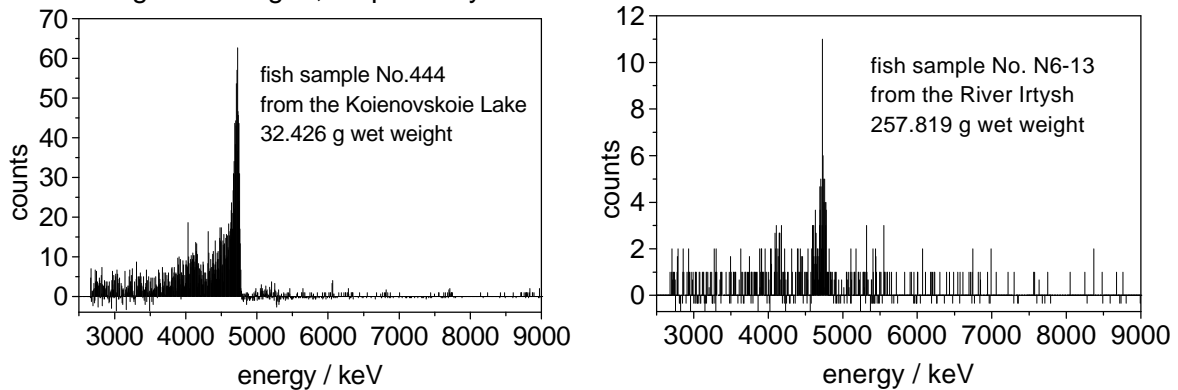


Fig.1: α -spectra of fraction 1 of two fish-samples. 20 h measuring time, background spectrum subtracted

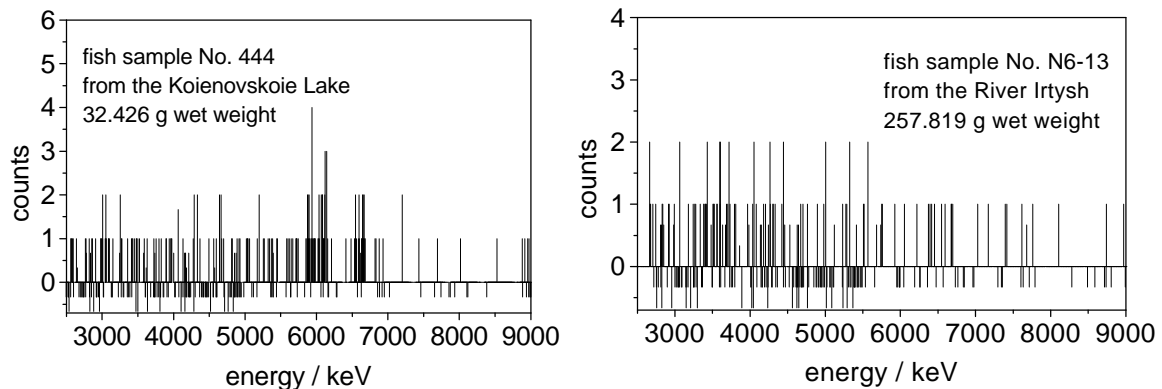


Fig.2: α -spectra of fraction 2 of two fish-samples. 20 h measuring time, background spectrum subtracted

In the fraction 2 of all samples no spectral lines of americium were found.

Future measurements, are planned with more sample masses in order to better determine the activities of the trivalent actinides.

PRELIMINARY RESULTS OF THE APPLICATION OF SIMS FOR THE LOCAL DETERMINATION OF RADIUM IN RADIOACTIVITY-CONTAINING ROCKS OF THE KÖNIGSTEIN URANIUM MINE

M. Thieme¹, F. J. Stadermann², L. Baraniak, G. Bernhard, H. Nitsche, K. Nindel³, J. Schreyer³

Forschungszentrum Rossendorf e.V., Institute of Radiochemistry

¹ Technische Universität Dresden, Institute of Materials Science

² Technische Hochschule Darmstadt, Fachbereich Materialwissenschaft

³ WISMUT GmbH, Chemnitz

The lateral distribution of ultra-traces of radium in natural rock material was recorded by secondary ion mass spectrometry (SIMS) in the presence of other members of the decay series.

Part of the research on the transport behaviour of radium downstream of the Königstein uranium mine /1/ was focused on the following issues:

- i) the distribution of Ra on the mesoscopic level, i.e., with a resolution of about 0.1 mm, in the radioactivity-containing cenomanian sandstone strata of the aquifer no. 4 located above the granite basement and
- ii) the identification of its specific mineralogic binding sites.

The radioactive equilibrium within this decay series was expected to be locally disturbed (Ra bound separately from U) because these sandstone strata are more or less affected by ground water streams and both elements are characterised by different solubility and retention properties. Sequential extraction, which was applied in parallel /2/, corroborated this assumption.

Concerning the locally resolved analysis of Ra, it should be noted that there are a number of experimental problems:

- i) Ra cannot be specifically detected by autoradiography using films /3/ or luminoradiography /4/ for recording alpha tracks;
- ii) the alpha and gamma lines of Ra-226 as the mostly abundant isotope suffer from more or less serious superposition effects due to the radiation of other nuclides. This prevents a direct spectrometric identification of the Ra radiation even if a local measurement would be achievable;
- iii) corresponding to the average specific radioactivity of #50 kBq/kg, the mass of Ra-226 is at best in the lower ppb range.

Therefore, an extremely sensitive method would be required to measure the Ra atoms (or ions) that are distributed within the sandstone. We applied secondary ion mass spectrometry which should cover the above-mentioned concentration range because of an expected high ionisation yield for Ra. Moreover, the method has a spatial resolution of about 1 µm.

First results are reported here using a Cameca ims 5f double-focussing magnetic sector field spectrometer. At first, the usual mass resolution of $M/\Delta M = 300$ was adjusted for positive secondary ions, combined with energy filtering. Rock samples of different strata were investigated in the as-received state and after H₂SO₄ leaching. A 2-nm Au film was deposited onto the polished cross sections to achieve electrical conductivity. Areas of 250@250 µm² were scanned. Test measurements were performed using a sample which was doped with 5@10⁻¹⁰ g Ra-226 on an area of about 1 mm². The results for three natural sandstone types showed that the energy filtering mode was not sufficient to suppress disturbing cluster species (among them also ¹⁹⁷Au²⁹Si⁺) against the weak ²²⁶Ra⁺ signal.

Measurements with a high mass resolution of $M/\Delta M = 5.700$ separated the peaks of ¹⁹⁷Au²⁹Si⁺ (225.9437 Da), ²⁰⁸PbH₂¹⁶O⁺ (225.9872 Da) and ²²⁶Ra (226.0254 Da). However, this mode causes a disadvantageous yield drop and requires frequent mass calibration. Finally, the search for radium was successful by recording the Ba signal in an enlarged area. It was shown earlier that the radium homolog barium is bound in a similar manner in the leached rock types /2/.

This study showed that ultra-traces of Ra can be directly detected by SIMS. Its lateral/spatial distribution in natural rock material was recorded in the presence of other members of the decay series, perhaps for the first time.

Fig. 1 shows a site where Ra could be unambiguously detected.

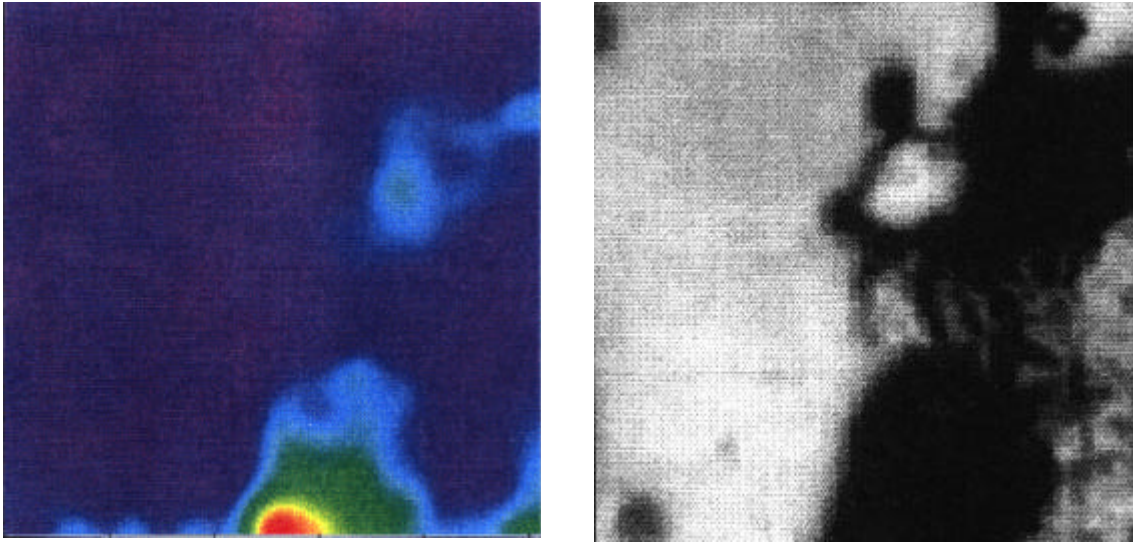


Fig. 1: Comparison of images of a polished sandstone sample (Wechsellagerung, leached); left: radium distribution according to SIMS (area: $250 \times 250 \mu\text{m}^2$, radium signal: relative intensities); right: photomicrograph of the same area.

Acknowledgment

The authors thank Dr. H. Wendrock, Institut für Festkörper- und Werkstofforschung Dresden e.V., for preparing the photomicrographs.

References

- /1/ Baraniak, L., Thieme, M., Schuster, G., Funke, H., Otto, A., Neubert, H.: *Stofftransportvorgänge des Radiums in gelaugten und ungelauften Sedimenten im Bereich der Lagerstätte Königstein (Radionuklidmigration)*. Abschlußbericht, Forschungszentrum Rossendorf e.V., Institut für Radiochemie, November 1995.
- /2/ Thieme, M., Baraniak, L., Berhard, G., Nindel, K., Schreyer, J., Nitsche, H.: Sequential Extraction on Radioactivity-containing Sedimentary Rocks of the Königstein Region, Saxony. In: Report FZR-123, Institute of Radiochemistry, Annual Report 1995, (1996), p. 34.
- /3/ Davies, J.H., Darmitzel, R.W.: Alpha Autoradiographic Technique for Irradiated Fuel. *Nucleonics* **23**, 86 (1965).
- /4/ von Seggern, H., Voigt, T., Knüpfer, W., Lange, G.: Physical Model of Photostimulated Luminescence of X-ray Irradiated BaFBr:Eu²⁺. *J. Appl. Phys.* **64**, 1405 (1988).

Organic Matter and its Interaction with Radionuclides

ISOLATION AND CHARACTERIZATION OF HUMIC ACID FROM A FLOODPLAIN OF THE RHEIN RIVER

M. Bubner, S. Pompe, A. Otto, K.H. Heise
Forschungszentrum Rossendorf e.V., Institute of Radiochemistry

We isolated humic acid as reference material from mud of the floodplain of the Rhein river. A combination of organic and inorganic extraction were devised to take into account the high content of inorganic and low molecular organic compounds, coming probably from industrial and urban products during the genesis of the humic material.

Results and discussion

In order to determine the influence of urban and industrial products during the genesis of humic acids we isolated and characterized humic acid from mud of a floodplain of the Rhein river, near Rheinstetten. The wet sample had a pH of 8. It was dried on air and analyzed.

pH	8.0			
moisture [%]	1.7			
elemental analysis (water-free sample)[%]	C	H	N	S
	5.6	0.7	0.3	0.06
inorganic oxides ^a [%]	SiO ₂	CaO	Al ₂ O ₃	Fe ₂ O ₃ K ₂ O MgO
	50.7	13.3	10.8	4.3 3.0 2.5
trace elements ^b [ppm]	Ti	Mn	Zn	Ba Sr Pb
	3880	470	450	430 280 134

^a rel. std. dev.: <±10%; ^b rel. std. dev.: <±5%

Tab. 1: Characterization of an air dried sample of mud from the floodplain of the Rhein river

compartment	% [wt.]
moisture	1.7
heptane extract	0.1
ethanol extract	0.3
non bound humic acid	0.4
earth alkali bound humic acid	1.4
residue	96

Tab. 2: Separation results of a mud sample from a floodplain of the Rhein river

The analytical results are summarized in Tab. 1. To isolate the humic acid the sample was dried under vacuum (13 Pa) and the low-molecular organics were separated by successively extracting them with heptane and ethanol. Non-bound humic acids were extracted with 1 M NaOH. The main humic acid fraction was separated with 2 M HCl from the alkaline earth containing soil matrix with 2 M HCl. Then the humic acid-containing precipitate was taken up in 2 M NaOH and precipitated with 2 M HCl. The results are summarized in Tab. 2. The isolated humic acid contained a high amount of inorganic materials. Therefore, the sample was further purified according Kim et al. /2/. The results of the chemical analysis of the purified humic acid are compared in Tab. 3 with two other humic acids that did not undergo further purification.

humic acid		I	II	III
elemental analysis:	C [%]	not determined	13.7	20.0
	H [%]		2.42	3.0
	N [%]		1.48	2.1
element analysis ^a :	Si [%]	1.3	2.5	6.6
	Ca [%]	1	2.7	0.16
	Al [%]	1.7	7.3	6.0
	Mg [%]	0.4	1.5	0.1
mval COOH per g humic ^b		0.62	0.74	1.12

I = humic acid, non bound to the sediment matrix, II = humic acid, bound by alkaline earth, classically isolated, III = humic acid, additional purified.

^a Determined with ICP/MS after decomposition with HNO₃; rel. std. dev.: <±30%.

^b Determined with calcium acetate exchange method; rel. std. dev.: <±10%.

Tab. 3: Characterization of humic acids isolated from a mud sample from a floodplain of the Rhein river

Conclusions

The results show that the alkaline earth, silicates and aluminum that are bound to humic acid cannot easily be removed. In order to remove most of these impurities the humic acid should undergo a multiple chemical treatment with NaOH and HCl. This however would significantly alter the chemical structure and perhaps also the functionality of the humic acid. In light of our results, it appears questionable if iron and aluminium can be reduced with this methods to trace levels.

We are currently devising a method to overcome this problem.

Acknowledgment

The authors thank W. Wiesener and M. Saupe for doing the element analysis, H. Görner for the determination of the elemental composition, M. Meyer and R. Ruske for the experimental work.

References

/1/ Stevenson, F.J.: *Humus chemistry, genesis, composition, reactions*. John Wiley and Sons, Inc, New York (1982).

SYNTHESIS OF URANIUM(VI) AND CALCIUM COMPLEXES WITH CARBOXYLIC AND HUMIC ACIDS

M. Bubner, S. Pompe, M. Meyer, R. Jander, G. Schuster, K.H. Heise
Forschungszentrum Rossendorf e.V., Institute of Radiochemistry

Uranyl complexes of organic carboxylic acids which represent structural elements of humic acids, and uranyl and calcium complexes of a natural and a synthetic humic acid were synthesized by ligand exchange starting from uranyl acetate or calcium acetate, respectively. These well-characterized substances serve as model and reference substances for structural investigations by EXAFS, ESCA and FTIR.

Experiments and discussion

Interpretation of the results from structural investigations of structures of uranyl-humic acid complexes by EXAFS, ESCA and FTIR necessitate the comparison of experimental data from substances with unknown structure with data from defined and well characterized models and reference substances /1, 2/. Therefore we synthesized uranyl complexes of organic acids with molecular structures corresponding to structural elements of humic acids, and humic acid complexes of a natural reference humic acid and a synthetic model humic acid with the maximum loading of uranyl and calcium. Solid complexes of carboxylic and humic acids were synthesized by exchanging the acetate ligand of uranyl acetate with either carboxylic or humic acid.

1. Uranyl complexes of organic carboxylic acids

Several different carboxylic acids, listed in Tab. 1, were chosen to prepare complexes with U(VI). Their carboxylate groups may simulate the carboxylate groups in humic acids.

Functionality - functional group	Carboxylic acid
aromatic carboxylic acid, unsubstituted	benzoic acid
aromatic carboxylic acid, OH- in o-position	salicylic acid
aromatic carboxylic acid, OH-blocked	o-methoxybenzoic acid
aliphatic dicarboxylic acid	malonic acid
aliphatic dicarboxylic acid, salt	malonic acid, monoammonium salt

Tab. 1: Carboxylic acids representing functional groups of humic acids

Due to the steric arrangement of the COOH-groups in the molecule and the low solubility of the forming complex, the reaction of stoichiometric amounts of the malonic acid led to pure uranyl

malonate. Aromatic carboxylic acids give mixed complexes with three ligands as shown in Fig. 1. The desired product can only be isolated if the acetic acid can be quantitatively removed. A special case of ligand exchange is the reaction of insoluble uranyl malonate with diammonium malonate yielding diammonium uranyl dimalonate /3/.

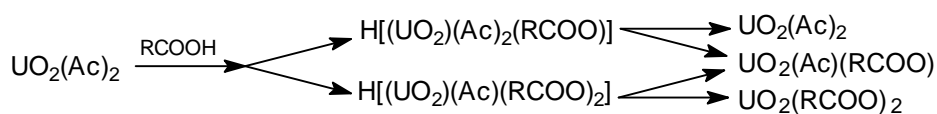


Fig. 1: Reaction scheme of the synthesis of carboxylato uranyl complexes

Uranyl Complex	Ratio of Reactants	Solvent	Reaction condition
$\text{UO}_2(\text{C}_6\text{H}_5\text{COO})_2$	1 : 3 (6)*	methanol	130°C, under vacuum*
$\text{UO}_2[\text{C}_6\text{H}_4(\text{OH})\text{COO}]_2$	1 : 2	methanol	100°C, lyophilization
$\text{UO}_2[\text{C}_6\text{H}_5(\text{OCH}_3)\text{COO}]_2$	1 : 2	methanol	100°C, lyophilization
$\text{UO}_2[\text{CH}_2(\text{COO})_2]\text{H}_2\text{O}$	1 : 1	water	20°C, filtration, lyophilization
$(\text{NH}_4)_2\text{UO}_2[\text{CH}_2(\text{COO})_2]_2$	1 : 1 **	water	0°C, filtration, lyophilization

* Repeating of the reaction after removing the volatile carboxylic acids in a molten ampoule

**Reaction of $\text{UO}_2[\text{CH}_2(\text{COO})_2]\text{H}_2\text{O}$ with $\text{CH}_2(\text{COONH}_4)_2$

Tab. 2: Reaction conditions of the uranyl complex syntheses

Tab. 2 summarizes the conditions of the syntheses, the manipulation for removing acetic acid and the composition of the products, based on elemental analysis and XRD-measurements.

2. Uranyl and calcium complexes of humic acids

For the reaction of uranyl or calcium acetate with humic acids suspended in water, highly purified Aldrich humic acid, A2, and a synthetic humic acid, type M1 /4/, were used. On the

basis of the determined mval COOH per g humic acid, 4,8 meq/g for A2 and 1,0 meq/g for M1, an one-fold excess of uranyl acetate and a ten-fold excess of calcium acetate were used for the complex formation. The products were isolated by centrifugation and lyophilization.

Humate	C [%]	H [%]	N [%]	Ca [%]	U [%]
A2-Ca calculated	49.2	3.9	0.6	8.7	-
A2-Ca experimental	50.5	3.8	0.7	8.1	-
M1-Ca calculated	61.6	5.5	0.2	1.9	-
M1-Ca experimental	60.8	5.4	0.4	2.0	-
A2-UO ₂ calculated	32.8	2.6	0.4	-	34.6
A2-UO ₂ experimental	32.3	2.3	0.4	-	35.0
M1-UO ₂ calculated	55.3	4.9	4.4	-	10.5
M1-UO ₂ experimental	49.9	4.6	3.9	-	12.5

Tab. 3: The elemental composition of the humic acid complexes

Ca/U [mol/mol]	reagent mixture (calcium acetate/uranyl acetate)	1/1	1/3	3/1
Ca/U [mol/mol]	solid A2-complex	1/1.7	1/5	1/0.5
	supernatant solution	1/0.7	1/2.2	1/0.12
Ca/U [mol/mol]	solid M1-complex	1/2.5	1/10	1/0.5
	supernatant solution	1/0.13	1/0.55	1/0.01

Tab. 4: Complexation of humic acids A2 and M1 with mixtures of calcium and uranyl acetate

Humic acid compl.	Ca/U[mol/mol] compl.	Ca/U[mol/mol] supern.sol.
A2	1/3.4	1/1.3
M1	1/8.6	1/0.5

Tab. 5: Ratio of Ca to U in solid complexes and the corresponding supernatant solution after interaction of calcium humates with uranyl acetate

Tab. 3 shows the elemental composition of the calcium and uranyl humates compared to those calculated for neutral complexes quantitatively saturated of the COOH-groups by either calcium or uranyl ions.

The difference in affinity of UO₂²⁺ and Ca²⁺ ions to the humic acids were also examined. For this purpose, the humic acids were reacted with one-fold excess of defined mixtures of uranyl and calcium acetate having molar proportions of 1:1, 1:3 and 3:1. The exchange of the cations between solid calcium humates and a one-fold excess of dissolved uranyl acetate was examined in a subsequent experiment. In all the experiments, the molar proportion were determined of Ca to U in the resulting solid product and in the supernatant solution. The results of these experiments are summarized in Tab. 4 and 5.

Results and conclusions

The availability of defined uranyl complexes of carboxylic acids is a prerequisite for investigations characterizing parameters of COO-binding in definite molecule structures. Such model compounds may serve for comparing unknown parameters of COO-binding in uranyl humate complexes. The synthesized carboxylato uranyl complexes have a defined elemental composition and a defined structure. The synthesized calcium and uranyl humates seem to be stoichiometric neutral complexes, according to elemental analysis. They are applicable for comparative studies of the binding parameters of uranyl ions in humic acid complexes and other carboxylato - functional analogs.

The reactions of humic acids with mixtures of calcium and uranyl acetate and the exchange of uranyl between calcium humate and uranyl acetate show a greater affinity of UO₂²⁺ ions to humic acid when compared to calcium. The synthetic humic acid, M1, shows a lower solubility of its uranyl complex, due to its lower COOH- content.

Acknowledgment

The authors thank W. Wiesener for ICP-MS analysis and H. Görner for elemental analysis.

References

- /1/ Denecke, M.A., Pompe, S., Moll, H., Heise, K.H., Reich, T., Bernhard, G., Nitsche, H.: EXAFS Studies on Anhydrous Complexes of Uranyl and Orthosubstituted Benzoic Acid. In: Report FZR-123, Institute of Radiochemistry, Annual Report 1995, 87 (1996).
- /2/ Denecke, M.A., Reich, T., Bubner, M., Pompe, S., Heise, K.H., Nitsche, H., Allen, P.G., Bucher, J.J., Edelstein, N.M., Shuh, D.K.: Differentiating between monodentate and bidentate carboxylate ligands coordinated to uranyl ions using EXAFS. In: This Report, Institute of Radiochemistry, Annual Report 1996, (1997) p. 40
- /3/ Herrero, J.A., Bermudez, J., Gutierrez Rios, E.: Derivados complejos de uranilo con ácido malónico (I). *Química e Industria* **18**, 15 (1972).
- /4/ Pompe, S., Bubner, M., Denecke, M.A., Reich, T., Brachmann, A., Geipel, G., Nicolai, R., Heise, K.H., Nitsche, H.: A Comparison of Natural Humic Acids with Synthetic Humic Acid Model Substances: Characterization and Interaction with Uranium(VI). *Radiochim. Acta* **74**, 135-140 (1996).

THERMOANALYSIS OF A SYNTHETIC AND A NATURAL HUMIC ACID AND THEIR CALCIUM- AND URANYL COMPOUNDS

G. Schuster, M. Bubner, S. Pompe, K.H. Heise, H. Nitsche
Forschungszentrum Rossendorf e.V., Institute of Radiochemistry

TG, DTG and DTA measurements were performed of the decomposition of a synthetic humic acid (R36) and a natural humic acid (A2) from Aldrich and their respective Ca and U(VI) compounds. Conclusions were done about the chemical structure and the influence of the metal cations on the thermal stability of the humic molecules. By reaction to definite compounds of the metals the content of bound metal was determined.

Experimental

We studied the thermal decomposition of a) a synthetic humic acid (R36) that was prepared from xylose, phenylalanine and glycine, b) a natural humic acid (A2) from Aldrich, and c) their respective calcium and uranium (VI) compounds. This compounds were prepared by the reaction of solutions of the humic acid and the metal acetates. Preparation and purification of the substances was described earlier /1, 2, 3/. About 5 mg were inserted in a Setaram thermoanalyzer, heated with 10°C/min up to 110°C where the temperature was held for 20 minutes. Then the temperature was increased to 1000°C and held for 10 minutes. The heating was done under a constant flow of oxygen (3 l/h). The determination varied between 0.1 and 0.6 %, depending on the substance investigated.

Results and Discussion

In a first endothermal reaction at about 80°C, 6 to 11 % moisture are evaporated (reaction 1). The main oxidation of the organic matter takes place in two exothermal reactions with peak temperatures of $T_p = 285$ to 340°C (reaction 2) and 370 to 450°C (reaction 3).

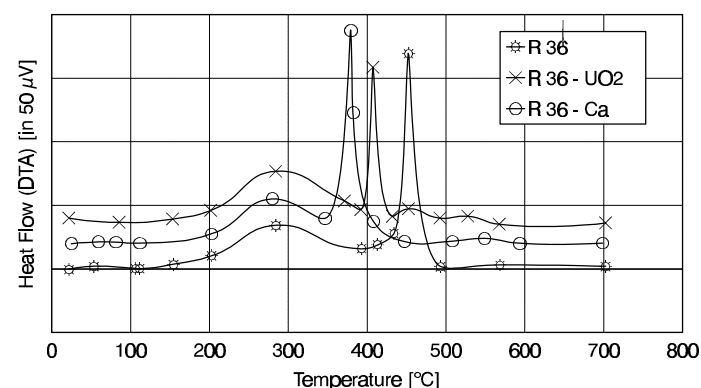


Fig. 1: DTA thermograms of synthetic humic acid R 36 and its Ca and uranyl compounds. (Y axis is displaced for clarity by 20 μ V for R 36-Ca and by 40 μ V for R 36-UO₂)

	δm_2 (aliphatic groups)	δm_3 (aromatic groups)	$\delta m_2 / \delta m_3$
R 36	51.4	42.9	1.2
A 2	24.6	73.8	0.3

Tab. 1: Mass loss of the reactions 2 and 3 and the ratio $\delta m_2 / \delta m_3$

Aliphatic and aromatic bonds in humic acids are broken above 350°C and 400°C, respectively, where oxidation occurs /4/. Therefore the mass loss of the exothermal reaction 2 is proportional to the aliphatic, and that of reaction 3 to the aromatic groups. According to these results, R 36 should have much more aliphatic and less aromatic groups than A 2. Tab. 1 summarizes the mass losses and their assignments.

After reaction 3 is completed, more than 85% of the organic matter is oxidized. The reaction temperatures for the individual compounds are summarized in Tab. 2. The shift of the temperature for reaction 3 is a measure of the thermal stability of the compound. This shifts may be due to the different metal-humic acid bond strength or to different steric proportions between the metal and humic acid groups. In the first case, a dependence should exist on the electronegativity and in the second case on the ionic radius. Neither dependencies could be found.

R 36 showed a fourth exothermal reaction at 530°C, and the calcium and uranyl complexes showed several small peaks above 450°C where the reaction to the final inorganic compounds occurred. The DTG thermograms of R36 and its respective Ca and U(VI) complexes are shown in Fig. 1.

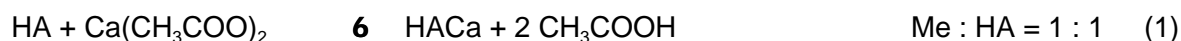
Aliphatic and aromatic bonds in humic acids are broken above 350°C and 400°C, respectively, where oxidation occurs /4/. Therefore the mass loss of the exothermal reaction 2 is proportional to the aliphatic, and that of reaction 3 to the aromatic groups. According to these results, R 36 should have much more aliphatic and less aromatic groups than A 2. Tab. 1 summarizes the mass losses and their assignments.

Sample	Reaction-temp. [°C]	δT [°C]
R36	448	
R36-Ca	403,9	- 44,1
R36-UO ₂	371	- 77
A2	393,9	
A2-Ca	383,5	- 10,4
A2-UO ₂	483,5	+ 89,4

Tab. 2: Reaction temperature shift for the reaction that degrades more than 85% of the organic matter

Calculation of the content of bound metal from the oxidation

The inorganic residues of the reactions are definitely CaO , U_3O_8 , and Na_2CO_3 . From their amount the content of bonded metal could be calculated. The calcium and uranium (VI) humates were prepared by reacting them with the respective metal acetates. This divalent metals can react in two different reaction paths /2/:



In both cases the two H^+ ions of the resulting acetic acid are dissociated from the carboxylic groups of the humic acid (HA).

Based on the determined amount of carboxylic groups per gram humic acid, which is 4.8 mequ/g for the A2 and 1 mequ/g for the R36, the theoretical metal content was calculated

Sample	Metal [%] calculated for Me:HA=2:1	Metal [%] calculated for Me:HA=1:1	Exp. Metal from TA	Exp. ratio from TA Me:HA	Exp. (TA) Me. value mequ/g
R 36 - Ca	3.6	1.9	1.8	1 : 1	0.9
R 36 - U	17.9	10.5	14.4	2 : 1 and 1 : 1	1.2
A2 - Ca	13	8.8	12.4	2 : 1	6.2
A 2 - U	44.3	34.6	34.6	1 : 1	2.9

Tab. 3: Theoretical and experimental metal contents of humic acid metal compounds and the molar Me:HA ratios

for both reaction paths and compared with the experimental values derives from TA (thermal analysis). The results are listed in Tab. 3. Calcium reacts with R36 in a 1:1 and with A2 in a 2:1 ratio. U(VI) shows with A2 a 1:1 and with R36 a mixed 1:1 and 2:1 ratio.

References

- /1/ Pompe, S., Bubner, M., Denecke, M.A., Reich, T., Brachmann, A., Geipel, G., Nicolei, R., Heise, K.H., Nitsche, H.: A Comparison of Natural Humic Acids with Synthetic Humic Acid Model Substances: Characterization and Interaction Uranium (VI). *Radiochimica Acta* **74**, 135-140 (1996)
- /2/ Bubner, M., Pompe, S., Meyer, M., Jander, R., Schuster, G., Heise, K.H.: Synthesis of Uranium(VI) and Calcium Complexes with Carboxylic and Humic Acids. In: This Report, Institute of Radiochemistry, Annual Report 1996, (1997) p. 22
- /3/ Kim, J., Buckau, G.: *Characterization of Reference and Site Specific Humic Acids*. Report RCM 02188, TU München, 1988
- /4/ Stevenson, F.: *Humus Chemistry*, J. Wiley and Sons, New York, 1994, p. 255

COMPLEXATION BEHAVIOR OF A SYNTHETIC HUMIC ACID WITH URANYL IONS IN COMPARISON TO A NATURAL HUMIC ACID BY TIME-RESOLVED LASER-INDUCED FLUORESCENCE SPECTROSCOPY

S. Pompe, A. Brachmann, G. Geipel, K.H. Heise, H. Nitsche
Forschungszentrum Rossendorf e.V., Institute of Radiochemistry

The complexation behavior of a synthetic humic acid (HA) and purified natural humic acid from Fluka with uranyl ions was investigated by time-resolved laser-induced fluorescence spectroscopy (TRLFS). The spectroscopic data were evaluated using the charge neutralization model of Kim and Czerwinski. Both humic acids show a comparable complexation behavior with uranyl ions (pH 3.90 ± 0.05 ; I: 0.1 M NaClO_4).

Experimental and results

The aim of this work was to compare the complexation behavior of a synthetic humic acid (type M42) prepared from glutamic acid monohydrate and xylose /1/ and of the purified HA from Fluka /2/ with U(VI) in aqueous solution. This should determine whether or not the synthetic HA can be used as a model substance to describe the complexation behavior of natural HA.

Concentration	Synthetic HA (M42)	Fluka-HA
HA [mg/L]	5	5
UO_2^{2+} [mol/L]	$1.0 \cdot 10^{-6}$ - $4.2 \cdot 10^{-6}$	$0.3 \cdot 10^{-6}$ - $2.9 \cdot 10^{-6}$

Tab. 1: Experimental conditions
(pH: 3.90 ± 0.05 ; I: 0.1 M NaClO_4)

The measurements were performed at pH 3.90 ± 0.05 and 22 ± 1 °C in 0.1 M NaClO_4 . Tab. 1 shows the humic acid and uranyl concentrations of the samples investigated. The proton exchange capacities (PEC) of the HA were determined with the calcium acetate method; they are 3.23 ± 0.05 meq/g for synthetic HA and 3.8 ± 0.1 meq/g for Fluka-HA. Uranyl solutions without HA present were measured for all samples in order to determine the depend-

ence of the relative fluorescence intensity on the uranyl concentration. The measurements were carried out with a Nd:YAG laser as an excitation source with an excitation wavelength of 266 nm. The laser energies applied were $450 \pm 50 \mu\text{J}$ for synthetic HA and $700 \pm 70 \mu\text{J}$ for Fluka-HA. A more detailed description of the measuring conditions is described in /1/.

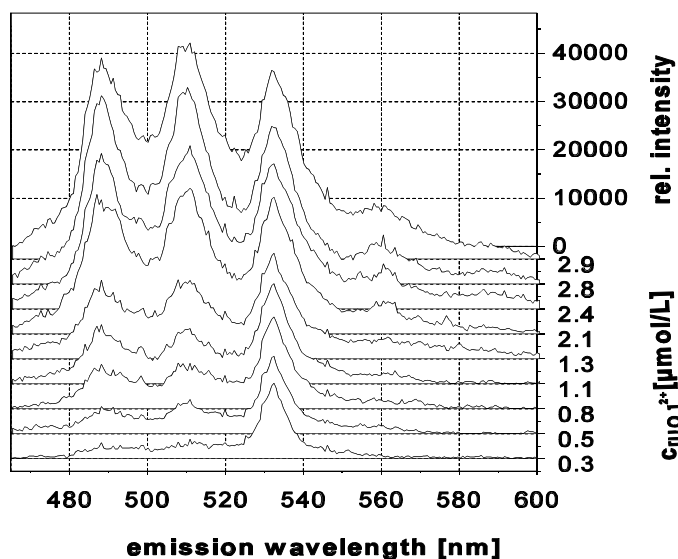
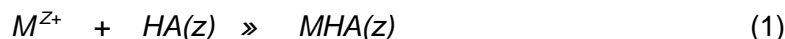


Fig. 1: Emission spectra of uranyl humate solutions (Fluka-HA) in dependence on the uranyl concentration

amount of UO_2OH^+ (< 2.2 %) is present at the applied experimental conditions. For all cases, no emission spectra of the uranyl humate complex was observed. The integrals of the relative fluorescence intensities between 465 and 600 nm were calculated from the spectra of the solutions without HA. The results were used to calibrate the fluorescence signal of the free uranyl ion in the solutions with HA.

The evaluation of the spectroscopic data was performed using the metal ion charge neutralization model of Kim and Czerwinski /4/, in which the complexation reaction of a given metal ion with humic acid is considered as a metal ion charge neutralization process. In this reaction the metal ion (M) occupies the number of proton exchange sites equal to its charge (z^+) (eq. 1).



In this model the loading capacity (LC), the mole fraction of the maximum available complexing sites of the humic acid, which varies with pH, metal ion, ionic strength and HA is introduced. The resulting complexation constants derived from this model are invariant of experimental conditions. The graphically determined loading capacities of the HA with uranyl ions and the complexation constants of the HA are:

	LC [%]	log β
Synthetic HA (M42)	0.23 ± 0.06 (3F)	6.16 ± 0.33 (3F)
Fluka-HA	0.24 ± 0.06 (3F)	6.04 ± 0.23 (3F)

Both HA show comparable results within the given errors. This result points to a similar complexation behavior of both HA with uranyl ions under the conditions applied.

Conclusions

Comparison of the behavior of a synthetic HA to a natural HA (Fluka) by TRLFS has shown both comparable loading capacities and complexation constants for uranyl ions. From this, we can conclude that our synthetic HA models the functionality of natural HA very well.

Acknowledgments

We thank A. Otto for help with the sample preparation and Dr. W. Wiesener, Zentralabteilung Analytik, for ICP-MS measurements.

References

- /1/ Pompe, S.: *Entwicklung huminsäureähnlicher Melanoidine als Funktionalitätsmodelle für Huminsäuren und ihr Vergleich mit Fluka-Huminsäure hinsichtlich ihres Komplexbildungsverhaltens gegenüber Uran(VI)*. Dissertation, TU Dresden, submitted.

- /2/ Pompe, S., Bubner, M., Denecke, M.A., Reich, T., Brachmann, A., Geipel, G., Nicolai, R., Heise, K.H., Nitsche, H.: A Comparison of Natural Humic Acids with Synthetic Humic Acid Model Substances: Characterization and Interaction with Uranium(VI). *Radiochim. Acta* **74**, 135 (1996).
- /3/ Brachmann, A.: *Zeitaufgelöste laserinduzierte Fluoreszenzspektroskopie zur Charakterisierung der Wechselwirkung des Uranylions mit Huminsäuren sowie Carboxylatliganden zur Simulation der Huminsäurefunktionalität*. Dissertation, TU Dresden, submitted.
- /4/ Kim, J.I., Czerwinski, K.R.: Complexation of Metal Ions with Humic Acid: Metal Ion Charge Neutralization Model. *Radiochim. Acta* **73**, 5 (1996).

INTERACTION OF Pb(II) AND Bi(III) WITH HUMIC ACID STUDIED BY TIME- RESOLVED LASER-INDUCED FLUORESCENCE SPECTROSCOPY (TRLFS)

A. Brachmann, G. Geipel, G. Bernhard, H. Nitsche
Forschungszentrum Rossendorf e.V. Institute of Radiochemistry

To determine the stability constants of lead and bismuth complexes with humic acid (FLUKA), we applied TRLFS using a Nd:YAG laser pumped OPO system. A description of the experimental setup is given elsewhere /2/.

The residues of the former uranium mining in Saxony and Thuringia contain two sources of these elements: The radioactive decay of naturally occurring uranium isotopes and paragenetic minerals of the uranium mineralisations. Weathering processes lead to the introduction of Bi(III) and Pb(II) into seepage waters where they can interact with humic substances.

Using the concept of metal ion charge neutralization /1/, we obtained the stability constants $\log \beta_{i=0.1M} = 3.7 \pm 0.2(2F)$ for Pb(II) - humate and $6.73 \pm 0.06(2F)$ for Bi(OH)₂ - humate.

Results and discussion

Bismuth and lead are main group elements and their aquo ions Bi³⁺ and Pb²⁺ do not show fluorescence in aqueous solution. However, humic acid is fluorescent when dissolved in water. The complex formation of humic acid with certain metal ions decreases the fluorescence signal

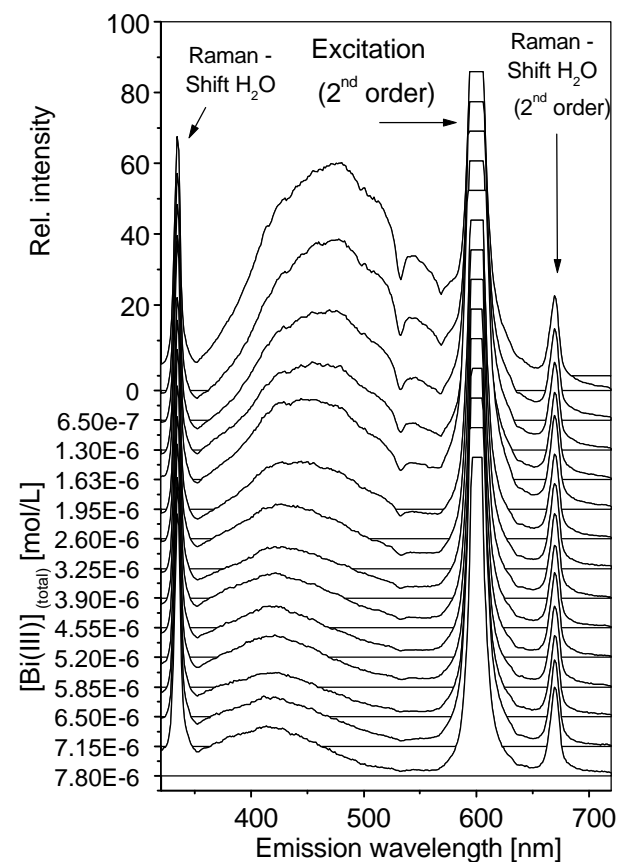


Fig. 1: Humic acid fluorescence as a function of $[Bi^{3+}]_{(total)}$

Fig. 1 shows humic acid fluorescence spectra as function of total Bi³⁺ concentration. Fluorescence of humic acid can be seen as a broad unstructured emission band in the spectral range from about 300 nm to 600 nm. The intensity decreases with increasing metal concentration due to the fluorescence depletion effect. The spectral band at 355 nm is due to Raman emission of

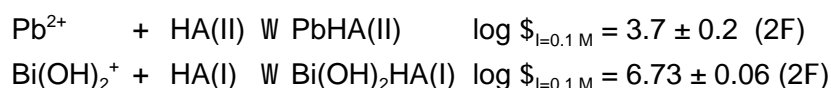
of the ligand which can be used to determine the concentration of the free humic acid. This method has been used by several authors to characterize the complexation of metal ions with fluorescent organic ligands and is known as *Fluorescence quenching titration* (e.g., /3/).

The experiments were carried out under atmospheric conditions. In order to avoid metal ion hydrolysis and carbonate complexation, the pH was held constant at about 4.5 and 4.0 for the lead - humic acid and the bismuth - humic acid experiments, respectively. Under these conditions only the Pb²⁺ aquo ion exists, and Bi(OH)₂⁺ is the main Bi(III) species. The experiments were performed at a constant ionic strength of 0.1 M NaClO₄ and a temperature of $23 \pm 1^\circ C$. TRLFS allows measurements at concentration ranges relevant to environmental conditions. This is particularly the case for the humic acid concentration which was 0.645 mg/L. To obtain evaluable analytical effects, the metal concentrations had to be increased above environmental levels. The metal-to-humic-acid ratios from 40 to 3000 and from 0.3 to 4 were used to study the Pb²⁺ humate and the Bi(OH)₂⁺ humate complexation, respectively.

the water molecule. Additionally, the second order of excitation wavelength (600 nm) and H₂O-Raman band (670 nm) which are generated in the spectrograph overlap with the humic acid fluorescence signal. Similar spectra of humic acid fluorescence were observed for Pb²⁺ - humate formation.

The influence of the complexed metal on the fluorescence intensity is not equally distributed over the entire spectral range. The extend of fluorescence depletion is most intense for those structural elements which are involved in the metal ion binding. Due to the complex nature of humic acid fluorescence, reliable spectra deconvolution is not possible. A distinctive metal - humate spectra was not observed. Therefore we used the decrease in fluorescence directly to calculate the free ligand concentration. The most intense depletion occurs in the spectral range from 470 nm to 500 nm for Bi(OH)₂⁺ - humate complexation, and from 530 nm to 550 nm for Pb²⁺ - humate complexation. The effects of the complexed metal ion on the electronic structure of the humic acid molecule are specific for each species. Therefore different spectral changes of the humic acid fluorescence are obtained.

The integrated fluorescence signal over the above-mentioned wavelength ranges was used to calculate the complex stability constants according to the method that was summarized by Brachmann /4/. Using the model of metal ion charge neutralization, the following complexation constants were derived:



Conclusions

We showed that complexation of Pb²⁺ and Bi³⁺ with humic acid occurs. Because of the relatively strong complex stability, the humate formation of these elements can compete with metal ion hydrolysis and complexation with other inorganic ligands. According to literature data, TRLFS studies on the complexation behavior of metal ions with humic substances have been carried out only using data derived from the fluorescence signal of metal ions (UO₂²⁺, Am³⁺, Cm³⁺). This study shows that also the ligand fluorescence can be used to characterize the complexation reactions.

References

- /1/ Kim, J.I., Czerwinski, K.R.: Complexation of Metal Ions with Humic Acid, Metal Ion Charge Neutralization Model. *Radiochim. Acta* **73**, 5-10 (1996).
- /2/ G. Geipel: Time-resolved Laser-induced Fluorescence Studies (TRLFS) - Experiences with a new laser system. In: Report FZR-94, Institute of Radiochemistry, Annual Report 1994, (1995) p. 19.
- /3/ Ryan, D.K., Weber, J.H.: Fluorescence Quenching Titration for Determination of Complexing Capacities and Stability Constants of Fulvic Acid. *Anal. Chem.* **54**, 986-990 (1982).
- /4/ Brachmann, A.: *Zeitaufgelöste laserinduzierte Fluoreszenzspektroskopie zur Charakterisierung der Wechselwirkung des Uranylions mit Huminsäuren und Carboxylatliganden*. Dissertation, TU Dresden, 1997.

COMPLEX FORMATION OF HEXAVALENT URANIUM WITH LIGNIN DEGRADATION PRODUCTS

L. Baraniak, M. Schmidt, G. Bernhard, H. Nitsche
Forschungszentrum Rossendorf e.V., Institute of Radiochemistry

The complexation of U(VI) with the lignin degradation products protocatechuic acid, ferulic acid, vanillic acid and vanillin was studied at I = 0.1 M by potentiometric pH titration. The stability constants were estimated from Bjerrum's formation function using (a) successive approximation and (b) Irving's least-squares treatment. To consider U(VI) hydrolysis, non-linear fitting of the pH titration curves was carried out with the multi-equilibria program SCOGS(version 2).

The natural disintegration of the highly stable lignin is a very slow process because only white rot fungi are able to start the radical depolymerisation of the phenolic matrix by their special enzyme system. The second step is the oxidative side-chain removal followed by phenol ring cleavage and the fast degradation of the non-aromatic fragments. In this process the oxidation of some more stable phenolic monomers occurs. Beginning with 4-hydroxy-3-methoxycinnamic acid (ferulic acid), the sequence leads over 4-hydroxy-3-methoxybenzaldehyde (vanillin) and

4-hydroxy-3-methoxy-benzoic acid (vanillic acid) to 3,4-dihydroxy-benzoic acid (protocatechuic acid). These compounds are also found in leachates of the hydrothermal wood treatment. Their phenolic hydroxyl and carboxylic groups are able to bind metals.

The complex stability constants were determined potentiometrically by measuring the hydrogen ion concentration in the system: uranyl perchlorate/complexant at constant ionic strength ($I = 0.1$ M, NaClO_4) and temperature in dependence of the added carbonate-free strong base titrant. The titrations were carried out with of an automatic titrator (model: Schott TPC 2000) equipped with a low-drift pH electrode (type: Orion-Ross 81/03), stirrer, inert gas inlet and titrant dosage capillary.

The evaluation of the pH titration curves was carried out: (1) on the classical theory of stepwise complex formation, analyzing Bjerrum's formation function (1921) by successive approximation:

$$\sum_{n=0}^{\infty} \beta_n [A]^n = 0, \text{ with } \beta_0 = 1; \quad \sum_{n=0}^{\infty} \beta_n k_1 [A] + \sum_{n=0}^{\infty} \beta_n k_1 k_2 [A]^2 = 0 \quad (1a, 1b)$$

or linear regression, as introduced by Irving and Rossotti /1/:

$$\frac{n}{(n+1)[A]} = \frac{(2+n)[A]}{(n+1)} k_1 k_2 + k_1 \quad (2)$$

and (2) by non-linear fitting of the unmodified pH titration curve with Sayce's multi-equilibria program "SCOGS" (Stability Constants of General Species) /2/ considering hydrolysis and the formation of mixed-ligand complexes.

The following hydrolysis constants of UO_2^{2+} as $\log Q_{xy}$ values, recalculated for $I = 0.1$ M by $\log Q_{xy} = \log K_{xy} + aI^{1/2} / (1+I^{1/2}) + bm_x$ were used /3/:

$\text{UO}_2(\text{OH})$:	-5.976	$\text{UO}_2(\text{OH})_2$:	-10.8	$\text{UO}_2(\text{OH})_3$:	-20.0	$\text{UO}_2(\text{OH})_4$:	-33.8
$(\text{UO}_2)_2(\text{OH})_2$:	-5.812	$(\text{UO}_2)_3(\text{OH})_4$:	-12.6	$(\text{UO}_2)_3(\text{OH})_5$:	-16.23	$(\text{UO}_2)_3(\text{OH})_7$:	-32.0
$(\text{UO}_2)_4(\text{OH})_7$:	-22.0						

Protocatechuic acid: 3,4-dihydroxybenzoic acid forms very stable complexes with U(VI). The evaluation of Bjerrum's formation function led to stability constants of the (1:1)- and (1:2)-complexes, which are in full agreement with the stability values, calculated by SCOGS curve fitting and given in the literature /4/, i.e., U(VI) hydrolysis is strongly suppressed in the presence of this complexant (Tab. 1).

Ferulic acid: Assuming the complex $[\text{UO}_2(\text{fer})]$ and $[\text{UO}_2(\text{fer})_2]^{2-}$ we find an increase of the corresponding $\log \beta$ -values with the U(VI) concentration and a strong deviation of the fit from the experimental curve in the pH range 4.5-6.2. The introduction of the acidic $[\text{UO}_2\text{H}(\text{fer})]^+$ led to constant values, which are independent on the U(VI) concentration and the fit discrepancy around pH 5 disappeared (Tab. 1). Additional consideration of $[\text{UO}_2\text{H}(\text{fer})_2]^-$ ($\log \beta$. 16), $[\text{UO}_2(\text{Hfer})_2]$ (-22) and $[\text{UO}_2(\text{fer})\text{OH}]^-$ (-0.05) did not contribute to a good curve simulation.

Vanillic acid: The interaction of U(VI) with vanillic acid results in a stepwise formation of mono-nuclear (1:1)- and (1:2)-complexes (Tab. 1). The stability constants, evaluated in the different ways, are in distinct conformity, i.e. hydrolysis plays no evident role in the pH range studied (3.6#pH#10.6).

ligand	$\text{pK}_{\text{diss.}}$	$\log \beta_{11}^{(5)}$ [MA] ⁶⁾	$\log \beta_{111}$ [MA(OH)]	$\log \beta_{12}$ [MA ₂]	$\log \beta_{12-2}$ [MA ₂ (OH) ₂]
¹⁾ H ₃ (pro)	4.26/8.64/13.1	14.8 ± 0.74	-	25.9 ± 1.0	-
²⁾ H ₂ (fer)	4.45/8.81	6.88 ± 0.56	11.9 ± 0.65	-	-
³⁾ H ₂ (vac)	4.35/8.71	7.16 ± 0.82	-	13.6 ± 1.1	-
⁴⁾ H(van)	7.18	4.47 ± 0.09	-	-	-3.95 ± 0.5

5) confidence interval at a probability of 0.95; 6) complex composition

Tab. 1: Stability of U(VI) complexes with protocatechuic acid¹, ferulic acid², vanillic acid³ and vanillin⁴ computed by non-linear curve fitting considering hydrolysis

Vanillin: Assuming the formation of the two species $[\text{UO}_2(\text{van})]^+$ and $[\text{UO}_2(\text{van})_2]$ the analysis of the formation functions according to Bjerrum and Irving/Rossotti results in corresponding complex stabilities. Considering U(VI) hydrolysis these results shift to lower values. The curve fitting was repeated under the assumption that in the course of the titration partially hydrolyzed complexes are formed. In case of $[\text{UO}_2(\text{van})]^+$ and $[\text{UO}_2(\text{van})_2(\text{OH})_2]^{2-}$ the best curve fits ($F_{\text{fit}} \# 0.025$) could be attained, giving the complex stabilities: $\log \beta_{11} = 4.47 \pm 0.09$ and $\log \beta_{12-2} = -3.78 \pm 0.74$, respectively (Tab.1). The exchange of $[\text{UO}_2(\text{van})]^+$ by $[\text{UO}_2(\text{van})(\text{OH})]^+$ or

[UO₂(van)(OH)₂]⁻ did not result in a more improved approximation. These species are therefore not as predominant as [UO₂(van)₂(OH)₂]²⁻.

Acknowledgments

This study was supported by the Sächsisches Ministerium für Wissenschaft und Kunst under contract no. 4.7541.88-FZR/402.

References

- /1/ Irving, H., Rossotti, H.S.: J. Chem. Soc. **1953**, 3397
- /2/ Sayce, I.G.: Talanta **15**, 1397 (1968)
- /3/ Baes, Jr., C.F., Mesmer, R.E.: *The Hydrolysis of Cations*, Krieger Publ. Comp., Malabar, Florida, 1986, pp. 176
- /4/ Jejurkar, C.R., Mavani, I.P., Bhattacharya, P.K.: Indian J. Chem. **10**, 1190 (1972)

INTERACTION OF U(VI) WITH WOOD DEGRADATION PRODUCTS A POTENTIOMETRIC STUDY

M. Schmidt, L. Baraniak, G. Bernhard, H. Nitsche
Forschungszentrum Rossendorf e.V., Institute of Radiochemistry

Carboxylic and phenolic hydroxyl groups of wood degradation products and their complex formation with U(VI) were determined by potentiometric titration. Considering U(VI)-hydrolysis, the formation constants were computed using the multi-equilibrium program SCOGS2.

During the process of mine flooding, wood can be hydrothermally degraded and its products may have an influence on contaminant migration. The degradation process was simulated in laboratory experiments using mine wood and distilled water under nitrogen at 90 bar and 70°C (W/N-p,T) /1/. Direct titration of the solution was carried out to determine the carboxyl- and phenolic hydroxyl content. They were found to be 2.9 meq/g TOC and 5.7 meq/g TOC, respectively. The dissociation constants (pK_{diss}) are 4.4 for the carboxylic and 9.3 for the phenolic hydroxyl groups (20°C, I = 0.1 M NaClO₄).

For the evaluation of formation constants, the solutions were treated as mixtures of two ligands. Different ratios of total ligand:U(VI) were titrated with carbonate-free NaOH under nitrogen. The

	total ligand:U(VI) = 8.2:1	total ligand:U(VI) = 16.4:1
UO ₂ A(OH)	-0.6 ± 0.4	-0.6 ± 0.4
UO ₂ B(OH) ₂	-4.3 ± 0.3	not detected
UO ₂ B(OH) ₃	-14.6 ± 0.4	(-12.6 ± 0.4)
UO ₂ B(OH) ₄	-24.9 ± 0.3	(-20.2 ± 0.6)

Tab. 1: Formation constants (log \$) of a wood degradation sample (W/N-p,T) with U(VI) at 20°C and 0.1 M NaClO₄ (A = carboxylic groups, B = phenolic hydroxyl groups)

formation constants considering hydrolysis of the U(VI) were determined using the program SCOGS2 /2/ (Tab. 1), \$ being defined as the cumulative formation constant:

$$\$ = \frac{[UO_2^{2+} Ligand_n (OH)^n]}{[UO_2^{2+}][Ligand]^n [OH]^{-n}}$$

(n = negative integer).

For a total ligand to U(VI) ratio of 16.4:1, no distinction between the complexes UO₂B(OH)₃ and UO₂B(OH)₄ (A = carboxylic groups, B = phenolic hydroxyl groups) was possible. Both can occur, but not at the same time. Neither the non-hydrolyzed complexes (UO₂A, UO₂B) nor complexes with two ligands (UO₂A₂(OH)_n, UO₂B₂(OH)_n, UO₂AB(OH)_n, (n=0,1,2) were necessary to fit the potentiometric data.

	total ligand:U(VI) = 2.3:1	total ligand:U(VI) = 4.1:1
UO ₂ A	11.5 ± 1.5	11.3 ± 1.5
UO ₂ A(OH)	4.6 ± 1.0	not probable
UO ₂ A ₂	not detected	(16.7 ± 1.4)*
UO ₂ B(OH)	4.9 ± 0.2	5.5 ± 0.4
UO ₂ B ₂ (OH)	(8.5)*	8.0 ± 6.7

* Complexes may be formed

Tab. 2: Formation constants (log \$) of a wood degradation sample (W/L-NB) with U(VI) at 20°C and 0.1 M NaClO₄ (A = carboxylic groups, B = phenolic hydroxyl groups)

A different extract obtained from the same mine wood (distilled water, 95°C, 1 bar, air (W/L-NB)) contained more carboxylic groups (7.8 meq/g TOC, pK_{diss} = 4.4) and phenolic hydroxyl groups (6.3 meq/g TOC, pK_{diss} = 8.5). Due to the presence of oxygen in the solution during the degradation process more functional groups were formed which are slightly more acidic than the functional groups of the degradation

products obtained under nitrogen. The stability constants with U(VI) show that stronger complexes were formed (Tab. 2).

In contrast to the other sample (W/N-p,T) non-hydrolyzed complexes and complexes containing two ligands were determined.

Conclusions

Mine wood degrades under hydrothermal conditions and functional groups are being formed. The higher the oxygen content in solution, the more acidic these groups are forming stabeler complexes with U(VI).

Acknowledgments

This work was supported by the Sächsisches Ministerium für Wissenschaft und Kunst under contract No. 4-7541.83-FZR/402.

References

- /1/ Jelen, K., Schiene, R., Fischer, K., Baraniak, L., Nitsche, H.: Investigation on the Hydrothermal Degradation of Wood in Flooded Mines. In: Report FZR-123, Institute of Radiochemistry, Annual Report 1995, p. 69, 1996.
- /2/ Perrin, D. D., Stunzi, H.: SCOGS2 A Nonlinear Least Squares Program for the Evaluation of Formation Constants of Metal Complexes. In: *Computational Methods for the Determination of Formation Constants* (D.J. Leggett, ed.) p. 71. Plenum Press, New York, 1985.

INTERACTION OF HEXAVALENT URANIUM WITH GLUCONIC ACID AND GLUCURONIC ACID

L. Baraniak, M. Schmidt, G. Bernhard, H. Nitsche
Forschungszentrum Rossendorf e.V., Institute of Radiochemistry

The interaction of U(VI) with gluconic acid and glucuronic acid was studied at I = 0.1 M by potentiometric pH titration. First results for stability constants, measured under the given conditions, were calculated by means of the multi-equilibria program SCOGS(version2), taking hydrolysis into account.

A great variety of cellulose degradation compounds with its different functional groups contributes to the complexation of heavy metals in natural waters. With regard to the remediation of mining sites the interaction of U(VI) with gluconic acid and glucuronic acid was studied by pH potentiometry.

Experimental methods, evaluation and results

The determinations were carried out by titrating solutions of uranyl perchlorate (5×10^{-5} - 5×10^{-4} M) and complexant (1×10^{-3} M) with strong base at constant ionic strength ($I = 0.1$ M, NaClO_4) and temperature (25°C) as described in the previous article. The evaluation was done by the "SCOGS" multi-equilibria program /1/ after the determination of the complexant's dissociation constant.

Gluconic acid: Assuming the interaction as a stepwise formation of mono-nuclear complexes, i.e. $[\text{UO}_2(\text{uco})_x]^{2-x}$ with $x \leq 3$, the SCOGS curve fitting leads to a set of constants ($\log \beta_{1,x} = 3.90/8.70/13.7$ for $x = 1-3$) with a curve approximation of $F_{\text{fit}} = 7.6 \times 10^{-2}$. If we consider partially hydrolyzed species the fit could be improved to $F_{\text{fit}} = 1.5 \times 10^{-2}$ with the result: $\log \beta_{1,2} = -1.43 \pm 0.95$ for $[\text{UO}_2(\text{uco})(\text{OH})_2]^-$ and $\log \beta_{1,3} = -9.76 \pm 3.8$ for $[\text{UO}_2(\text{uco})(\text{OH})_3]^{2-}$ (Tab. 1). Additional introduction of other hydrolyzed species resulted in a loss of fit accuracy.

complexant [A]	$\text{pK}_{\text{diss.}}$	$\log \beta_{1,1} [\text{UO}_2\text{AOH}]$	$\log \beta_{1,2} [\text{UO}_2\text{A}(\text{OH})_2]^-$	$\log \beta_{1,3} [\text{UO}_2\text{A}(\text{OH})_3]^{2-}$
¹⁾ H(uco)	3.78 ± 0.028	-	-1.43 ± 0.95	-9.76 ± 3.8
²⁾ H(uro)	3.57 ± 0.021	-1.41 ± 0.40	-5.63 ± 0.21	-

Tab. 1: Stability of U(VI) complexes with gluconic acid¹ and glucuronic acid² computed by non-linear pH curve fitting considering hydrolysis

Glucuronic acid: In this case we found a similar behavior. The interaction constants of the complexes $[\text{UO}_2(\text{uro})_x]^{2-x}$ with $x \leq 3$ changed evidently with the uranium-complexant ratio. Considering hydrolysis, we found the best fit assuming the species $[\text{UO}_2(\text{uro})(\text{OH})_2]^-$ with $\log \beta_{1,2} = -5.61 \pm 0.15$ (Tab. 1). The additional introduction of the neutral complex $[\text{UO}_2(\text{uro})(\text{OH})]$ led to $\log \beta_{1,1} = -1.43 \pm 0.4$ and $\log \beta_{1,2} = -5.64 \pm 0.17$ without any changes in the fit. Other

species e.g. $[(\text{UO}_2)_2(\text{uro})(\text{OH})_2]^+$ and $[(\text{UO}_2)_2(\text{uro})_2(\text{OH})_3]^-$ do not exist in such solutions and the occurrence of $[\text{UO}_2(\text{uro})_2]$ and $[\text{UO}_2(\text{uro})_2\text{OH}]^-$ has less probability.

Conclusions

The interaction of U(VI) with gluconic acid and glucuronic acid do not lead to a series of pure complexes. Our pH curve fittings pointed out that mono-nuclear complexes with one organic ligand and two or three hydroxyl groups in the first coordination sphere are formed. Escandar et al. /2/ describe a similar situation for the formation of gluconato complexes of Cd(II), Hg(II) and Pb(II) (Tab. 2). They concluded that the complexation occurs mainly via carboxylic groups and that neighboring hydroxyl groups are involved in the coordination.

The introduced species for the best fitting of the pH titration curve are assumed and their existence should be verified by independent methods such as, for example, infrared (FTIR) and laser-fluorescence spectroscopy (TRLFS) as well as X-ray absorption spectroscopy (EXAFS).

metal ion $[\text{M}^{2+}]$	$\log \beta_{11} [\text{MA}]^+$	$\log \beta_{11-1} [\text{MA}(\text{OH})]$	$\log \beta_{11-2} [\text{MA}(\text{OH})_2]^+$	$\log \beta_{22-3} [\text{M}_2\text{A}_2(\text{OH})_3]^-$
Cd^{2+}	2.3	-	-15.7	-
Hg^{2+}	-	-0.09	-4.03	-
Pb^{2+}	2.49	-	-11.8	-10.7

Tab. 2: Gluconato complex stabilities of Cd(II), Hg(II) and Pb(II) according to Escandar et al. /2/

Acknowledgments

This study was supported by the Sächsisches Ministerium für Wissenschaft und Kunst under contract no. 4.7541.88-FZR/402.

References

- /1/ Sayce, I.G.: Talanta **15**, 1397 (1968)
 /2/ Escandar, G.M., Salas Peregrin, J.M., Gonzalez Sierra, M., Martino, D., Santoro, M., Frutos, A.A., Garcia, S.I., Labadie, G., Sala, L.F.: Polyhedron **15**, 2251 (1996)

DETERMINATION OF LIGNIN-REDUCING CAPACITY BY ALKALINE FERRICYANIDE TITRATION

B. Mack, L. Baraniak, G. Bernhard, H. Nitsche
 Forschungszentrum Rossendorf e.V., Institute of Radiochemistry

The reducing capacity of methanol-leached spruce lignin was determined by ferricyanide titration to be 11.5 ± 0.3 meq/g. The reduction is a first order process with a rate constant of $1.24 \cdot 10^{-6} \text{ s}^{-1}$.

Experimental method and results

The reducing capacity of natural organic soil and water-borne material such as humic acid, fulvic acid or lignin have been known for a long time /3, 4/. The redox activity of humic substances is attributed to phenolic structures. Only few investigations, however, focussed on the fundamental redox properties of these systems. Attempts were made to determine the standard potential of humic acid from single point measurements /1/. The redox capacity can be found by potentiometric titrations /2-4/.

Object of our investigations was a methanol-leached spruce lignin which was precipitated from the organic solution by addition of carbon dioxide. The reducing capacity of lignin was determined at pH 9.3 in a boric acid buffer. The oxidation of phenols in alkaline media occurs under formation of phenoxide ions. Literature data show that the phenoxide ion rather than the undissociated phenol is releasing the electrons /2/. The dissociation constant ($\text{pK}_{a,1}$) of many polyphenols is about 9. Potassium ferricyanide is commonly used as oxidizing agent for the studies of natural phenols /2/.

Only few data exist in the literature on the reaction rate of natural systems with potassium ferricyanide. The reaction time to reach equilibrium for humic acid is between 4 and 12 hours /2, 3/. The oxidation of lignin under these conditions takes about 10 days /4/. A reducing capacity of 1.7 meq/g was found for peat humic acid /2/.

Lignin solutions containing 0.5 mg were mixed with increasing amounts of potassium ferricyanide. The samples were gently shaken and the potentials were measured at different times. All measurements were done under nitrogen with a platinum ring electrode against a silver / silver chloride 3 M KCl reference cell (EMC 30, Meinsberg).

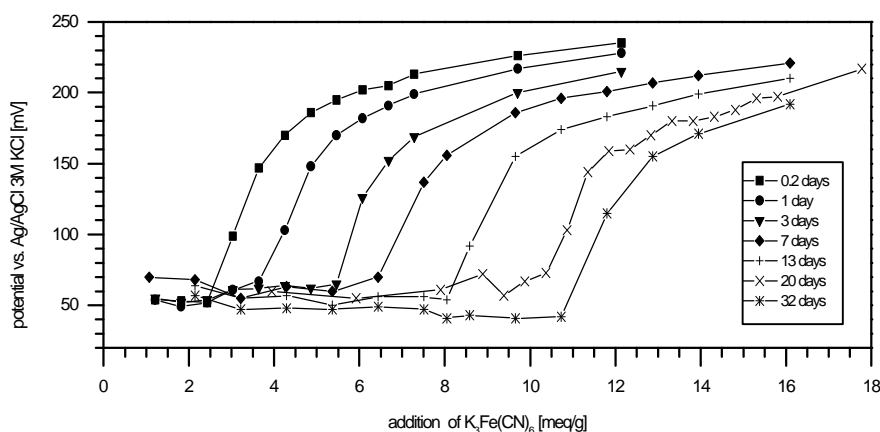


Fig. 1: Potentiometric titration curves for lignin at different times (pH 9.3, boric acid, room temperature).

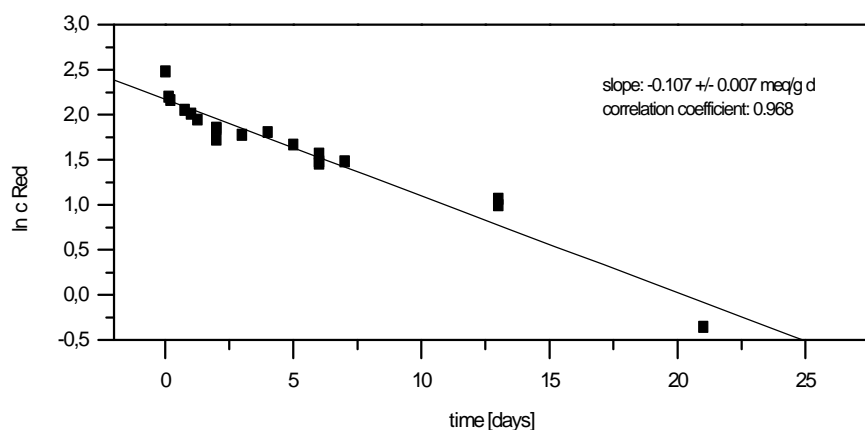


Fig. 2: Decrease of reducing groups in lignin as a function of time (initial concentration $[\text{Red}_0] = 11.5 \text{ meq/g}$).

The time dependency of the redox potential is shown in Fig. 1. After 21 days, more than 99.5% of the reactive groups were oxidized. The reducing capacity was determined to $11.5 \pm 0.3 \text{ meq/g}$ from two measurements series (series 1, 11.8 meq/g and series 2, 11.2 meq/g).

The reaction rate was estimated. The lignin oxidation by ferricyanide is a first order process (Fig. 2) with a reaction rate constant of $(1.24 \pm 0.08) \cdot 10^{-6} \text{ s}^{-1}$.

Lignin shows a much higher reducing capacity than humic acid under the same conditions. This means lignin is able to reduce higher substance amounts than humic acid in environmental processes.

Acknowledgments

We thank N. Zier and R. Schiene, Technische Universität Dresden, Institute of Plant and Wood Chemistry, Tharandt, for supplying the lignin samples.

This study was supported by the Sächsisches Ministerium für Wissenschaft und Kunst under contract no. 4.7541.88-FZR/512

References

- /1/ Szilagyi, M.: Soil Sci. **115**, 434 (1973)
- /2/ Matthiessen, A.: In: *Humic substances in the global environment and implications on human health*, Senesi, N., Miano, T.M. (eds.), (1994)
- /3/ Helburn, R.S., MacCarthy, P.: Anal. Chim. Acta **295**, 263 (1994)
- /4/ Moskotov, N.G.: Chim. Drev. **4**, 67 (1977)

ANALYSIS OF CARBOHYDRATES DISSOLVED FROM PITWOOD UNDER MINE FLOODING CONDITIONS

K. Jelen¹, R. Schiene¹, H. Koch¹, K. Fischer¹, L. Baraniak, H. Nitsche
Forschungszentrum Rossendorf e.V., Institute of Radiochemistry

¹ Technische Universität Dresden, Institute of Plant and Wood Chemistry, Tharandt

Carbohydrates were analyzed stemming from hydrothermal treatment of pitwood under acidic and neutral conditions. The composition of the hydrothermal extracts was studied as a function of time.

In the process of uranium mine flooding in Saxony and Thuringia, Germany, hemicelluloses of the pitwood may become structurally changed and degraded /1, 2/. The conditions prevalent in the mine have been simulated in our experiments on a wood sample obtained from the remediation company Wismut GmbH. They are summarized in Tab. 1.

samples	hydrothermal condition			
	temperature (EC)	pressure (bar)	time	notes/model
W/N-p,T	70	90	67 days	de-ionized water stationary system
W/L-NBS	100	normal pressure	5 h	mine water Königstein (pH 2)
W/L-TS	40	normal pressure	1 year	mine water Königstein (pH 2)
W/L-NB-f-h	100	normal pressure	total: 72 h	de-ionized water fresh water supply
W/L-NBS-f-h	100	normal pressure	total: 72 h	mine water Königstein (pH 2)
W/L-NB-s-h	100	normal pressure	up to 72 h	de-ionized water stationary system

Tab. 1: Hydrothermal mine-wood extraction conditions

hydro-thermal extract	total content monosaccharide [mass % of wood]	monosaccharide content [% total monosaccharide content]			
		arabinose	galactose	glucose	xylose/ mannose
W/N-p,T	1.21 ± 0.12	76.8	12.3 ± 1.1	-	10.9 ± 1.0
W/L-NBS	0.19 ± 0.02	84.1	6.29 ± 0.6	5.33 ± 0.5	4.27 ± 0.4
W/L-TS	1.09 ± 0.11	80.7	6.90 ± 0.7	3.58 ± 0.3	8.84 ± 0.8

Tab. 2: Results of monosaccharide analysis of the hydrothermal extracts

sugars are xylose and mannose. The main component of monomeric sugars is arabinose (Tab. 2). This means that (1) the largest proportion of xylose and mannose is not hydrolysed and therefore available in the extract as oligosaccharides, and (2) arabinose is preferentially subject to hydrolytic cleavage because of its side-chain position in the above-specified hemicellulose. If the wood is treated for one year with acidic water from the Königstein mine (W/L-TS), one percent of monosaccharides were isolated relative to the total wood mass. Due to the short extraction time of only five hours, the monosaccharide content of the sample W/L-NBS is low when it is compared with the amount obtained from long-term treatment in acidic medium and in deionized water under pressure.

The time dependency of the wood degradation shows (1) that 1-2% of the wood is decomposed to monosaccharides and (2) after an extraction time of about 30 h, the total monosaccharide content in the stationary system is higher than in the systems with fresh water supply (Fig. 1).

The monosaccharide concentration increases more as a function of leaching time in the stationary than in the freshwater system. The higher concentration in the stationary system may be due to the additional penetration of the inner wood sphere by the remaining leachate. Moreover, it could be shown that for the experiments with acidic mine water influx only a minor change of the total monosaccharide content occurs in comparison with the system with deionized water (W/L-NB-f-h).

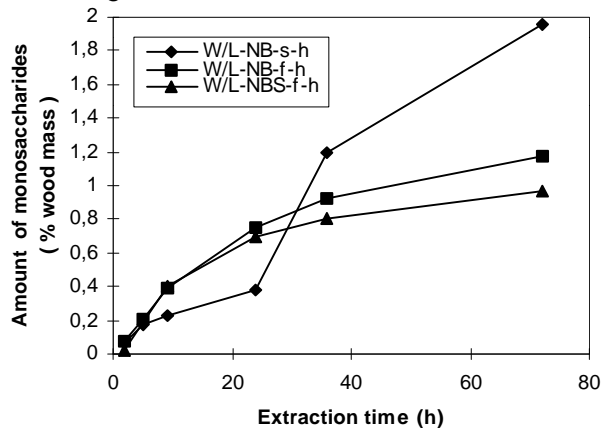


Fig. 1: Monosaccharide content in dependence on the time

Acknowledgment

This work was supported by the Sächsische Ministerium für Wissenschaft und Kunst under contract No. 4-7541.83-FZR/402.

References

- /1/ Fengel, D., Wegener, G.: *Wood-Chemistry, Ultrastructure, Reactions*, De Gruyter, Berlin, 1984
- /2/ Thompson, N.S., Heller, H.H., Hankey, J.D., Smith, O.: *Pulp paper Mag. Can.* **67**, 541 (1966)

EXPERIMENTS FOR THE DISPOSAL OF CARBON-14 LABELED ORGANIC MATERIAL: 1. MINERALIZATION OF ORGANIC MODEL COMPOUNDS BY AMMONIUM PEROXYDISULFATE

E. Förster, H. Petzold¹, M. Rösseler¹, K. Wolf, K.H. Heise, H. Nitsche
 Forschungszentrum Rossendorf e.V., Institute of Radiochemistry
¹Universität Leipzig, Kontrollbereich Permoserstraße

Spent carbon-14 labeled organic compounds and their inactive surrogates were, with few exceptions, completely mineralized by wet oxidation at 90 - 100°C using acidified ammonium peroxydisulfate. The activity of the evolved ¹⁴CO₂ was determined by a novel gas cuvette combined with a commercially available proportional counter tube.

Peroxydisulfate (S₂O₈²⁻) is one of the strongest oxidants (standard electrode potential in acid solution E° = + 2.13 V /1/). Acidified solutions of ammonium peroxydisulfate are stable at room temperature but become a rapid oxidant at elevated temperatures (80 - 100°C) which stimulate the generation of the free sulfate radical SO₄^{•-} (E° ~ + 2.6 V). This radical initiates, in the presence of organics, a chain reaction including the production of OH[•] and organic free radicals /2/.



The resulting product is harmless ammonium sulfate. Because of its properties, peroxydisulfate found a widespread use to convert the organic materials to water, carbon dioxide and inorganic materials (e.g., /2/). We have employed this process for wet combustion of our organic model substances.

Experimental

A 250 ml three-necked reaction flask was equipped with a magnetic stirrer bar, a reflux condenser and a 100 mL dropping funnel with a pressure equalizing tube. The condenser was connected to a cupric oxide filled quartz tube (catalyst) followed by a safety bottle and two gas traps. The catalyst in the quartz tube was heated at about 650°C. A 50 mL solution or dispersion of an organic compound (equating on equivalent of 4 millimole carbon) in 0.05 M sulfuric acid was placed in a reaction flask and subsequently heated and stirred for 4 hours at a temperature of 95 - 100°C. Twenty five mL of a 1.9 M solution of ammonium peroxydisulfate was slowly added (4 - 5 drops/min.). Evolving CO₂ and other volatile products were swept away by a N₂ gas stream and passed to the catalyst and the gas traps. Carbon dioxide was absorbed in 0.1 M sodium hydroxide and was determined by titration (only the inactive CO₂). The nitrogen gas stream (about 17 mL/min.) was circulated with a peristaltic pump. Chlorine, formed by the oxidation of any chlorides in the sample, is removed from the gas stream by a U-tube which

substance name	% CO ₂ yield	
	without catal. oxidation	with catal. oxidation
Acetophenone	92	98
Succinic acid	96	100
1,2-Dibromoethane	13	24
4-Hydroxybenzoic acid	-	97
2-Nitrophenol	47	84
Palmitic acid (C ₁₆)	2	-
Nonanoic acid	93	-
Phenol	83	87
Thiourea	95	98
Trapidil ®*	86	97
2-Xylene	25	39

* pharmaceutical agent

Tab. 1: Mineralization of some inactive organic substances with ammonium peroxydisulfate

contained crystalline stannous chloride. Additional experiments were conducted with the radioactive acetic acid [2-¹⁴C] sodium salt, and 4-hydroxy-benzoic acid [ring UL-¹⁴C] at low activity levels (max. 10 µCi). The radioactivity of ¹⁴CO₂ was measured by a gas flow cuvette connected with a commercially available proportional counter tube (type LB 6280). It was positioned between the catalytic oxidation tube and the safety bottle.

Results and Discussion

Tab. 1 shows the recovery of CO₂ from the mineralization of selected organics with ammonium peroxydisulfate with or without the additional thermal catalytic oxidation.

Some substances were incompletely

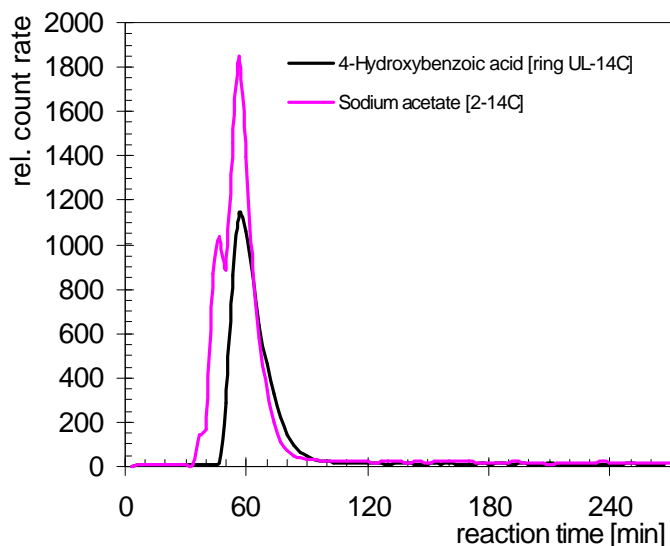


Fig. 1: Kinetics of mineralization by ammonium peroxydisulfate of labeled sodium acetate and 4-hydroxybenzoic acid.

References

- /1/ Lids, D.R., Frederikse, H.P.R. (eds.): *CRC Handbook of Chemistry and Physics*, 75th Ed., CRC Press, Boca Raton, 1994-1995, p. 8-28, 8-29
- /2/ Cooper, J.F., Wang, F., King, K., Shell, T., Farmer, J.C., Adamson, M.: Demonstration of Omnivorous Non-Thermal Mixed Waste Treatment: Direct Chemical Oxidation using Peroxydisulfate. In: Report UCRL-ID-123193 (Progr. Rep. SF2-3-MW-35 Oct. - Dec. 1995), Lawrence Livermore National Laboratory

mineralized into carbon dioxide because of their insolubility in the aqueous phase and their low chemical reactivity.

Fig. 1 presents the kinetics of the mineralization for two C-14 labeled model substances by measuring the β -radiation of the produced $^{14}\text{CO}_2$. The degradation into C-14 carbon dioxide after a short incubation period was vigorous. Complete mineralization was achieved after about 120 min. The residual solutions contained a little radioactivity ($< 0.02 \mu\text{Ci}$).

Acknowledgment

This study was supported by Sächsisches Ministerium für Wissenschaft und Kunst under contract No. 4-7581.312/20.

EXPERIMENTS FOR THE DISPOSAL OF CARBON-14 LABELED ORGANIC MATERIAL: 2. MINERALIZATION OF ORGANIC MODEL SUBSTANCES USING HYDROGEN PEROXIDE AND A MIXTURE OF TRANSITION METAL SALTS

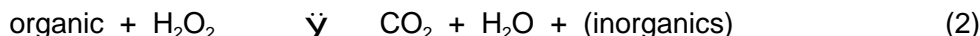
E. Förster, H. Petzold¹, M. Rösseler¹, K.H. Heise, H. Nitsche
 Forschungszentrum Rossendorf e.V., Institute of Radiochemistry
¹Universität Leipzig, Kontrollbereich Permoserstraße

The oxidation of non-labeled organic model compounds by hydrogen peroxide and a catalytic mixture of transition metal salts was investigated to obtain a method for the conversion of radioactive ^{14}C organic compounds. The recovery (as % CO_2) was general $> 80\%$, with the exceptions of chloroacetic acid, palmitic acid, 1,2-Dibromo-ethane and 2-xylene.

Hydrogen peroxide is a cheap and relatively strong oxidant ($E^\circ = +1,78 \text{ V}$). However it reacts quite slowly with the most organic substrates. It may be required to activate the peroxide with UV irradiation or with transition metal ions at elevated temperature. Activation improves the reactivity toward a substrate through the formation of stronger oxidizing species such as hydroxyl (OH^*) or hydroperoxyl (HO_2^*) free radicals. The Fenton-reaction e.g., uses Fe-II salts in acidic conditions to produce OH^* free radicals. The decomposition of H_2O_2 is catalyzed by transition metal ions and predominates in the absence of organics in the reaction mixture:



If organics are present in the reaction mixture the following reaction occurs together with reaction (1):



The Fenton-oxidation involves the formation of various refractory byproducts like acetic and oxalic acids and their homologs /1/.

Recently, Falcon and coworkers /2/ used a mixture of Fe(II), Cu(II) and Mn(II) salts to achieve

almost complete oxidation due to a possible synergistic effect. They also determined the optimal proportions of the catalytic mixture Fe:Cu:Mn. The H₂O₂ decomposition (1) can be suppressed by slowly adding the hydrogen peroxide to the reaction mixture. We used the method of Falcon and coworkers to convert organic model compounds.

Experimental

In a 100-mL three-necked flask, equipped with a magnetic stirrer bar, a 10-mL dropping funnel with pressure equalizing tube, a gas inlet tube and a reflux condenser was placed a solution containing 28 mg of iron(II) sulfate heptahydrate, 25 mg of copper(II) sulfate pentahydrate, 22 mg manganese(II) sulfate tetrahydrate and the organic compound of interest (the amount is calculated for 4 mmol of carbon) in 50 mL of water. The pH was adjusted to 3.0 using 0.05 M sulfuric acid. 5.0 mL of 35% hydrogen peroxide was placed in the dropping funnel. A quartz combustion tube connected with two gas absorption traps containing 0.2 M NaOH was attached to the upper end of the condenser. The quartz tube was filled with a wire CuO catalyst and was heated to 650°C. Then the reaction mixture was stirred at 95 - 100° C and the hydrogen peroxide was added dropwise from the dropping funnel over a period of about 2 hours (1 - 2 drops per min). A N₂ stream (17 mL/min) was continuously circulated through the apparatus by a peristaltic pump. The CO₂ evolved in this process was transported by the gas stream and absorbed in 0.2 M NaOH. The absorbed CO₂ was determined with a titrimetric method described by Winkler /3/, which we have slightly modified.

Results and Discussion

The procedure described here illustrates a practical and convenient method especially for the mineralization of water soluble organic substances. The results are shown in Tab. 1.

The oxidation leads to low recovery rates if hydrophobic (e.g., palmitic acid) or volatile substances (e.g., 1,2-dibromoethane or 2-xylene) are used. While the reaction proceeds, the pH value of the solution may change to basic values. In this case, the catalysts may precipitate as hydroxides.

Tab. 1: Wet mineralization of some organic substances using hydrogen peroxide and the catalytic mixture of Fe-II, Mn-II and Cu-II salts

substance name	% CO ₂ recovery	substance name	% CO ₂ recovery
Aniline	94.9	Methyl alcohol	95.5
Succinic acid	95.6	2-Toluic acid	95.0
1-Butanol	90.5	2-Nitrophenol	87.8
Chloroacetic acid	73.9	Palmitic acid (C ₁₆)	3.8
1,2-Dibromoethane	38.5	Phenol	81.2
Acetic acid, Na-salt	98.0	Trapidil ®*	86.7
Ethyl acetate	97.9	Triethylamine	100.1
4-Hydroxybenzoic acid	96.3	2-Xylene	53.6

* pharmaceutical agent (subst. Triazolo pyrimidine)

Acknowledgment

This study was supported by Sächsisches Ministerium für Wissenschaft und Kunst under contract No. 4-7581.312/20

References

- /1/ Srinivas, C., Ramaswamy, M., Theyyuni, T.K.: *Wet Oxidation of Spent Ion-Exchange Resins Using Hydrogen Peroxide*. Report BARC/1994/E/041, Bhabha Atomic Research Centre Bombay, India 1994
- /2/ Falcon, M., Fajerweg, K., Foussard, J.N., Puech-Costes, E., Maurette, M.T., Debellefontaine, H.: *Wet Oxidation of Carboxylic Acids with Hydrogen Peroxide*. *Environ. Technol.* **16**, 501 - 513 (1995)
- /3/ Jander, G., Jahr, K.F.: *Maßanalyse*, 15th ed., de Gruyter, Berlin, New York 1989, p. 144

Application of X-Ray Absorption Spectroscopy

ARSENITE AND ARSENATE CONCENTRATION RATIOS IN AQUEOUS MIXTURES BY XANES

M.A. Denecke, T. Reich, H. Friedrich, G. Bernhard, T. Knieß¹, D. Rettig, T. Zorn, H. Nitsche
 Forschungszentrum Rossendorf e.V., Institute of Radiochemistry
¹ Institute of Bioinorganic und Radiopharmaceutical Chemistry

Relative concentrations of As(III) and As(V) present in mixtures can be determined by a least squares fit of their XANES spectrum with a linear combination of the pure component spectra.

An edge-shift greater than 3 eV is observed in As K-edge x-ray near edge structure, XANES, spectra of As(III) and As(V) compounds. This shift is great enough to allow a qualitative determination of the arsenic oxidation state in samples with unknown arsenic speciation /1/. The XANES of As(III) and As(V) compounds also exhibit pronounced white lines, WL, formally corresponding to a dipole-allowed 1s64p transition. The prominence of these XANES features makes them useful for a quantitative determination of relative concentrations of As(III) and As(V) present in mixtures. The mixture's XANES spectrum can be modeled as the sum of XANES spectra of the individual, pure components.

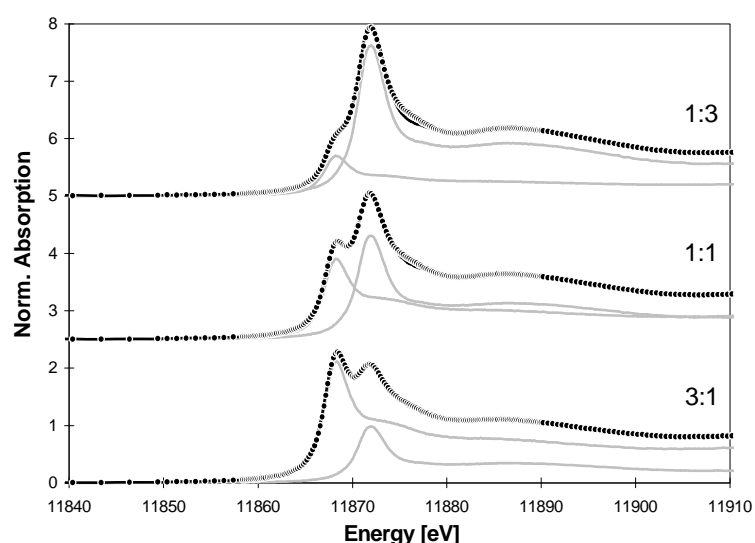


Fig. 1: Experimental XANES of solution samples containing As(III) : As(V) concentration ratios indicated (dotted curve), the fit (solid curve), and the individual arsenite and arsenate components (grey curves).

As(III) and As(V) concentrations in the 1:3, 1:1, and 3:1 $\text{AsO}_3^{3-} : \text{AsO}_4^{3-}$ mixtures were determined by a least squares fit of their XANES with a linear combination of the pure component AsO_3^{3-} and AsO_4^{3-} spectra. A similar XANES fit procedure for the determination of the amount of Se(IV) and Se(VI) in samples containing selenium has been reported /3/.

SAMPLE PREPARATION*		EXPERIMENT					
		XANES				Polarography	
		Absorption		1st derivative			
As(III)	As(V)	As(III)	As(V)	As(III)	As(V)	As(III)	As(V)**
75	25	71.0	28.5	70.7	26.4	66	34
50	50	47.0	52.8	48.1	52.8	45	55
25	75	23.8	74.6	22.2	72.2	21	79

* Calculated from stoichiometry and weights of As_2O_3 and $\text{H}_3\text{AsO}_4 \cdot 0.5\text{H}_2\text{O}$ used for the preparation of the stock solutions.

** Calculated from the polarographic results for As(III) and the total arsenic concentration of the sample.

Tab. 1: Relative concentrations of As(III) and As(V), expressed in percent, for solution mixtures obtained from fits of their XANES (± 0.003) and first derivative spectra (± 0.006), compared to results from polarographic measurements.

0.019 M aqueous solutions of arsenite (AsO_3^{3-}), arsenate (AsO_4^{3-}), and mixtures of the two having concentration ratios of 1:3, 1:1 and 3:1, were prepared from AsO_3^{3-} and AsO_4^{3-} stock solutions. Transmission As K-edge XANES spectra of these samples were recorded at the Hamburger Synchrotronstrahlungslabor, HASYLAB, beamline X1.1, using a Si(311) double-crystal monochromator detuned to about 50% of the maximum incident flux. All samples were measured in 1.3 cm diameter polyethylene cuvettes of 4 mL volume. The arsenic concentration in the samples yielded an edge-jump of less than 0.3, thereby avoiding thickness effects in the region of the spectrum's WL /2/. The relative $\text{AsO}_3^{3-} : \text{AsO}_4^{3-}$ mixtures were determined by a least squares fit of their XANES with a linear combination of the pure component AsO_3^{3-} and AsO_4^{3-} spectra. A similar XANES fit procedure for the determination of the amount of Se(IV) and Se(VI) in samples containing selenium has been reported /3/. The XANES spectra of the mixtures, the fitted spectra and the individual AsO_3^{3-} and AsO_4^{3-} components are depicted in Fig. 1. The WL maxima of the AsO_3^{3-} and AsO_4^{3-} spectra are at 11868.3 and 11872.2 eV, respectively. These remain distinguishable in the XANES spectra of the mixtures. Fits to both absorption and first derivative spectra (not shown here) gave excellent agreement between experiment and fit. The fits, depicted as solid lines, can hardly be differentiated from the experimental spectrum, depicted as dots. Varying the energy

range for the fit did not significantly alter the goodness of the fit nor did it influence the results obtained for the As(III) : As(V) ratio.

Tab. 1 summarizes the relative concentrations of As(III) and As(V) obtained from the fits and compares them to those obtained from polarographic As(III) determination. The fits to the absorption data yielded results similar to fits to first derivative spectra. The results from the XANES curve fitting are in better agreement with the values expected, according to the sample preparation, than those from the polarographic determination. The XANES fits lead to a quantitative determination of the relative As(III) concentration to within 6%. This is better than the 10% error estimated for determinations using polarography.

The success of this method for the determination of relative concentrations of As(III) and As(V) in mixtures renders studies on other environmentally relevant samples feasible. A significant advantage of XANES analysis is that samples can be studied without prior separation of the arsenic species from the matrix.

References

- /1/ Denecke, M.A., Moll, H., Pompe, S., Rettig, D., Friedrich, H., Bernhard, G., Reich, T., Nitsche, H.: Determination of the Arsenic Oxidation State in Environmentally Relevant Waters by XANES Spectroscopy. In: Report FZR-123, Institute of Radiochemistry, Annual Report 1995, p.90.
- /2/ Goulon, G., Goulon-Ginet, C., Cortes, R., Dubois, J.M.: On Experimental Attenuation Factors of the Amplitude of the EXAFS Oscillations in Absorption, Reflectivity and Luminescence Measurements. *J. Physique* **43**, 539 (1982).
- /3/ Pickering, I.J., Brown, G.E., Tokunaga, T.K.: Quantitative Speciation of Selenium in Soils Using X-Ray Absorption Spectroscopy. *Environ. Sci. Technol.* **29**, 2456 (1995).

DIFFERENTIATION BETWEEN MONODENTATE AND BIDENTATE CARBOXYLATE LIGANDS COORDINATED TO URANYL IONS USING EXAFS

M.A. Denecke, T. Reich, M. Bubner, S. Pompe, K.H. Heise, H. Nitsche, P.G. Allen¹, J.J. Bucher¹, N.M. Edelstein¹, D. K. Shuh¹

Forschungszentrum Rossendorf e.V., Institute of Radiochemistry

¹Lawrence Berkeley National Laboratory, Chemical Sciences Division

The possibility is explored of detecting the carbon atoms in bidentate and monodentate coordinated carboxylate ligands in uranyl complexes by EXAFS analysis, including multiple-scattering pathways. The EXAFS results are compared to XRD data reported in the literature.

We have investigated the U L_{III}-edge EXAFS of two carboxylato uranyl complexes of known structure: sodium triacetatodioxouranium(VI), Na[UO₂(C₂H₃O₂)₃] (**I**) /1/ and dibenzoatodioxouranium(VI), UO₂(C₇H₅O₂)₂ (**II**) /2/. This study was aimed at exploring the possibility of differentiating between bidentate (**bi**) and monodentate (**mono**) coordinated carboxylate ions. The UO₂²⁺ cation in **I** is surrounded by three carboxylate ligands, stemming from three acetate ions, coordinated exclusively in a **bi** fashion. The benzoate carboxylate group in **II** bridges two neighboring UO₂²⁺ units; each O atom exhibits **mono** coordination to uranium.

The fact that **bi**-coordinated carboxylate groups generally exhibit longer metal-oxygen bond distances than their **mono** counterparts /3/ can be used for interpreting EXAFS data from UO₂²⁺-complexes based on fits of the first two oxygen coordination shells (U-O_{ax} and U-O_{eq}). However, interpretation of data based solely on U-O_{eq} distances ($R_{U-O_{eq}}$) can be inconclusive; information from further-distant shells is often needed. Obtaining this information from the analysis of EXAFS data can be complicated by the presence of multiple scattering (MS) pathways along the O=U=O unit and along atoms in the coordinating carboxylate groups. For example, the near-collinear arrangement of carbon atoms in the **bi** configuration can cause amplitude enhancement of scattering on the distal carbon atom. Detecting a carbonyl carbon atom, C, in **mono** coordination may be difficult due to overlap of single scattering (SS) with MS oscillations.

In order to evaluate the possibility of detecting the carbon atoms in **bi** and **mono** complexes, the MS pathways were calculated using FEFF6 /4/ and used in the analysis of EXAFS data for compounds **I** and **II**. These results were compared to XRD data reported in the literature.

U L_{III}-edge EXAFS transmission spectra of **I** and **II** were measured at the Stanford Synchrotron

Radiation Laboratory, SSRL, (beamline 2.3) using a Si(220) double-crystal monochromator detuned to 50% of the maximum incident flux. The samples were dispersed in Teflon and pressed as 1.3 cm diameter pellets. The k^3 -weighted $U L_{III}$ EXAFS for **I** and **II** and their corresponding Fourier transforms (FT) are shown in Fig. 1. The FT for **II** exhibits no peaks distinctly above the background noise at distances greater than $R_{U-O_{ax}}$ and $R_{U-O_{eq}}$. $R_{U-O_{eq}}$ in **I** is significantly longer than in **II** and the FT shows more distant coordinations shells. Also noticeable is, although **I** has no atoms between 2.85 and 3.98 Å away from uranium, its FT spectrum exhibits intensity around $R_{(C')} \sim 3$ Å.

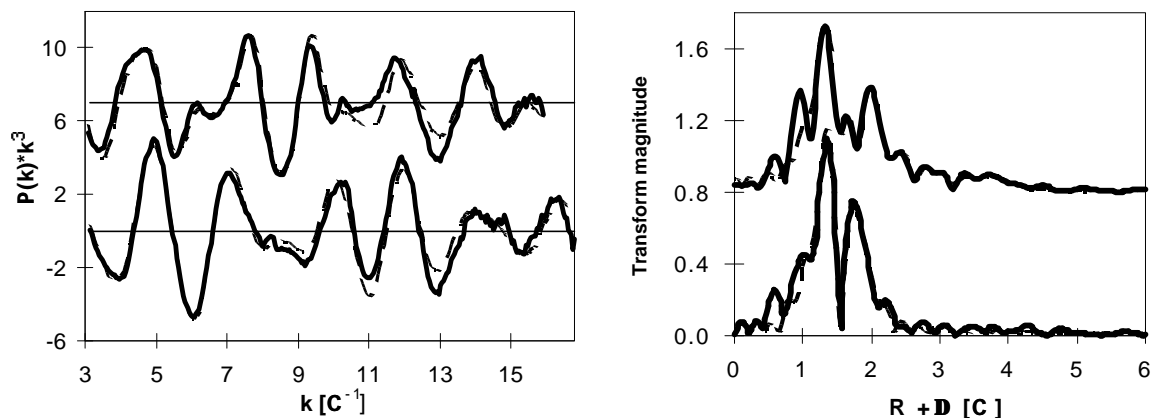


Fig. 1: k^3 -weighted $U L_{III}$ -edge EXAFS spectra and their corresponding Fourier transform for **I** (above) and **II** (below). The solid line is the experimental data; the dashed line is the result of the fit described in the text.

The dashed lines in Fig. 1 depict the results from fits of the spectra using SS and the following MS paths: **MS**, the four-legged MS path involving both axial oxygen atoms ($U \text{---} O_{ax1} \text{---} U \text{---} O_{ax2} \text{---} U$); **MS-C**, the three-legged path between $U-O_{eq}-C$ atoms; **MS-E/A**, MS pathways between $O_{ax}-U-O_{eq}$, and the MS path leading to the focussing effect along the linear $U-C-C'$ in the **bi** ligated compound **I**, **MS-C'**. The fit results for the interatomic distances to uranium (R) coordination numbers (N), and Debye-Waller factors (F^2) in both compounds are shown in Tab. 1 and compared to XRD results.

Shell	N	R [Å]	F^2 [Å ²]
I			
O_{ax}	2 [*] (2)	1.78 (1.76)	0.002
O_{eq}	4.3 (6)	2.49 (2.47)	0.005
C	2.5 (3)	2.89 (2.85)	0.002
Na	3 [*] (3)	3.98 (3.93)	0.016
C'	5 (3)	4.40 (4.35)	0.006
II			
O_{ax}	2 [*] (2)	1.76 (1.75)	0.002
O_{eq}	4.1 (4)	2.29 (2.28)	0.004
C	5.3 (4)	3.42 (3.46)	0.010

^{*}Held constant during fit.

Tab. 1: EXAFS structural parameters for **I** and **II** compared to XRD values /1/, /2/ (in parentheses).

obtain physically meaningful results. The peaks near 3 Å in the FT spectrum of **I** can only be accounted for by including **MS-E/A** and **MS** paths into the fit.

These results show that identifying **bi** carboxylate ligands coordinated to a uranyl unit based on their usually relatively long $R_{U-O_{eq}}$ bond lengths can be substantiated by detecting the carboxyl

F^2 for the MS paths was assumed to be the sum of F^2 from the SS paths for the atoms involved and the $O_{eq}-C$ bond distance was taken to be 1.26 Å. In this way the MS paths could be included in the fit without increasing the number of variable parameters by linking their parameters with the corresponding SS values. $N_{O_{ax}}$ was kept constant at 2 and N_{Na} was held constant at 3, the value obtained from an initial fit to filtered data. The edge shift (E_0) was held constant at the value obtained from a fit to the first two shell filtered data.

In the case of **II**, detecting atoms further distant than the first two bond distances is not possible; if the existence of the carboxyl C atom were not known, it would not have been included in the fit. The oscillations from the SS path of this C atom and the **MS-E/A**, **MS-C**, and **MS** paths in **II** tend to cancel each other out leaving only a weak signal. There is also no evidence for more distant atoms in the spectrum; these weak backscatterers are too far away to be observed. In contrast, although the $U-C'$ bond distance in **I** is 4.35 Å, this atom shows up with a rather large intensity due to the **MS-C'** path.

Moreover, the **MS-C'** path must be included in the fit to

C and distal C' atoms in the analysis of U L_{III}-edge EXAFS spectra. MS paths involving these atoms and the first two shells O_{ax} and O_{eq} must be included in the analysis. Only the O_{ax} and O_{eq} bond distances are evident in the EXAFS of the compound having **mono** bridging carboxylate ligands, **II**. Substantiating the mode of coordination by detecting further distant C atoms is not possible in this case.

Acknowledgments

Measurements were made at SSRL, which is operated by the U.S. Department of Energy, Office of Basic Energy Sciences, Divisions of Chemical Sciences and Materials Science.

References

- /1/ Templeton, D.H., Zalkin, A., Ruben, H., Templeton, L.K.: Redetermination and Absolute Configuration of Sodium Uranyl (VI) Triacetate. *Acta Cryst.* **C41**, 1439 (1985).
- /2/ Cousson, A., Proust, J., Pages, M., Robert, F., Rizkalla, E.N.: Structure of Dibenzoatodioxouranium (VI). *Acta Cryst.* **C46**, 2316 (1990).
- /3/ Carrell, C.J., Carrell, H.L., Erlebacher, J., Glusker, J.P.: Structural Aspects of Metal-Ion-Carboxylate Interactions. *J. Am. Chem. Soc.* **110**, 8651 (1988).
- /4/ Rehr, J.J., Zabinsky, S.I., Albers, R.C.: High-Order Multiple Scattering Calculations of X-Ray-Absorption Fine Structure. *Phys. Rev. Lett.* **69**, 3397 (1992).

STRUCTURAL ANALYSIS OF URANIUM(VI) COMPLEXES WITH SIMPLE CARBOXYLIC ACIDS IN AQUEOUS SOLUTION USING EXAFS

T. Reich, V. Brendler, M.A. Denecke, P.G. Allen¹, J.J. Bucher¹, N.M. Edelstein¹, D.K. Shuh¹, H. Nitsche

Forschungszentrum Rossendorf e.V., Institute of Radiochemistry

¹ Lawrence Berkeley National Laboratory, Berkeley, CA, USA

Structural analysis of eight aqueous uranyl carboxylates by EXAFS reveals three basic types of near-neighbor environments.

Aqueous solutions of uranyl acetate (**1**), phthalate (**2**), maleate (**3**), malonate (**4**), succinate (**5**), malate (**6**), citrate (**7**), and tartrate (**8**) were prepared by dissolving uranyl nitrate hexahydrate and the corresponding acid in bidistilled water. Prior to sample preparation, the uranium and ligand concentrations and the pH value of the solutions were calculated to yield only one uranyl species. For the speciation calculations, we used published complexation constants and acid dissociation constants and included the hydrolysis equilibria of the uranyl ion. According to these calculations, more than 95% of the uranium in solution was present as the desired uranyl complex with a specific uranium to ligand ratio, U(VI):L (see Tab. 1).

Ligand (L)						U(VI) :L ratio						
No.	Acid	mol/L	U(VI) mol/L	pH	(of the complex)	No.	Uranyl complex	R(Å)	U-O _{eq} N	F ² (Å ²)	U-X X	R(Å)
1	acetic	1.10	0.05	3.7	1:3	1	acetate	2.44	6	0.008	C	4.34
2	phthalic	0.06	0.02	4.6	1:1	2	phthalate	2.37	6	0.010		
3	maleic	0.01	0.001	4.2	1:1	3	maleate	2.37	6	0.010		
4	malonic	0.20	0.05	3.9	1:2	4	malonate	2.36	5	0.007	U	3.96
5	succinic	0.50	0.05	4.0	1:1	5	succinate	2.48	5	0.008	C	4.37
6	malic	0.10	0.05	3.2	2:2	6	malate	2.37	5	0.005	U	3.97
7	citric	0.10	0.05	3.9	2:2	7	citrate	2.38	5	0.007	U	3.94
8	tartaric	0.10	0.05	3.4	2:2	8	tartrate	2.36	4	0.006	U	3.95

Tab. 1: Sample composition and calculated U(VI) speciation using published complex formation constants.

Tab. 2: EXAFS structural parameters of aqueous uranyl complexes.

Structural parameters for the aqueous uranyl complexes **1-8** were determined by uranium L₃-edge EXAFS analysis (see Tab. 2).

Although a variety of aliphatic and aromatic uranyl carboxylates were studied, the near-neighbor environment of uranium in these aqueous complexes can be grouped into three basic types, i.e., A, B, and C. The Fourier transforms of the uranium L₃-edge EXAFS for one representative of each type (A-C) are shown in Fig. 1. Uranyl acetate (**1**) and succinate (**5**) belong to type A coordination and are characterized by bidentate ligation of the COO⁻-group with a U-O_{eq} bond

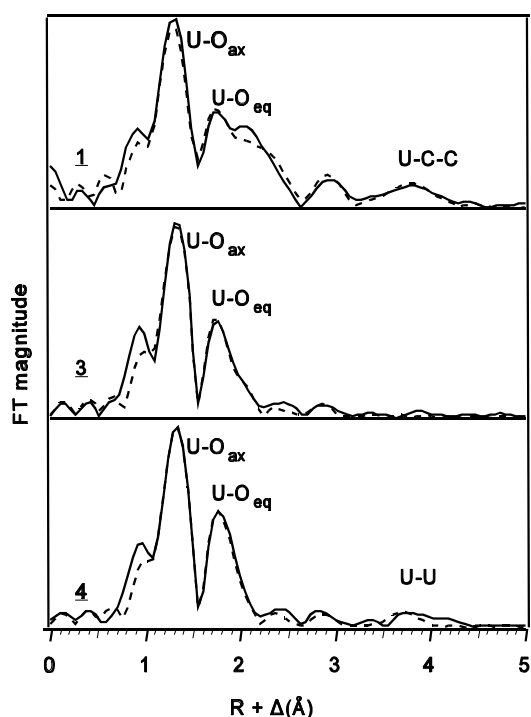


Fig. 1: Fourier transforms of U L_{3} -edge EXAFS data for aqueous uranyl acetate (1), maleate (3), malonate (4). The solid lines are the experimental data. The dashed lines are the best theoretical fit of the data.

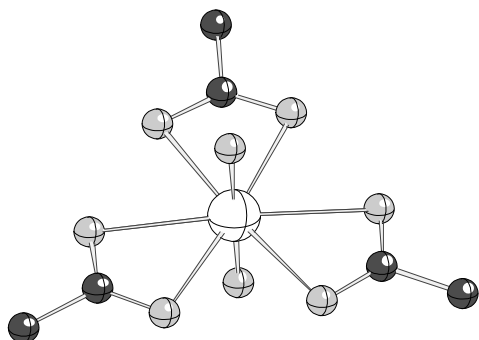


Fig. 2: Structural model for the uranyl tri-acetate having the empirical formula $UO_2(Ac)_3$.

distance larger than 2.42 Å. The assignment of bidentate coordination is supported by the detection of an additional carbon coordination shell at 4.3 Å due to multiple-scattering enhancement along a linear U-C₁-C₂ arrangement. A structural model for the uranyl acetate solution (1), where three acetate ligands adopt a bidentate geometry, is shown in Fig. 2.

Coordination of types B and C is characterized by monodentate ligation of the COO⁻-group with a typical U-O_{eq} distance of 2.37 Å. Aqueous uranyl carboxylates of type C differ from type B by the detection of an additional coordination shell due to single-scattering U-U interaction at 3.9 Å C. Such a U-U coordination shell is not observed for type B complexes (samples 2 and 3). In malic, citric, and tartaric acids, both the α -hydroxyl group and the COO⁻-groups play a key role in the formation of 2:2 dimers in solution. A detailed account of the EXAFS analysis and the structural model derived for complexes 6-8 was published recently /1/.

The structural parameters obtained for different coordination modes may be used to guide the EXAFS analysis of interaction products of uranium(VI) with naturally occurring organic macromolecules such as humic and fulvic acids and lignin which possess many carboxylic and hydroxyl groups.

Acknowledgments

The help of G. Grambole and A. Otto and the advice of E. Förster during sample preparation are gratefully acknowledged. EXAFS measurements were made at Beamline 2-3 at SSRL, which is operated by the US Department of Energy.

References

- /1/ Allen, P.G., Shuh, D.K., Bucher, J.J., Edelstein, N.M., Reich, T., Denecke, M.A., Nitsche, H.: EXAFS Determinations of Uranium Structures: The Uranyl Ion Complexed with Tartaric, Citric, and Malic Acids. *Inorg. Chem.* **35**, 784 (1996)

STRUCTURAL INVESTIGATIONS OF TECHNETIUM AND RHENIUM COMPLEXES BY EXAFS. 2. STUDIES OF Tc AND Re OLIGOGLYCINE COMPLEXES

R. Jankowsky¹, B. Noll¹, H. Spies¹, B. Johannsen¹, T. Reich, H. Nitsche
Forschungszentrum Rossendorf e.V., Institute of Radiochemistry
¹Institute of Bioinorganic and Radiopharmaceutical Chemistry

Structural parameters for the first three coordination shells of several aqueous Tc(V) and Re(V) oligoglycine complexes were measured by EXAFS spectroscopy. A more detailed account of these studies can be found in /1/.

Experimental

Starting from a solution of $^{99}TcO_4^-$ in water, aqueous technetium complexes with the oligoglycine ligands Gly₄, Gly₅, and Gly₆, where Gly stands for the glycol residue, were prepared by an upscaled synthesis as described in /2/. Due to the thermal instability of these complexes at room temperature, samples were kept at -10°C after partial lyophilization. The rhenium complexes with Gly₄ and Gly₅ were prepared immediately before measurements without further

lyophilization by mixing ReO_4^- , Sn^{2+} , and tartrate solutions and adding the corresponding oligoglycine ligand. Technetium K-edge and rhenium L_{III} -edge x-ray absorption spectra were collected at room temperature in transmission and fluorescence modes, respectively. The Tc samples were measured at Hamburger Synchrotronstrahlungslabor, HASYLAB. The Re complexes were measured at Stanford Synchrotron Radiation Laboratory, SSRL.

Results

The extended x-ray absorption fine structure (EXAFS) of the Tc and Re spectra was analyzed according to the standard procedure described in /3/. The EXAFS structural parameters obtained are given in Tab. 1. The first coordination shell of the Tc and Re complexes consists of one oxygen atom at a distance of ca. 1.69 Å from the central atom. This is a typical value for the monooxotechnetium species in Tc(V) complexes. The same Tc(V) oxidation state was determined by analysis of Tc K-edge energies and is described in more detail elsewhere /1/.

In all Tc complexes, approximately four light atoms like nitrogen or oxygen were detected at an average distance of 2.05 Å. If all four atoms are nitrogen, they could represent three amide and one amine nitrogen atoms of the oligoglycine ligand. This would mean that the NH_2 group of the peptide is involved in the technetium complexation. In the Re(V) complexes, the average Re-N distance is 1.97 Å, i.e., slightly shorter than in the corresponding Tc(V) complexes.

The third coordination shell of the Tc(V) and Re(V) complexes could only be fit if a heavy backscatterer is included, i.e., technetium and rhenium at 2.85 Å and 2.91 Å, respectively. This was an unexpected result. A plausible explanation for the presence of Tc-Tc and Re-Re interactions at ca. 2.9 Å remains to be found. Also, the presence of an additional coordination shell at ca. 4 Å in the Fourier transforms of the Tc complexes needs to be analyzed in future studies including analysis of multiple-scattering paths along the peptide backbone carbonyl oxygen atoms.

Tab. 1: EXAFS structural parameters for the Me-X coordination shells, where Me is Tc or Re.

Complex	Near-neighbor atom, X	Coordination number, N_x	Distance, Me-X (Å)	F^2 (Å ²)
Tc-Gly ₄	O	0.8	1.67	0.003
	N	3.8	2.03	0.007
	Tc	1.1	2.86	0.009
Tc-Gly ₅	O	0.8	1.69	0.002
	N	4.3	2.07	0.008
	Tc	0.9	2.85	0.008
Tc-Gly ₆	O	0.7	1.68	0.002
	N	3.6	2.06	0.008
	Tc	1.1	2.82	0.009
Re-Gly ₄	O	1 [*]	1.70	0.002
	N	4 [*]	1.96	0.004
	Re	1 [*]	2.91	0.008
Re-Gly ₅	O	1 [*]	1.70	0.002
	N	4 [*]	1.98	0.005
	Re	1 [*]	2.92	0.009

Experimental uncertainties of N_x and distance Me-X are $\pm 30\%$ and ± 0.02 Å, respectively.

^{*} Held constant during the fit.

In summary, EXAFS analysis confirmed that the oxidation state of Tc and Re in aqueous oligoglycine complexes is +5. All Tc(V) and Re(V) oligoglycine complexes studied have similar structural parameters for their first three coordination shells. The peptide nitrogen atoms seem to be involved in a complicated complexation with the Tc and Re atoms. The observed metal-metal interaction at distances below 3 Å indicates the formation of binuclear complexes in solution.

References

- /1/ Jankowsky, R., Noll, B., Spies, H., Johannsen, B., Reich, T., Nitsche, H.: XAS of Tc and Re complexes of oligoglycine ligands and Tc tartrate. In: Report FZR-165, Institute of Bioinorganic and Radiopharmaceutical Chemistry, Annual Report 1996 (1997) p.72
- /2/ Jankowsky, R., Noll, B., Spies, H., Johannsen, B.: Synthesis and characterization of technetium and rhenium oligoglycine complexes and Tc tartrate. In: Report FZR-165, Institute of Bioinorganic and Radiopharmaceutical Chemistry, Annual Report 1996 (1997) p.67
- /3/ Koningsberger, D.C., Prins, R. (eds.): *X-ray absorption. Principles, applications, techniques of EXAFS, SEXAFS and XANES*. John Wiley & Sons, New York (1988).

X-RAY ABSORPTION SPECTROSCOPIC AND MÖSSBAUER STUDIES OF REDOX AND CATION-ORDERING PROCESSES IN MANGANESE FERRITE *

G. Bonsdorf¹, M.A. Denecke, K. Schäfer², S. Christen¹, H. Langbein¹, W. Gunßer³

Forschungszentrum Rossendorf e.V., Institute of Radiochemistry

¹ Technische Universität Dresden, Institut für Anorganische Chemie

² Universität Leipzig, Fakultät für Physik und Geowissenschaften

³ Universität Hamburg, Institut für Physikalische Chemie

X-ray absorption spectra of manganese ferrites were recorded at the Mn K-edge to determine the manganese valences of differently prepared samples from the energy shift of their x-ray absorption edges relative to the Mn K-edge position of the reference samples MnO, Mn₃O₄ and Mn₂O₃. The site occupation ratio of Fe³⁺ cations on tetrahedral (A) and octahedral (B) sites of the spinel structure was determined from Mössbauer spectra taken at 4.2 K in an external magnetic field of 6 Tesla.

The manganese ferrite samples were prepared by the decomposition of a freeze-dried Mn-Fe₂-formate precursor. Decomposition in an oxidizing atmosphere (air) at 400°C yielded a spinel phase similar to the defect spinel $-(\text{Fe,Mn})_2\text{O}_3$. From the x-ray absorption spectra shown in the figure below, a value of 2.8 was obtained for the Mn valence of this phase.

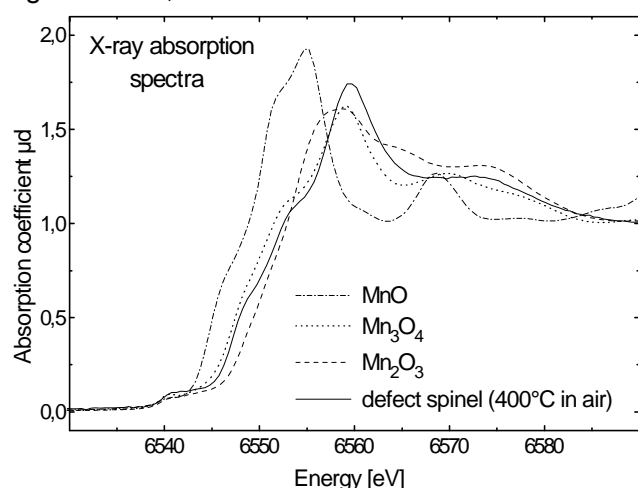


Fig. 1: Mn K-edge x-ray absorption of manganese compounds indicated.

In the spectrum of the sample treated at 500°C, 33% Fe ions were found on tetrahedral sites.

Excluding any cation vacancies, the following cation distribution was deduced from this: $(\text{Mn}_{0.34}\text{Fe}_{0.66})_A[\text{Mn}_{0.66}\text{Fe}_{1.34}]_B\text{O}_{4+*}$. Assuming that Mn³⁺ ions occupy exclusively octahedral sites and Mn²⁺ ions only tetrahedral sites, this cation distribution corresponds to a Mn valence of 2.67, which is in accord with the value of 2.7 obtained from the x-ray absorption spectra. In the manganese ferrite treated at 1000°C an absence of Mn³⁺ cations was found and only 16% Fe cations have been observed to occupy tetrahedral sites.

* The results of this study are being published in: Bonsdorf, G., Denecke, M.A., Schäfer, K., Christen, S., Langbein, H., Gunßer, W.: Solid State Ionics (in press).

POLARIZED X-RAY-ABSORPTION SPECTROSCOPY OF THE URANYL ION: COMPARISON OF EXPERIMENT AND THEORY *

E.A. Hudson¹, P.G. Allen¹, L.J. Terminello¹, M.A. Denecke, T. Reich

Forschungszentrum Rossendorf e.V., Institute of Radiochemistry

¹ Glenn T. Seaborg Institute for Transactinium Science, Lawrence Livermore National Laboratory, University of California, Livermore, USA

The x-ray linear dichroism of the uranyl ion (UO₂²⁺) in the uranium L₃-edge extended x-ray absorption fine structure (EXAFS), and L₁- and L₃-edge x-ray absorption near edge structure (XANES), has been investigated both by experiment and theory. A striking polarization depend-

ence is observed in the experimental XANES and EXAFS for an oriented single crystal of uranyl acetate dihydrate [$\text{UO}_2(\text{CH}_3\text{CO}_2)_2 \cdot 2\text{H}_2\text{O}$], with the x-ray polarization vector aligned either parallel or perpendicular to the bond axis of the linear uranyl cation (O-U-O). Single-crystal results are compared to experimental spectra for a polycrystalline uranyl acetate sample and to calculations using the *ab initio* multiple-scattering (MS) code FEFF 6. Theoretical XANES spectra for uranyl fluoride (UO_2F_2) reproduce all the features of the measured uranyl acetate spectra. By identifying scattering paths which contribute to individual features in the calculated spectrum, a detailed understanding of the L_1 -edge XANES is obtained. MS paths within the uranyl cation have a notable influence upon the XANES. The measured L_3 -edge EXAFS is also influenced by MS, specifically when the x-ray polarization is parallel to the uranyl species. These MS contributions are extracted from the total EXAFS and compared to calculations. The best agreement with the isolated MS signal is obtained by using nonoverlapped muffin-tin spheres in the FEFF 6 calculation. This contrasts the L_1 -edge XANES calculations, in which overlapping was required for the best agreement with experiment.

* abstract; article published in: Phys. Rev. B **54**, 156 (1996)

Behavior of Colloids and Aerosols

COMPARISON OF METHODS FOR COLLOID PARTICLE SIZING: FILTRATION, CENTRIFUGATION, PHOTON CORRELATION SPECTROSCOPY (PCS), AND SCANNING ELECTRON MICROSCOPY (SEM)

H. Zänker, G. Hüttig, H. Moll, H. Nitsche

Forschungszentrum Rossendorf e.V., Institute of Radiochemistry

Several methods of determining submicron particle size distributions were tested on an artificial model colloid (silica particles) and on a real environmental sample. The susceptibilities of the different methods to artifacts are discussed and a strategy for particle sizing is developed.

A puzzling problem in colloid research is that experimental results can dramatically depend on the experimental technique used to investigate a colloid. This is due to the tendency of colloidal suspensions to change when ambient conditions are altered, i.e., due to the thermodynamic instability of colloids. Two techniques of colloid research of entirely different physical principles were first tested on a 'model colloid': the relatively invasive technique of filtration and the almost non-invasive technique of PCS.

A sample of suspended silica particles was prepared by acidifying a 0.1 molar solution of sodium silicate with HClO_4 to a pH value of 3.92 ± 0.05 . Particles were grown during a period of 8 days. Eight PCS measurements were taken on day 8 of the experiment. PCS results showed that the vast majority of the particles was in the size range below 80 nm with the main peak being in the 50 to 80 nm region.

Fig. 1 gives an autocorrelation function and the corresponding light-intensity- weighted size distribution. Fig. 2 shows the filtration scheme we applied first. Nuclepore filters of 47 mm diameter were used. With this filtration scheme a classification of the submicron particles into 4 size classes should be reached. The lower size limits of these classes should differ by factors of 2.5, 8 and 3.3 from that of the corresponding neighbor class. All the filtrates were analyzed for their silicon concentrations by ICP-MS. The results are given in Fig. 2. The figure indicates that most of the particles had been removed by the 400 nm Filter. This is in sharp contrast to the PCS results (Fig. 1). Alternatively, we used the filtration scheme depicted in Fig. 3. This scheme avoided filtration to complete dryness (dead-end filtration) and the experiments were done parallel to each other and not in sequence. The ICP-MS results of the filtrates from the filtration according to this second scheme are given in Fig. 3. These results are striking: when using this filtration regime, there is good agreement between the filtration experiment and the PCS measurements.

Our experiment shows that dead-end filtration was not suited to characterize the particles under study. Finding 50 to 80 nm and smaller particles primarily on the 400 nm filter results in a misinterpretation of the true particle size by almost one order of magnitude. The main reason of this failure is obviously 'self-coagulation' during the process of filtration [1,2]. Filtration according to Scheme 2 (Fig. 3) reduced the filtration artifacts considerably. Further steps toward artifact reduction could be made using a stirring cell or performing a cross-flow filtration. Filtration, however, is generally not a reliable technique of particle size determination in the submicron size range and particle sizes determined by filtration should always be viewed with caution. Our experiment also demonstrates the need for applying more than one method for particle-sizing in the submicron size range. Using several (at least two) techniques validates the results and increases the probability for recognizing artifacts.

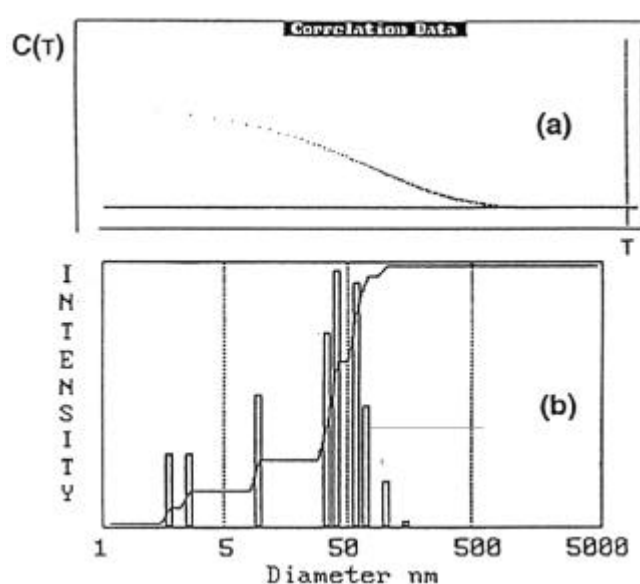


Fig.1: Typical PCS results from a sodium silicate solution after 8 days (silicate concentration 0.1 mol/L, pH 3.92 ± 0.05). (a) Autocorrelation function, (b) NNLS deconvolution of the autocorrelation function.

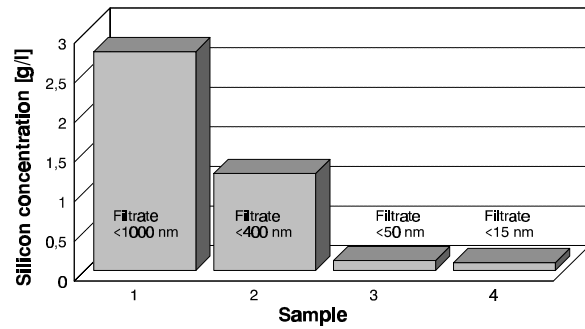
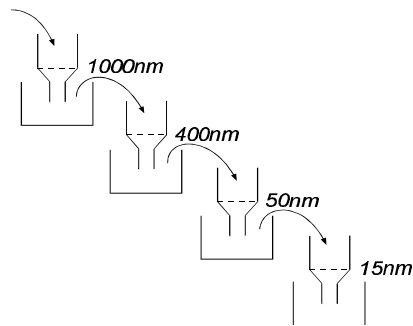


Fig. 2: Silicon concentration in the filtrat (right) of the sequential dead-end filtration (Scheme left). Initial silicon concentration: 0.1 mol/L; pH 3.92 ± 0.05 ; age of the solution: 8 days.

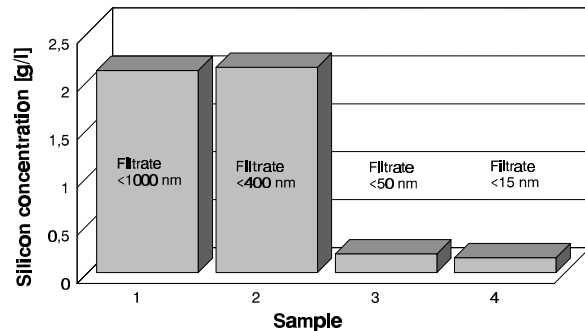
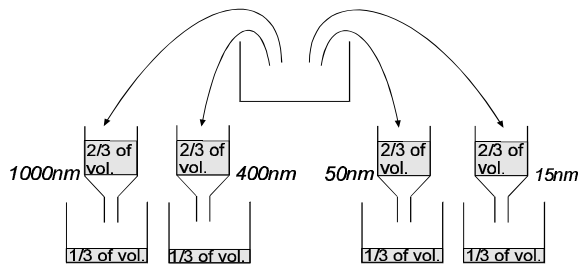


Fig. 3: Silicon concentration in the filtrat (right) of the filtration (Scheme 2 left; only 1/3 of the volume is filtered, the rest is discarded). Initial silicon concentration: 0.1 mol/L, pH 3.92 ± 0.05 , age of the solution: 8 days.

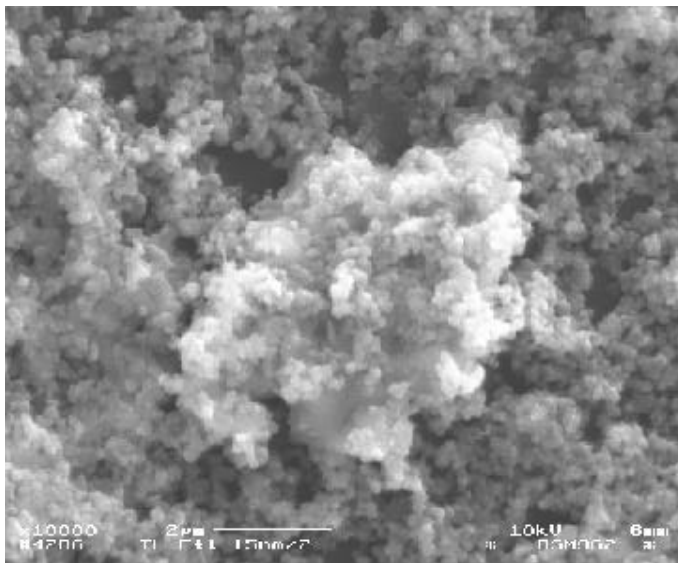


Fig. 4: SEM micrograph of the particles in the backwater of a sanitary landfill on a 15 nm Nuclepore filter (Prefiltration through a 1000 nm filter)

The experience gained from these tests on artificial 'model particles' was applied to study colloids in environmental samples. Submicron particles from backwater of a sanitary landfill that is located on top of a uranium mine tailing were investigated using two independent methods of particle separation (filtration and centrifugation) and two independent sizing methods (PCS and SEM) /3/. The PCS measurements (after the appropriate separation steps) revealed submicron particles from 30 to 300 nm. This was in good agreement with the SEM micrograph shown in Fig. 4 where individual particles of this size range can be identified. The large agglomerate in the picture also consists of these small particles and is likely a result of the filtration process. One can therefore

assume that the particles of 30 to 300 nm move freely through the backwater and not as larger agglomerates as the one that is shown in the center of the micrograph.

References

- /1/ Buffle, J., Leppard, G.G.: Environ. Sci. Technol. **29**, 2176-2184 (1995)
- /2/ Zänker, H., Hüttig, G., Christalle, E., Richter, W.: First Results of Sequential Filtration of Groundwater From an Aquifer in the Upper Elbe Valley Sandstone. In: Report FZR-123, Institute of Radiochemistry, Annual Report 1995 (1996) p.50
- /3/ Zänker, H., Richter, W., Hüttig, G., Nitsche, H., Wiesener, W., Mende, A.: *Characterization of Submicron Particles in an Environmentally-Relevant Water: Backwater From a Sanitary Landfill on a Uranium Mine Tailing at Freital, Saxony*. Report FZR-155, Forschungszentrum Rossendorf e.V., Oct. 1996 (in German)

DETERMINATION OF THE PARTICLE DIAMETER OF INDUSTRIAL TiO₂ IN AQUEOUS SUSPENSION IN THE PRESENCE OF A DETERGENT

W. Richter, H. Zänker, E. Förster
 Forschungszentrum Rossendorf e.V., Institute of Radiochemistry

The particle size of TiO₂ in aqueous suspension was measured by filtration and photon correlation spectroscopy. The results showed agglomerated particles of 110±50 nm diameter. The particles were stable to both sonication and the addition of surfactants.

A UV-activated oxidation of C-14-labeled organic substances in a colloidal suspension of TiO₂ was developed by Förster et al. /1/. The particle size of the TiO₂ in the suspension is one important parameter for this process. We tested two different TiO₂ Powders (P25 (DEGUSSA) /2/ and Hombikat UV100 (Sachtleben Chemie GmbH, Duisburg). According to the producers, the size of the primary particles was about 21 nm and <10 nm for the P25 and UV100 powder, respectively. We measured the size of the TiO₂ particles with the photon correlation spectroscopy BI-90 (Brookhaven Instruments Corp.). The powders were suspended in water together with the surfactant Präwozell®-N9 (Buna AG Schkopau) which is a non-ionogenic tenside based on nonylphenole and ethenoxide. The laser power was 400 mW, the laser wavelength 514.5 nm, and the temperature 25°C.

Prior to the measurements on the TiO₂ suspensions, we tested the solvent (Milli-Q water) and the surfactant solution. The Milli-Q water, showing a photomultiplier count rate of only 1 to 2 kcps, was virtually free of scatterers. However, the tenside solution showed a remarkable count rate (124 kcps) at a dilution of 1:500. The deconvolution of the autocorrelation function obtained from this tenside solution yielded a particle size of 6±3 nm. This suggests that tenside micelles had formed. After a dilution of this solution to 1:25000, the count rate decreased to 6 kcps, a value low enough to allow an unperturbed sizing of the TiO₂ particles.

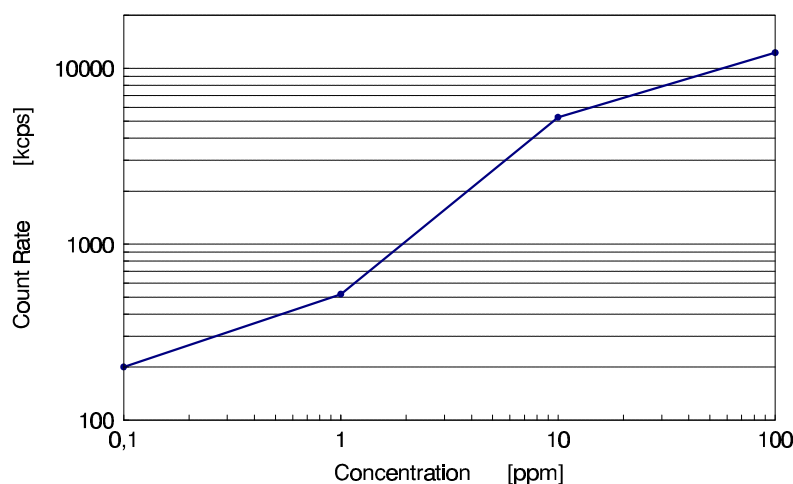


Fig. 1: Count rate of the TiO₂ suspension (P25) in dependence on the colloid concentration

The most favorable concentration range for photon correlation spectroscopy (PCS) lies between 1 and 10 ppm. Tab. 1 gives the results of PCS. The size of the suspended TiO₂ particles was found to be 110±50 nm.

Concentration [ppm]	Count rate [kcps]	Particle size [nm]
10	5258	152±50
1	519	65±30
0.1	189.5	100±50

This dilute tenside solution was used to make a 100 ppm TiO₂ suspension. Following a ultra sound sonication of 5 min, the TiO₂ particle size was measured with the BI-90. Because the powder type UV100 sedimented within minutes, we will report only the measurements on the P25 titanium dioxide in the following. From the 100 ppm stock solution, dilutions as low as 0.1 ppm were made and measured with the BI-90. Fig.1 shows the dependence of the count rate on the TiO₂ concentration.

Tab. 1: Results of particle sizing from the TiO₂ suspension (P25, Degussa)

Fig. 2 shows a transmission electron micrograph of the TiO₂ powder (provided by the manufacturer). Comparing the micrograph and the PCS results for the particle size of the powder, one can assume that PCS detects relatively stable agglomerates that are also visible in Fig. 2 and that are not sufficiently separated in the aqueous suspension, despite the detergent. The application of a more concentrated tenside solution as well as a longer ultra sound sonication did not result in a reduction of the particle size of the TiO₂ suspension.

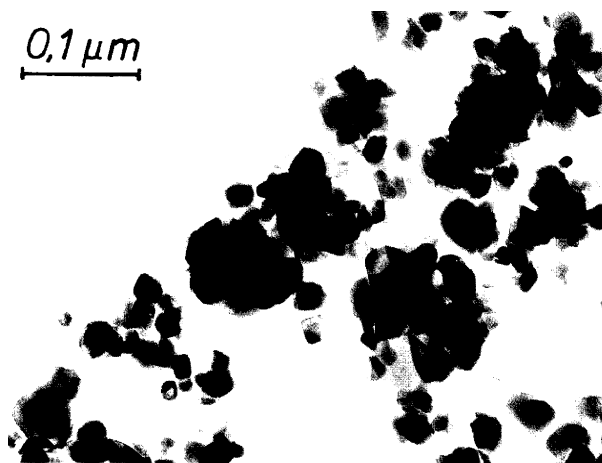


Fig. 2: Transmission electron micrograph of the P25 type TiO_2 powder taken by the producer /1/

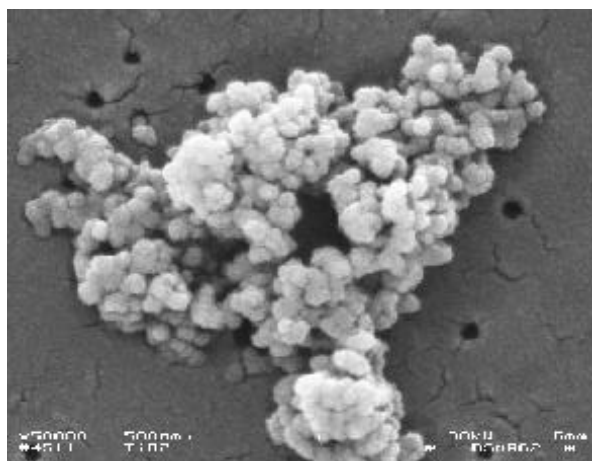


Fig. 3: Scanning electron micrograph of the TiO_2 particles on an 100 nm Nucleporefilter

The PCS results do not, however, exclude the presence of particles in the size range of about 20 nm reported in /2/. Because of the r^6 -dependence of the scattered light intensity on the radius r of a particle, small particles are often masked by larger ones in light scattering experiments. The small particles become only 'visible' by PCS then if the larger ones are removed from the suspension. We removed larger particles by filtration through a 100 nm and a 50 nm Nuclepore filter (Costar GmbH). Fig. 3 shows a scanning electron micrograph of the deposits on the 100 nm filter which confirms the existence of the 100 nm agglomerates found by PCS. The PCS results obtained from the filtrates are given in Tab. 2.

Sample	Count Rate [kcps]	Particle size [nm]
unfiltered	594	160±50
Filtrate 100nm	357	100±20
Filtrate 50nm	5.5	7±4; 30±10

Tab. 2: Results of the PCS measurements on filtrates from the TiO_2 suspensions of 1 ppm (P25, Degussa)

It is obvious from this table that a large proportion of the particles are removed by the two filters and that these removable particles emit most of the scattered light. In particular, the 50 nm filtration causes a strong count rate decrease. The count rate after this filtration lies in the range that should, according to our experience, be regarded as the lower detection limit of our photon correlation spectroscope /3/. The results of particle sizing for this filtrate, however, make physical sense if one takes into consideration that the accuracy of the particle sizing with PCS on such very dilute colloidal suspensions is only within a factor of two. These results confirm that there is a small amount of particles of the size range given by the producer of the TiO_2 powder.

The conclusion can be drawn from our experiment that most of the suspended particles were in the size range of 110±50 nm. A comparison with a TEM micrograph suggests that these particles were agglomerates which cannot be split into smaller particles by mild methods of dispersion such as adding a detergent or us sonication. However, the measurements also show that a small portion of the particles was in the size range indicated by the producer of the TiO_2 powder. These small particles should presumably be regarded as the 'primary particles' that form the agglomerates.

References

- /1/ Förster, E., Heise, K.H., Wolf, K., Nitsche, H.: TiO_2 -Photocatalyzed Oxidation of Organic Compounds. In: Report FZR-123, Institute of Radiochemistry, Annual Report 1995 (1996) p.77
- /2/ *Hochdisperse Metalloxide nach dem Aerosil®-Verfahren*. Schriftenreihe Pigmente Nr. 56, Degussa AG, 1989
- /3/ Richter, W., Zänker, H., Hüttig, G.: Testing of a Photon Correlation Spectroscope with Low-Concentration Colloids. In: Report FZR-123, Institute of Radiochemistry, Annual Report 1995 (1996) p.47

DETECTION OF AEROSOL LOSSES IN GLASS VESSELS

D. Rettig, P. Merker, H. Nitsche
 Forschungszentrum Rossendorf e.V., Institute of Radiochemistry

Several electrostatic depletion effects were determined using polydisperse aerosols under defined flow, geometry, and aerosol diameter and concentration conditions.

The electrostatic deposition of particles in sampling lines and aerosol vessels of non-conductive materials is difficult to characterize. In experiments with monodisperse aerosols, McMurry and Rader /1/ as well as Liu et al. /2/ observed high particle losses in electrostatically-charged Teflon film bags and in plastic tubes, which were charged by bending and flexing. Liu et al. minimized the losses by wrapping the external surface of the plastic tubing with an aluminum foil. Crump, Flagan, and Seinfeld /3/ determined the particle loss rate of monodisperse aerosols in a glass vessel and could explain their experimental results by only considering diffusional and gravitational losses. However, they suspected that the scatter of their data was an indication of an uncontrolled electrical charge effect.

Our method directly determines the loss of electrical charged particles from polydisperse aerosols in vessels of non-conductive materials. The experimental conditions (18 L/h flow, 300 mL volume, 15 - 300 nm particle diameter, $< 2 \cdot 10^5/\text{cm}^3$ particle concentration) offer the advantage of minimizing the influence of effects such as gravitational settling, impaction or diffusion loss to the wall, charge redistribution, and population decrease due to coagulation. We have studied the electrostatic aerosol loss in different glass vessels (of quartz (QG), borosilicate glass (BG), and silicate glass (SG)) in comparison to that in Teflon (T) and steel (S) vessels. All glass vessels were pre-treated with distilled water, heated to 250 °C and equilibrated with laboratory air of 30% humidity. Before and during the aerosol loss measurements the outside of the glass vessels was exposed to one of the following conditions:

- (1) in laboratory atmosphere surrounded by a grounded Faraday cage,
- (2) slightly wiped with a cloth before the experiment, and
- (3) totally immersed in an electrolytic bath containing 3% sodium chloride in water.

The aerosols were generated in an atomizer (2g/L NaCl), passed through a diffusion dryer, diluted with dry air (5% humidity), neutralized in a TSI 3077 neutralizer and then passed through the appropriate experimental vessel (SG, BG, QG, T, S) or a simple steel tube connector (C) which served as an arbitrary reference with negligible particle loss. The emerging aerosol was then classified (in mobility equivalent particle diameter D_m classes) in a TSI 3934 Scanning Mobility Particle Sizer (SMPS). We removed the neutralizer from the SMPS and determined only the positively charged particles. A defined and constant fraction of all particles in each mobility class were measured with the unmodified SMPS. The particle loss fraction (LF) is calculated from the particle concentration in the experimental vessel and the steel tube reference (C). Examples for the LF 's from neutralized and solely atomized aerosols (without the TSI 3077 neutralizer upstream from the vessel) are given in Fig. 1, and those of the positively charged particles from neutralized aerosols are given in Fig. 2.

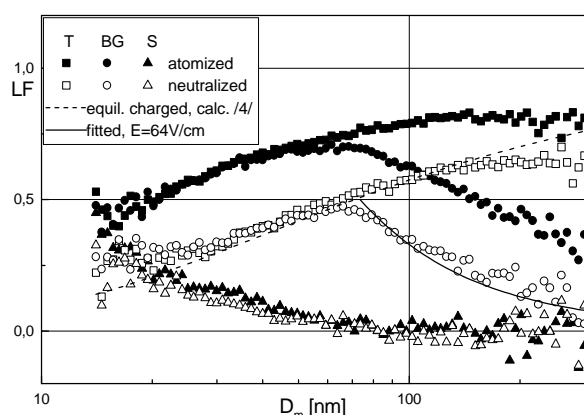


Fig. 1: Aerosol loss fraction (LF) of all particles from atomized and neutralized aerosol in vessels in the laboratory atmosphere and Faraday shielding.

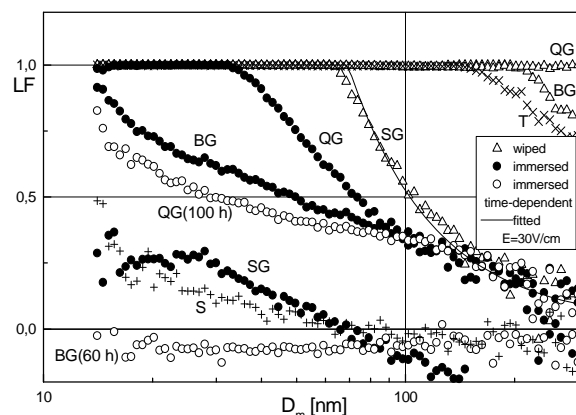


Fig. 2: Loss fraction (LF) of positive particles from neutralized aerosol in vessels after wiping and after immersion in an electrolytic bath.

All singly and multiply-positive and negative charged particles with diameters less than 150 nm are totally removed in the Teflon vessel. Fig. 1 shows the experimental particle loss from neutralized aerosols compared to all particles present, excluding neutral particles for equilibrium conditions that were calculated according to Wiedensohler /4/. A smaller fraction of all charged particles with diameters greater than a certain value are removed in *BG* vessels under experimental condition (1), as described above (Fig. 1). Electric fields arise from the contact-electric or tribo-electric charging of the outside surface by wiping and create a high *LF* (Fig. 2). This is due to the electric field lines passing through the space inside the vessel and terminating at locally different charges outside the vessel. Assuming the appropriate geometry, we can fit the experimental *LF* with the formula for electrostatic precipitation (Fig. 1 and 2). From this, the electric field strength (*E*) is calculated. Removing the outside surface charging by immersing the vessels into an electric conducting liquid instantly reduces the particle losses in *SG* vessels to the level of the steel vessel *S* (Fig. 2). However, in *BG* and especially in *QG* vessels, long times are necessary for *LF* reduction. A build-up of charged particles at some sites of the inner surface during the action of the outer charge may have occurred. The charge of the particles vanishes slowly due to capturing opposite charged particles and due to electrolytic conduction on the inner surface of the vessels. The conductivity is high in the thick alkali and alkaline-earths-containing swelling layers of the *SG*, lower in the thinner layers of the *BG* vessels, and negligible on the *QG* surfaces. We found equal transmissions of steel, borosilicate, and silicate tubes as well as of flexible pipes of polyvinylchloride for aerosols when the outside was electrolytically shielded with the salt bath.

References

- /1/ McMurry, P.H., Rader, D.J. : *Aerosol Sci. Technol.* **4**, 249 (1985)
- /2/ Liu, B.Y.H., Pui, D.Y.H., Rubow, K.L., Szymanski, W.W. : *Ann. Occup. Hyg.* **19**, 251 (1985)
- /3/ Crump, J.G., Flagan, R.C., Seinfeld, J.H. : *Aerosol Sci. Technol.* **2**, 303 (1983)
- /4/ Wiedensohler, A.: *J. Aerosol Sci.* **19**, 387 (1988)

TRANSPORT OF RADON DAUGHTERS BY SALT AEROSOLS

P. Merker, D. Rettig

Forschungszentrum Rossendorf e.V., Institute of Radiochemistry

The adsorption of radon decay products on sodium chloride and ammonium sulphate aerosols under laboratory conditions was investigated. The salt aerosols were produced using an atomizer. Adsorption has been measured by α -spectrometry after filtering the aerosol.

An important indoor radiation exposure to the public is due to the inhalation of radon decay products. The estimated health risk associated with this is much higher than those due to other environmental carcinogens /1/. Radon decay products are chemically active, unlike their inert gaseous parent. They can attach to surfaces, such as aerosols, walls or other indoor surfaces and can also deposit on lung tissue. Potential health hazards depend, in part, on the concentration of the daughter isotopes and on its mobility. Thus, the fraction of decay products attached to aerosols is an important determinant of radon progeny behavior.

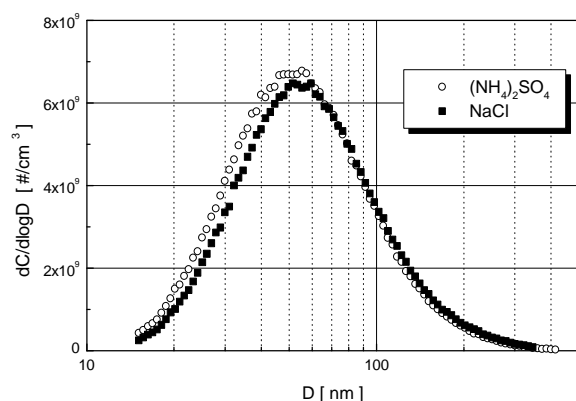


Fig. 1: Typical size distribution of used aerosols

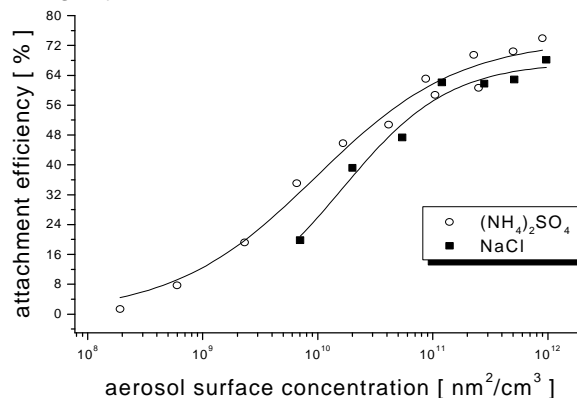


Fig. 2: Attachment of radon daughters to salt aerosols

Laboratory experiments were conducted to determine the effect of the nature and the concentration of aerosols on its ability to attach radon decay products. Salt aerosols were produced by atomizing aqueous solutions and drying the aerosol using a modified commercially available generator (TOPAS, model SLG 270). Aerosol concentration and size distribution were measured using a scanning mobility particle sizer (TSI, model 3934). Typical results are shown in Fig. 1.

The aerosol was mixed with radon-containing air (typical 750 Bq) in a 0.5 L glass vessel. Ten minutes after mixing, the whole gas volume was pumped off from the vessel to a filter sampler. To determine the number of radon daughter atoms attached to aerosol particles, the Po-214 decays on the filter were measured on-line by a PIPS-silicon detector for 4 hours. After this time nearly all short-lived decay products have decayed. The measured total counts were normalized to the expected number of counts calculated from the radon activity and the decay time in the mixing vessel (10 min). The resulting attachment efficiencies were determined for aerosol volume concentrations ranging over two and four orders of magnitude for NaCl and $(\text{NH}_4)_2\text{SO}_4$, respectively (Fig. 2).

According to Fig. 2, the attachment of radon daughters to ammonium sulphate seems to be higher than to sodium chloride, especially at low aerosol surface concentration. A substantial scattering of data points at higher concentrations was observed. We are currently improving the experimental setup in order to decrease the scattering at high aerosol concentration.

References

/1/ Nazaroff, W.W., Nero, A.V.: *Radon and its decay products in indoor air*. J. Wiley, 1988

DIFFERENT SHAPES OF AEROSOLS GENERATED BY ATOMIZATION

D. Rettig, P. Merker, R. Müller¹

Forschungszentrum Rossendorf e.V., Institute of Radiochemistry

¹ Zentralabteilung Analytik

The aerosols of sodium chloride and ammonium sulfate used in adsorption and transport experiments of radon decay products /1/ have been characterized by the particle size distribution, the total particle mass concentration and the shape of the aerosol particles. Hollow ammonium sulfate spheres and crystalline sodium chloride particles were observed.

The polydisperse aerosols of sodium chloride and ammonium sulfate are produced by spraying solutions of both salts of the same mass concentration with a Collison atomizer and drying the droplets and particles with a diffusion dryer as described in /2/.

For the determination of the particle size distribution, the aerosols are diluted and passed through the scanning mobility particle sizer (SMPS) /2/. For an independent determination of the mass concentrations, the aerosol substances are sampled on fibrous glass filters, extracted in water, and examined by chemical analysis (CA) for SO_4^{2-} or Cl⁻, respectively.

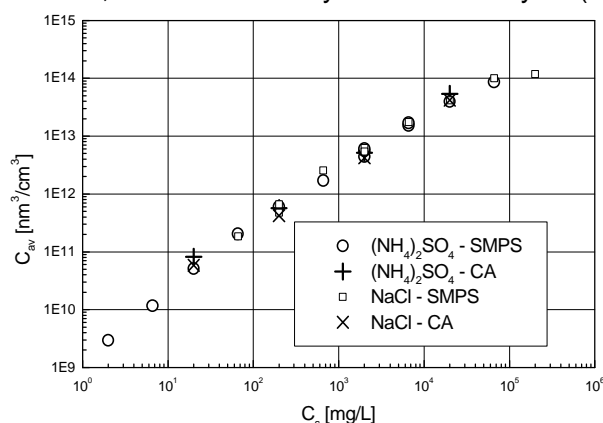


Fig. 1: Total volume concentrations C_{av} of the aerosol particles generated by atomizing solutions of different concentrations C_s of NaCl and $(\text{NH}_4)_2\text{SO}_4$ determined by CA and with the SMPS

Fig.1 depicts the total volume concentration of the aerosols from CA (after conversion of the mass to the volume concentration by the theoretical density) and that from the SMPS measurements (assuming spheres and summation over all particles) as a function of the salt mass concentration in the atomizer.

To observe their shapes, the particles from a small part (1 L in 4.5 min) of the total aerosol flow (250 L/h) were separated on microporous polyester membrane filters. The SEM images of the sodium chloride particles always showed cubic shapes with more or less rounded corners and edges (Fig. 2). The ammonium sulfate particles are spheres (Fig. 3). Only with mechanical pressure were we able to crack greater aggregates of the spheres

and to find that the spheres were hollow (Fig. 4). The weakest parts of the sphere walls are in the region where single spheres are grown together. There, they seem to sink into each other and break more easily.

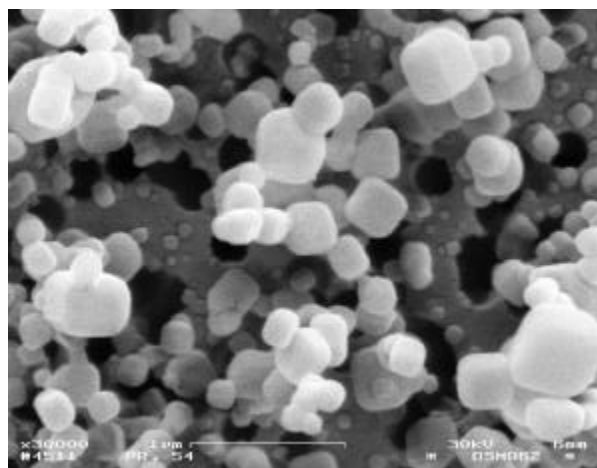


Fig. 2: Filtered NaCl particles generated from a solution of 6.6 g/L

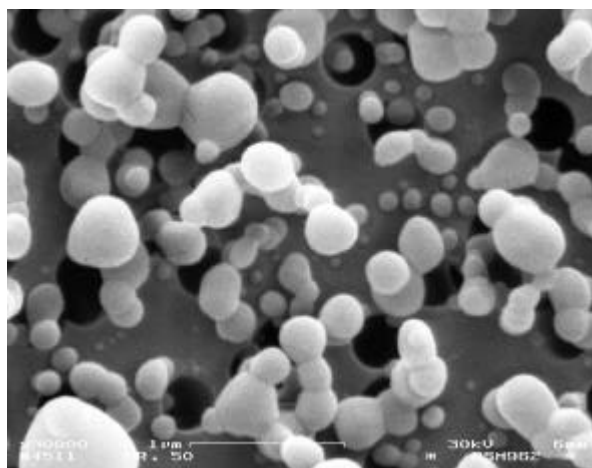


Fig. 3: Filtered $(\text{NH}_4)_2\text{SO}_4$ particles generated from a solution of 6.6 g/L

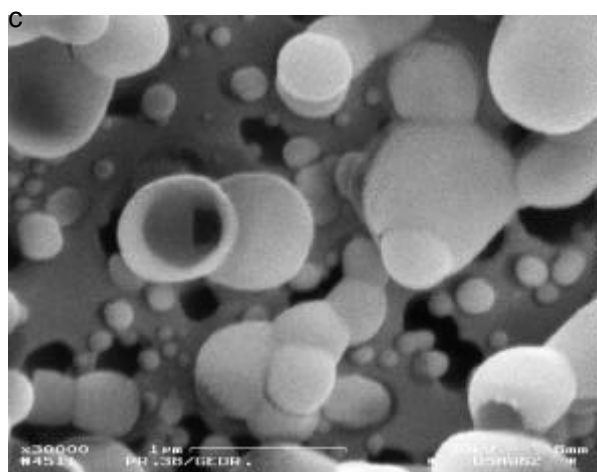


Fig. 4: Filtered $(\text{NH}_4)_2\text{SO}_4$ particles generated from a solution of 66g/L

According to Raabe /3/, the type of particles produced will depend upon the conditions of drying as well as the chemical nature of the materials. If droplets are dried rapidly, essentially shells may be formed by the encrustation of the surfaces. We see from the SEM micrographs that drying by free evaporation of the water into the surrounding gas is hindered where neighboring spheres attach to each other. The re-dissolution into the inner liquid competes with the evaporation, thereby weakening the crust at these areas.

Despite these differences in particle shape between the two salts, we did not see any characteristic differences in the particle spectra, in the total aerosol number, or in the vol-

ume concentrations outside the range of experimental error ($F=9\%$, Fig. 1). (The SMPS results may have some systematic losses in comparison with the CA). Therefore, we assume that coagulation processes superpose the extremely short droplet drying process, thereby compensating the initial differences in the aerodynamic or mobility properties of the aerosols. What is true for the similarity of the aerodynamic properties may not be true for the inner structure of the primary particles. Differences in these properties may significantly influence the adsorption of the individual particles. Therefore, we are planning to further investigate the crystalline or non-crystalline properties of the particles.

References

- /1/ Merker, P., Rettig, D.: Transport of Radon Daughters by Salt Aerosols. In: This Report, Institute of Radiochemistry, Annual Report 1996, (1997) p. 52
- /2/ Rettig, D., Merker, P.: Generation and Characterization of Sodium Chloride Aerosols. In: Report FZR-123, Institute of Radiochemistry, Annual Report 1995, (1996) p. 55
- /3/ Raabe, O.G.: The Generation of Aerosols of Fine Particles, in: Liu, B.Y.H.: *Fine Particles, Aerosol Generation, Measurement, Sampling, and Analysis*. Academic Press, Inc. 1976

Chemistry of the Heaviest Elements

REACTION GAS CHROMATOGRAPHY OF OXIDE AND HYDROXIDE SPECIES OF MOLYBDENUM - SIMULATION AND EXPERIMENT

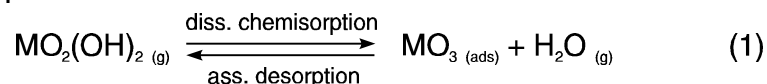
A. Vahle, S. Hübener, R. Dressler¹, B. Eichler¹, A. Türler¹

Forschungszentrum Rossendorf e.V., Institute of Radiochemistry

¹ Paul Scherrer Institut Villigen, Laboratory of Radio- and Environmental Chemistry

The reaction gas chromatography of oxide and hydroxide species of molybdenum in thermochromatographic columns was simulated with a microscopic model. Calculated thermochromatograms were compared to experimental results.

In the O_2 - $H_2O_{(g)}$ / $SiO_{2(s)}$ -system all group 6 elements are transported via reaction gas chromatography, governed by the surface reactions dissociative adsorption and associative desorption ($M = Cr, Mo, W$) /1/.



To describe reaction gas chromatography the microscopic model proposed by Zvara /2/ has been extended /3/.

Simulations of gas chromatography can be done with a Monte Carlo procedure based on this model. The method has been applied to thermochromatographic surface reaction studies with oxide and hydroxide species of molybdenum in open tubular quartz columns. Positions and shapes of thermochromatographic zones were calculated in dependence of reaction type, humidity of the carrier gas, and exposure time and were compared to experimental results.

The reaction gas chromatographic transport of molybdenum via reaction (1) through a thermochromatographic column has been studied already and is summarized in /1/. For all simulations, the thermodynamic state functions evaluated by conventional methods or estimated from literature data in /1/ were used. Thermochromatograms were calculated assuming the real experimental conditions described in /1/.

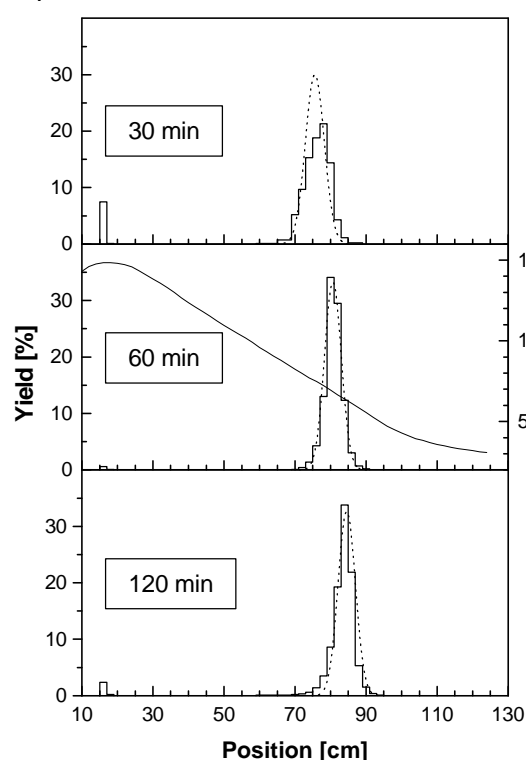


Fig. 1: Thermochromatograms of molybdenum in trace amounts at different exposure times.

solid: experimental data
dotted: Monte Carlo simulation with
) $H_{diss,ads}^E = -50$ kJ/mol and
) $S_{diss,ads}^E = -47$ J/(molK)

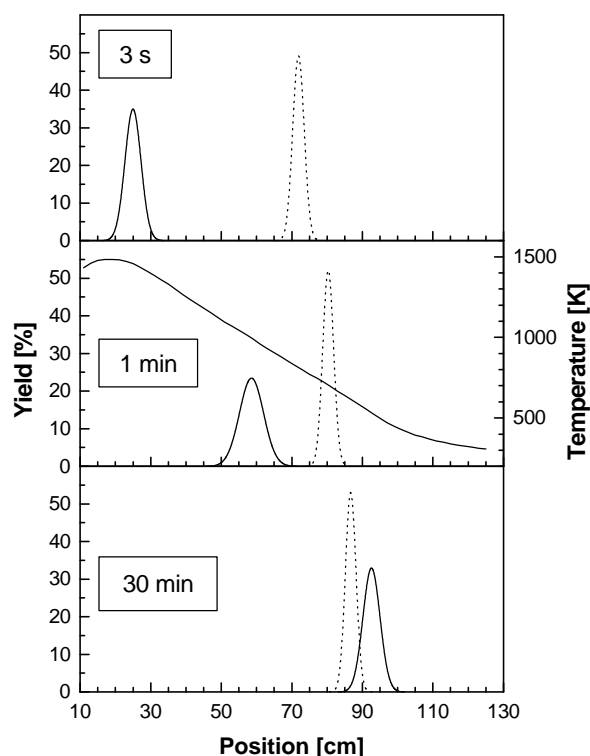


Fig. 2: Monte Carlo simulation of thermochromatography for different basic reactions and exposure times.

solid: $MoO_2(OH)_{2(g)} \rightleftharpoons MoO_3(ads) + H_2O(g)$
) $H_{diss,ads}^E = -35.4$ kJ/mol
dotted: $MoO_2(OH)_{2(g)} \rightleftharpoons MoO_2(OH)_{2(ads)}$
) $H_{ads}^E = -145.9$ kJ/mol

As can be seen from Fig. 1, both simulated peak positions and shapes correspond very well

with the experimental results under the assumption that molybdenum is transported according to reaction (1). This holds also at different water vapour pressures of the carrier gas /3/. The best correspondence between simulation and experiment was obtained with a value of $\Delta H_{\text{diss.ads}}^{\text{E}} = -50 \text{ kJ/mol}$. The same enthalpy was evaluated from experiments by conventional methods /1/.

As an example for potential applications, thermochromatograms for different basic reactions and exposure times were calculated by Monte Carlo simulations based on the model of Zvara and the extended model and are compared in Fig. 2. The simulation shows that the invariable species $\text{MoO}_2(\text{OH})_2$ transported via simple reversible adsorption would quickly reach the region of its deposition temperature and then move very slowly. In contrast, chromatography according to reaction (1) via dissociative adsorption - associative desorption with $\Delta H_{\text{diss.ads}}^{\text{E}} = -35.4 \text{ kJ/mol}$ /1/ is characterized by a slow but steady migration. The peak shapes of the deposition zones also depend significantly on the basic reaction. Narrow peaks are obtained if the chromatography is governed by simple reversible adsorption, whereas broader peaks are obtained for chromatography according to reaction (1). All simple reversible adsorption processes are characterized by similar values of $\Delta S_{\text{ads}}^{\text{E}}$, which has no effect on position or shape of the peak. In contrast, $\Delta S_{\text{diss.ads}}^{\text{E}}$ affects the migration velocity of the deposition zone as well as its shape. As demonstrated here the Monte Carlo simulation of reaction gas chromatography on the base of the extended model /3/ is an essential and reliable tool to model, evaluate, and interpret gas-solid chromatography experiments. Contrary to all other evaluation methods it allows to calculate the shape of thermochromatographic deposition zones.

Acknowledgments

These studies were supported by the BMBF of the FRG under contract 06 DR 101 D and 06 DR 666 I (4)/1.

References

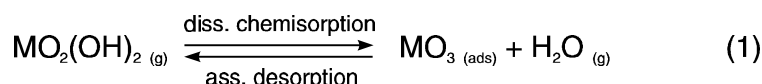
- /1/ Vahle, A., Hübener, S., Eichler, B.: Thermochromatographic Studies of Oxide and Hydroxide Species of Molybdenum - Model Experiments with Respect to the Physico-Chemical Characterization of Element 106. *Radiochim. Acta* **69**, 233 (1995)
- /2/ Zvara, I.: Simulation of Thermochromatographic Processes by the Monte Carlo Method. *Radiochim. Acta* **38**, 95 (1985)
- /3/ Vahle, A., Hübener, S., Dressler, R., Eichler, B., Türlér, A.: Reaction Gas Chromatography of Oxide and Hydroxide Species of Molybdenum - Simulation and Experiment. *Radiochim. Acta*, accepted for publication

ON-LINE ISOTHERMAL GAS CHROMATOGRAPHY WITH SHORT-LIVED MOLYBDENUM AND TECHNETIUM ISOTOPES IN THE $\text{O}_2\text{-H}_2\text{O}_{(\text{g})}/\text{SiO}_{2(\text{s})}$ -SYSTEM

A. Vahle, M. Böttger, M. Grantz, S. Hübener
Forschungszentrum Rossendorf e.V., Institute of Radiochemistry

In preparation for an experiment to study the chemical properties of element 106 (seaborgium, Sg), model studies were performed with short-lived molybdenum isotopes. The behavior of technetium as a homologue of element 107 (nielsbohrium, Ns) was also studied.

In order to study the reaction



which is assumed to be valid for all group 6 elements (including Sg) in the $\text{O}_2\text{-H}_2\text{O}_{(\text{g})}/\text{SiO}_{2(\text{s})}$ -system /1/, on-line isothermal gas chromatography experiments were performed using short-lived molybdenum isotopes as model nuclides.

Among other fission products, short-lived Mo and Tc isotopes were produced from the ^{235}U fission target of the radiochemistry gas-jet /2/ at the U-120 cyclotron of the Forschungszentrum Rossendorf with neutrons produced in the reaction $^9\text{Be}(\text{d}, \text{n})^{10}\text{B}$. For the rapid transport of the fission products, the He/MoO₃-version (1.0 l/min) of the radiochemistry gas-jet was used.

A quartz wool plug for destroying the aerosol particles was placed in the first section of the furnace which was kept at 1100 EC. The temperature of the 40-cm-long isothermal part of the

column was varied between 500 EC and 1000 EC. The recluster unit was operated with an Ar/KCl aerosol. The KCl clusters loaded with volatile species were collected on a glass fibre filter and measured on-line with a HPGe detector. Moist oxygen with a partial pressure of water of about 12 kPa was used as reactive gas at a flow rate of 0.5 l/min.

Fig. 1 shows elution yields of the isotope ^{104}Mo as a function of the isothermal temperature in the chromatographic column. The given yields are relative to a direct catch measurement using an empty quartz glass tube at room temperature. The isotopes ^{103}Mo and ^{105}Mo were also measured and gave similar yield curves.

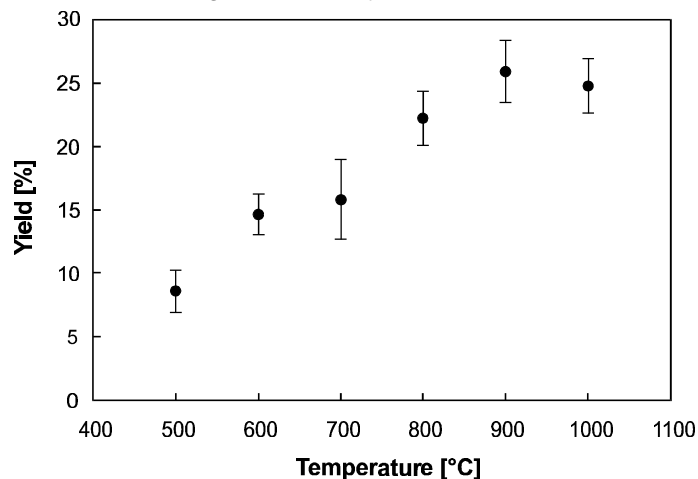


Fig. 1: Yield curve measured for ^{104}Mo and reaction (1)

The elution yield depends significantly on the temperature of the isothermal part of the column. With increasing temperature, a flat increase was obtained as typically for reaction gas chromatography /3/. The yield plateau was reached at a temperature of 900EC. In case of longer lived ^{101}Mo ($t_{1/2} = 14.6$ min), the yield plateau is already reached at temperatures above 500EC. However, the yield was expected to be higher than measured in the experiments for both the short-lived isotopes $^{103-105}\text{Mo}$ and the longer lived isotope ^{101}Mo . Only a small part of the losses results from the radioactive decay in the chromatographic column. In the temperature range studied, the retention time in the chromatographic column is in the order of a few seconds to minutes. Heavy losses are caused by the interaction between volatile species and the surface of the recluster chamber before the species are reattached to aerosol particles. High temperatures have a negative effect on the recluster yield. In case of short-lived isotopes, additional considerable losses are a result of the radioactive decay in the recluster chamber due to the dwell time of about one minute.

With respect to possible future experiments with element 107 preliminary investigations to the behavior of short-lived Tc isotopes were performed.

For all Tc isotopes, the short-lived ^{103}Tc ($t_{1/2} = 54.2$ s) as well as the longer lived ^{101}Tc ($t_{1/2} = 14.2$ min), ^{104}Tc ($t_{1/2} = 18.2$ min) and ^{105}Tc ($t_{1/2} = 7.6$ min), yield plateaus were obtained in the temperature range 400 EC - 1000EC. The elution yield was 50 ± 10 % compared to the direct catch. At temperatures of # 600 EC a slight increase of the yield was measured as a result of the higher recluster yield at decreasing temperature.

As expected, due to higher volatilities /4/, oxides and hydroxides of Tc pass the chromatographic system under study at temperatures below 1000 EC faster and with higher yields than the corresponding Mo species. Therefore, the $\text{O}_2\text{-H}_2\text{O}_{(g)}/\text{SiO}_{2(s)}$ -system should be better suited to investigate group 7 than group 6 elements.

Acknowledgments

This work was supported by the BMBF, contract 06 DR 666 I (4)/1, and was performed in cooperation with the GSI Darmstadt.

References

- /1/ Vahle, A., Hübener, S., Eichler, B.: Thermochromatographic Studies of Oxide and Hydroxide Species of Molybdenum - Model Experiments with Respect to the Physico-Chemical Characterization of Element 106. *Radiochim. Acta* **69**, 233 (1995)
- /2/ Hübener, S., Heyne, H., Hüttig, G., Roß, A., Brückner, R., Guratzsch, H., Fischer, S., Binder, R.: Design and Characteristics of the Radiochemistry Gas-Jet. In: Report FZR-43, Institute of Radiochemistry, Annual Report 1993, p. 55 (1994)
- /3/ Vahle, A., Hübener, S., Dressler, R., Eichler, B., Türler, A.: Monte Carlo Simulation of Reaction Gas Chromatography of Group 6 Elements. In: Report FZR-123, Institute of Radiochemistry, Annual Report 1995, p. 99 (1996)
- /4/ Steffen, A., Bächmann, K.: Gas Chromatographic Study of Volatile Oxides and Hydroxides of Re, Tc, Os, Ru and Ir-II. *Talanta* **25**, 677 (1978)

THERMOCHROMATOGRAPHY OF HEAVY ACTINIDES - DETERMINATION OF THE SUBLIMATION ENTHALPY OF ES

S. Taut, S. Hübener, B. Eichler¹, H.W. Gäggeler^{1,2}, M. Schädel³, I. Zvara⁴

Forschungszentrum Rossendorf e.V., Institute of Radiochemistry

¹ PSI Villigen, ² Universität Bern, ³ GSI Darmstadt; ⁴ JINR Dubna, Flerov Laboratory of Nuclear Reactions

The adsorption of Cf, Es, and Fm on several metals was studied thermochromatographically. Based on the adsorption data and the correlation between adsorption and sublimation heats, we calculated the Es sublimation enthalpy of 167 ± 15 kJ/mol (95 %). This is significantly higher than the value obtained by direct vapor pressure measurements (133 kJ/mol /1/). However, our value fits better to the theory.

Theoretical calculations using different approaches /2, 3, 4/ indicate that the sublimation enthalpies decrease smoothly from Cf to No. This is in contrast to the opposite trend of the experimental values for Es (133 kJ/mol /1/) and Fm (143 kJ/mol /5/). Therefore, we checked these values based on the correlation between the sublimation and adsorption enthalpies, experimentally well established for metallic adsorbate bonding /6/, especially in case of the lanthanides /7/.

Our experimental setup, the procedure, and the data analysis is described elsewhere /8/. The actinides were produced at the UNILAC (GSI) in the $^{248}\text{Cm} + ^{22}\text{Ne}$ reaction and at the U-400 (FLNR) and the Philips cyclotron (PSI) in the $^{248}\text{Cm} + ^{18}\text{O}$ reaction.

In all experiments a separation was observed on the chromatographic column in the order Cf, Es, and Fm. This is supported by the EICHLER-MIEDEMA model /9/, developed for understanding the adsorption enthalpy at zero coverage which predicts this position of Es between Cf and Fm.

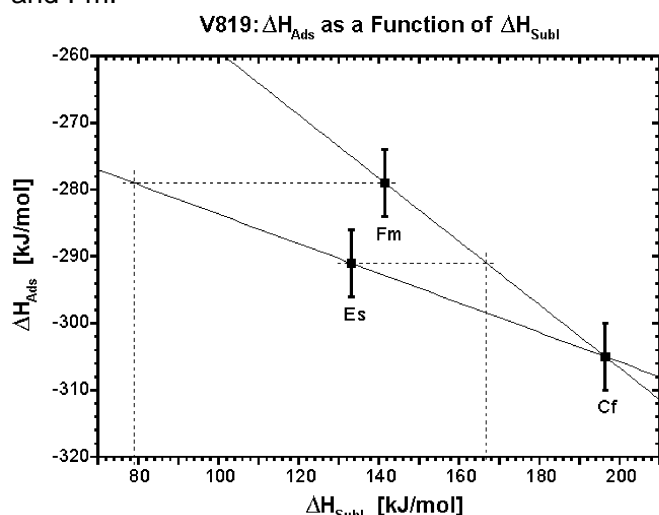


Fig. 1: Calculation of sublimation enthalpies of Es and Fm based on the proportionality between adsorption and sublimation enthalpies

Obviously, the magnitude of the metallic properties of Es determining the adsorption behavior must be between those of Cf and Fm and one has to expect that the sublimation enthalpy of Es is between those of Cf and Fm. Based on the proportionality mentioned above, one can calculate the sublimation enthalpies of Fm and Es from the measured adsorption heats. Fig. 1 illustrates the procedure for the case of adsorption on Mo.

If the sublimation enthalpies of Cf, Es, and Fm are correct, the adsorption sublimation enthalpy pairs should yield a straight line in the diagram. This is not the case. Because Cf has been well investigated, one may assume that its sublimation enthalpy /10/ is correct and there exist two possibilities: If the reported Es sublimation enthalpy is correct, then the Fm sublimation enthalpy would be about 79 kJ/mol, or if the Fm value is correct, then the Es sublimation enthalpy would be about 167 kJ/mol.

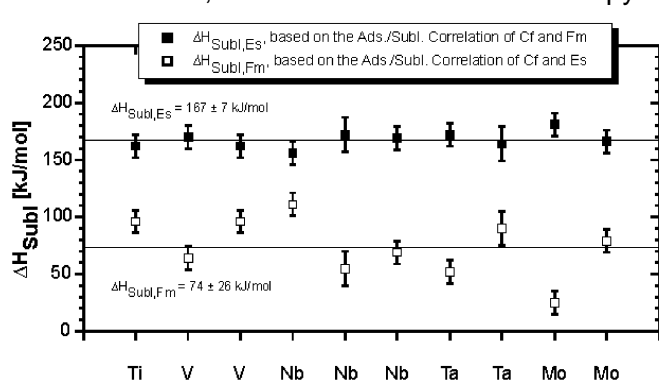


Fig. 2: Calculated sublimation enthalpies of Es and Fm

The results of these calculations for all experiments are shown in Fig. 2. For Es a sublimation heat of 167 ± 15 kJ/mol (95 %) results, which is typical for a metallic divalent element. The sublimation enthalpy of Fm would be 74 ± 52 kJ/mol (95 %), far too small for the metallic divalent Fm.

The sublimation enthalpy of Es calculated here agrees well with the expected value based on theoretical calculations using different approaches /2, 3, 4/. This is shown in Fig. 3, depicting the adsorption data of this work together with theoretically

and experimentally obtained sublimation enthalpies of Cf, Es and Fm.

The similar trends of the desorption and sublimation enthalpies emphasize the possibility to derive sublimation enthalpies from adsorption experiments even for the actinides beyond Fm.

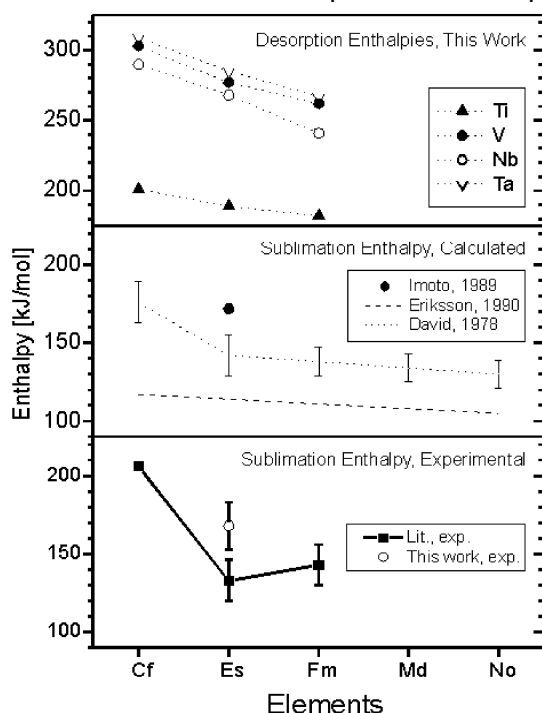


Fig. 3: Thermo chromatographic Desorption and Macroscopic Sublimation Enthalpies of Cf, Es and Fm

- /8/ Taut, S., et al.: Thermo chromatography of Actinides on Metal Columns at High Temperatures. Report FZR-123, Institute of Radiochemistry, Annual Report 1995, 101 (1996)
- /9/ Eichler, B.: *Bestimmung der Adsorptionswärme gasförmiger Metalle auf festen Metalloberflächen (Empirisches Modell)*. Report ZfK-396 (1979)
- /10/ Ward, J.W.: Electronic Structure and Bonding in Transuranics: Comparison with Lanthanides. *J. Less-Common Met.* **93**, 279 (1983)

Acknowledgments

This work was supported by DFG, contract Hu642/1-1.

References

- /1/ Kleinschmidt, P.D., Ward, J.W., Matlack, G.M. Haire, R.G.: The Cohesive Energy of Einsteinium Metal. *High Temp. Sci.* **19**, 267 (1985)
- /2/ Eriksson, O., Brooks, M.S.S., Johansson, B.: Calculated Cohesive Properties of Lanthanide and Lanthanide-Like Actinide Elements. *J. Less-Common Met.* **158**, 207 (1990)
- /3/ David, F., Samhoun, K., Guillaumont, R., Edelstein, N.: Thermodynamic Properties of 5f Elements. *J. Inorg. Nucl. Chem.* **40**, 69 (1978)
- /4/ Imoto, S.: Computed Energy Levels of Actinide Configurations. *J. Nucl. Mat.* **166**, 68 (1989)
- /5/ Haire, R.G., Gibson, J.K.: The enthalpy of sublimation and thermodynamic functions of fermium. *J. Chem. Phys.* **91**, 7085 (1989)
- /6/ Eichler, B.: *Trennung von Radionukliden durch Verflüchtigungsprozesse*. Thesis, Technische Universität Dresden (1976)
- /7/ Nikulin, V.K., Potechina, N.D.: Effekt izmeneniya valentnovo sostoyaniya atomov redkosemelnykh elementov pri adsorbicii na perechodnykh metallach. *Fiz. Tverd. Tela* **20**, 3354 (1978)

THERMOCHROMATOGRAPHY OF NO-259

S. Taut, S. Hübener, B. Eichler¹, A. Türlér¹, H.W. Gäggeler², S.N. Timokhin³, I. Zvara³
 Forschungszentrum Rossendorf e.V., Institute of Radiochemistry

¹ Paul Scherrer Institut Villigen, Switzerland

² Universität Bern, Switzerland

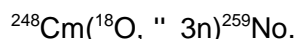
³ Flerov Laboratory of Nuclear Reactions Dubna, Russia

For the first time the adsorption of No on several metals was studied by thermo chromatography.

In continuation of thermo chromatographic adsorption studies of the heaviest actinides /1, 2/ the adsorption of No on several metals was studied.

The experimental setup used in this work was similar to the one described in /2/. We chose a temperature of 1480 K at the starting position in the column and a quartz support tube for the thermo chromatographic columns. These columns, made from metallic Ti, V, Nb, Ta and Mo foils, were wrapped in a Ta lining to protect them from oxygen emitted from the quartz tube. Helium was used as carrier gas with a flow rate of 230 cm³ per minute. It was purified from water and oxygen with molecular sieve and a Ti getter, respectively.

No-259 was produced both at the U-400 cyclotron (FLNR) and at the Philips cyclotron (PSI) in the reaction



The reaction products were collected in Ti catcher foils. After irradiating the target for 4 hours they were used as thermo chromatographic samples without further preparation.

After the thermochromatography the nuclide distributions along the columns were measured off-line by alpha spectroscopy. Fig. 1 shows the activity distribution of ^{259}No and other actinide nuclides on a Nb column.

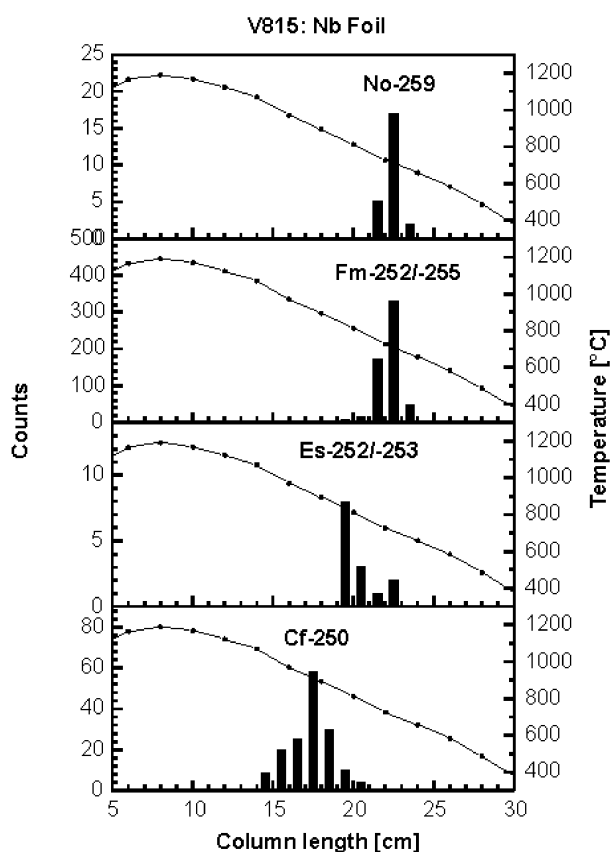


Fig. 1: Thermochromatogram of ^{259}No on a Nb Column

Actinide	Column	Deposition Temp. [K]	Adsorption Enthalpy [kJ/mol]
Cf	Ti	810	-201
	V	1250	-303
	Nb	1173	-290
	Ta	1250	-309
	Mo	1260	-305
Es	Ti	760	-189
	V	1140	-277
	Nb	1083	-268
	Ta	1150	-284
	Mo	1200	-291
Fm	Ti	730	-182
	V	1080	-262
	Nb	973	-241
	Ta	1080	-267
	Mo	1150	-279
No	Ti	710	-177
	V	1060	-258
	Nb	973	-241
	Ta	1040	-258
	Mo	1140	-277

* only one event registered

Tab. 1: Deposition Temperatures and Adsorption Enthalpies of Actinides

The program TECRAD /3/ was used to derive adsorption enthalpies from the deposition temperatures. Tab. 1 summarizes our experimental deposition temperatures and the calculated adsorption enthalpies.

The different adsorption enthalpies of Cf, Es and Fm reflect the tendency from metallic tri- to divalency in the second part of the actinide series.

Nobelium is always adsorbed at the position of Fm. This allows the conclusion, that at Fm the metallic divalency is fully developed. This is in agreement with previous investigations of Md /4/.

Acknowledgments

The authors wish to express appreciation to G.V. Buklanov and N. Trautmann for providing the ^{248}Cm targets. This work was supported by Deutsche Forschungsgemeinschaft, contract Hu642/1-1.

References

- /1/ Hübener, S., et al.: Thermochromatographic studies of heavy actinides in metal columns. *J. Alloys Comp.* **213/214**, 429 (1994)
- /2/ Taut, S., et al.: Thermochromatography of Heavy Actinides - Determination of the Sublimation Enthalpy of Es. accepted by *Radiochimica Acta*
- /3/ Funke, H., Hübener, S., Ross, A., Eichler, B.: Contribution to the Evaluation of Thermochromatographic Experiments. In: Report FZR-43, Institute of Radiochemistry, Annual Report 1993 (1994) p. 53
- /4/ Hübener, S., et al.: Characterization of some Metallic State Properties of Mendelevium and other Actinoids by Thermochromatography. *Radiochimica Acta* **31**, 89 (1982)

CALCULATION OF RATE CONSTANTS OF THE BASIC REACTIONS OF REACTION GAS CHROMATOGRAPHY - TRACE AMOUNT COMPONENTS IN LAMINAR GAS FLOW

M. Grantz

Forschungszentrum Rossendorf e.V., Institute of Radiochemistry

Trace amount components in gas phase follow other statistical rules than main components of the carrier gas. These statistical rules are based on dilution effects. Instructions for the calculation of the rate constant of adsorption and the rate constant of streamline flow in a laminar gas flow for trace amount components are set out.

Any component in the gas phase that has an extremely small concentration - # 10^{-6} volume percent - is called a trace amount component, abbreviated in the following tac. The transport of tac is governed by collisions with the carrier gas. The mean free path δ_x of a species x is the natural parameter to discrete the tube. In the suggested problem the tube radius is much greater than the mean free path. As laminar flow is considered, the radial velocity profile is parabolic and is discreted in this work by:

$$v_{(r, x)} = v_0 [1 - j^2 (j_{m,x} + \frac{1}{2})^{-2}] \quad (1)$$

where $(j_{m,x} + \frac{1}{2})$ is the ratio $(r_{\max} \delta_x^{-1})$, r_{\max} the tube radius, and $0 \neq j \neq j_{m,x}$ is an integer number that discrete the tube into a sum of hollow cylinders with volume flow $V_{(r, x)} t^{-1} = 2j B \delta_x^2 v_{(r, x)} \cdot v_0$ is the maximum flow velocity in the tube.

Let a tac be just desorbed from the tube wall, so at first one has to consider the chance of tac to become a *free* particle in the gas flow in respect to recollision with the wall. This means, that we separate the zone of transport over macroscopic distances along the tube from a radial oriented zone in the gas phase, in that the tac is in a standby position. Geometric factors set up a power series in $4B$ scattering, which yields for the total collision probability with the wall within the approximation that only molecules in the first δ zone hit the wall and that the hypotenuse of a molecule located in this zone next to the wall to the wall is of constant length δ :

$$O_{\text{ads, h}} = (dS/4B) \sum_{p=0}^{\infty} 3_{l=0}^4 (dS/4B)^{2p+1} [1 - 2(dS/4B)]^{2p+1} = 0,2327 \quad (2)$$

with h as average scattering angle of the unit sphere $(dS/4B)_h = \frac{1}{2} I_0^{B/2} d2(1 - \cos 2)$, l is the number of collisions inside the first δ zone and p the probability of rediffusion into the first δ zone from inner hollow cylinders. The chance of collision with the wall is for the first ($l = 1$) and the first three collisions ($1 \neq (p+l) \neq 3$) 87,9% and 99,995% of the total collision probability with the wall respectively. The same considerations lead to the same results for tac to get into the inner zones of the tube. Therefore molecules that are three mean free paths or more away from the wall of the tube can be handled as *free* particles in respect to the existence of the tube wall $1/1$. The quantitative analysis of this problem in kinetic gas theory is new.

The transport of tac along the tube is done by collisions with the carrier gas. The slow velocity of laminar flow [$v_0 \neq 16 \text{ m s}^{-1}$] is a small disturbance of molecular movement given by Maxwell distribution and its average velocity v_M [$v_M \cdot 730 \text{ m s}^{-1}$; Ar, 1000 K] and therefore separable. This is valid especially in the region next to the tube wall, where the laminar flow is vanishing small. The tac distribute according to equation (2): 23% of the desorbed particles will hit the wall without becoming *free* particles. Other 23% will be *free* particles in the laminar gas flow. The rest of 54% will stay inside the standby zone.

For small Knudsen numbers adsorption of *free* particles is related to a probability of collision with the wall instead of drifting through the surfaces of the inner hollow cylinders. The "collisions" with surfaces of inner cylinders are a measure of collisions with other molecules in gas phase. When $\delta_{w, cg}$ is the probability factor of collision with the wall, the rate constant of collision with the wall of the carrier gas is given by:

$$k_{w, cg} = \delta_{w, cg} v_{M, cg} \delta_{cg}^{-1} = (j_{m, cg} + \frac{1}{2}) 2^{-1} [(j_{m, cg} + \frac{1}{2})^2 + (j_{m, cg} - \frac{1}{2})^{-1}] v_{M, cg} \delta_{cg}^{-1} \quad (3)$$

The calculation of the probability factor of collisions with the wall for tac - as a free particle - is more difficult, since the lack of interchange effects has to be taken into consideration. In short it is the difference between a particle and any particle. The interchange effects are characteristic for components of the carrier gas, because it's the pressure dominating substance and the particles are indistinguishable. Also, the pressure forces the carrier gas into regions of less

laminar flow velocity. The probability of a radial place of tac in a carrier gas is given then by averaging over possible location, the laminar flow velocity of the carrier gas at that place and the time of residence of tac there! The probability factor of collision with the wall for tac as *free* particle can be calculated by:

$$\delta_{w, \text{ tac, free}} = \{1 + [1 - j_{m, \text{ tac}}^2 (j_{m, \text{ tac}} + \frac{1}{2})^{-2}]^{-1} (j_{m, \text{ tac}} + \frac{1}{2})^{-1} (j_{m, \text{ tac}} - 1)^{-1} [1 + j_{m, \text{ tac}} - 2 j_{m, \text{ tac}}^3 (j_{m, \text{ tac}} + \frac{1}{2})^{-1} - j_{m, \text{ tac}}^2 (j_{m, \text{ tac}} - 1)^2 (j_{m, \text{ tac}} + \frac{1}{2})^{-2}]\}^{-1} \quad (4a)$$

The rate constant of collision with the wall as an upper limit for adsorption for tac is given by:

$$k_{w, \text{ tac, tot}} = 0_{w, h} (1 + \delta_{w, \text{ tac, free}}) v_{M, \text{ tac}} \delta_{\text{tac}}^{-1} \quad (4b)$$

Where n_x is the particle density in the gas phase of species x. This definition means, that two tac do not interact with another in a macroscopic paraboloid given by the tube radius, v_0 , and the average time of tac spent in the gas phase.

Streamline flow of desorbed tac as a *free* particle in a laminar flow of carrier gas is a function of velocity averaged over the transported volume and secondly of momentum transfer from carrier gas to tac. The average value of $v_{(r, \text{ tac})}$ is found at the half value of the normed generating function of the averaging integral and the rate constant of streamline flow is:

$$k_{\text{sif, tac, free}} = 0,800(227) v_0 \delta_{\text{cg}}^{-1} m_{\text{cg}} m_{\text{tac}}^{-1} \quad (5)$$

The transport of tac as free particle in the gas phase by streamline flow is faster as the average laminar flow velocity of a carrier gas of equal mass. This effect is again a consequence of interchange effects of the molecules of the carrier gas. The rate constant is a product of averaging. Therefore tac and carrier gas follow the same physical interactions but not the same statistics. The error of about 28% is calculated from the normed slope $[V_{(r)} v_{(r)}]$ versus $[j (j_m + \frac{1}{2})^{-1}]$ by averaging with a 2:1:1 weighting of maximal value and the half values. As laminar flow is considered, there is no experimental parameter to influence this error.

The distribution of immediate collision with the wall, residence inside the standby zone and *free* particle gives a total streamline flow rate constant of:

$$Y k_{\text{sif, tac, tot}} = \{(1 - 2 0_{w, h}) (2 j_{m, \text{ tac}} + 1)^{-1} + 0.8 0_{w, h}\} v_0 \delta_{\text{cg}}^{-1} m_{\text{cg}} m_{\text{tac}}^{-1} \quad (6)$$

Acknowledgments

The support of these studies by the BMBF of the Federal Republic of Germany under contract 06 DR 666 I (4)/1 are gratefully acknowledged. I thank Dr. S. Hübener and R. Dressler for productive discussions.

References

/1/ Zvara, I.: Radiochim. Acta **38**, 95 (1985)

OLGA EXPERIMENTS WITH ²⁶¹104 UNDER CHLORINATING AND BROMINATING CONDITIONS

H.W. Gäggeler^{1,2}, B. Eichler², D.T. Jost², D. Piguet², A. Türlér², G.V. Buklanov³, V.Ya. Lebedev³, S.N. Timokhin³, M.V. Vedeneev³, A.B. Yakushev³, I. Zvara³, S.Hübener

Forschungszentrum Rossendorf e.V., Institute of Radiochemistry

¹ Universität Bern, Department of Chemistry and Biochemistry, Bern, Switzerland

² Paul Scherrer Institut, Laboratory of Radio- and Environmental Chemistry, Villigen, Switzerland

³ Joint Institute for Nuclear Research, Flerov Laboratory of Nuclear Reactions, Dubna, Russia

With the On-Line Gas Chromatography Apparatus OLGA III the retention times of element 104 chloride and bromide were measured in a quartz column using the isotope ²⁶¹104 with a half-life of 78 s. With HCl as chlorinating agent element 104 was found to quantitatively pass through the column at 150EC, whereas with HBr this temperature shifted to about 300EC. Under both halogenating conditions, the homologous element Hf passed through the column at higher temperatures than element 104, in agreement with expectations.

A target (diameter 8 mm) containing $1.01 \pm 0.06 \text{ mg/cm}^2$ ²⁴⁸Cm, covered by about 200 Fm/cm² Gd (30 % enriched in ¹⁵²Gd) on a 10 Fm Be foil was bombarded with 0.5 - 0.7 pFA of a 99 MeV ¹⁸O beam at the vertical beam line of the 4m cyclotron at FLNR Dubna. From the target recoil-

ing products were thermalized in the heavy-ion gas-jet chamber from PSI /1/ and transported with a He/C gas-jet through a 2 mm polyethylene capillary of about 5 m length to the OLGA system. Here, the graphite particles were collected on a quartz wool plug kept at about 950 to 1000 EC. To that position about 300 ml/min of HCl or HBr gas were added to form volatile halides which were then transported along a 2 m 1.0 mm i.d. quartz column kept at an isothermal but variable temperature. Behind the column the molecules were reattached to KCl particles and transported through a 5 m long 2 mm i.d. capillary to the PSI tape system for counting (45 s steps).

A typical α -spectrum collected during a two hour OLGA run with HBr gas at 300 EC from all 6 detectors is depicted in Fig. 1. Besides small lines at 6.6 and 7.7 MeV, from ^{211}Bi and ^{214}Po (decay product of ^{214}Bi), a group of 5 counts is found between 8.3 and 8.4 MeV. We assign this group to $^{261}104$ and its daughter ^{257}No . This assignment is corroborated by the decay of this event group (insert in Fig. 1).

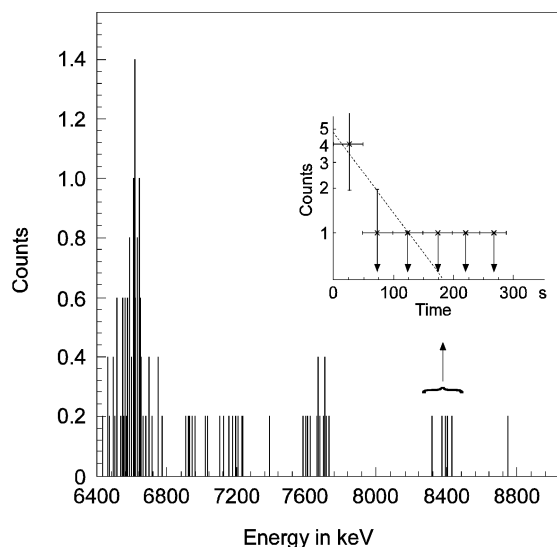


Fig. 1: Sum of all α -events collected with the 6 detectors during an OLGA run at 950/300°C with 300 ml/min HBr gas

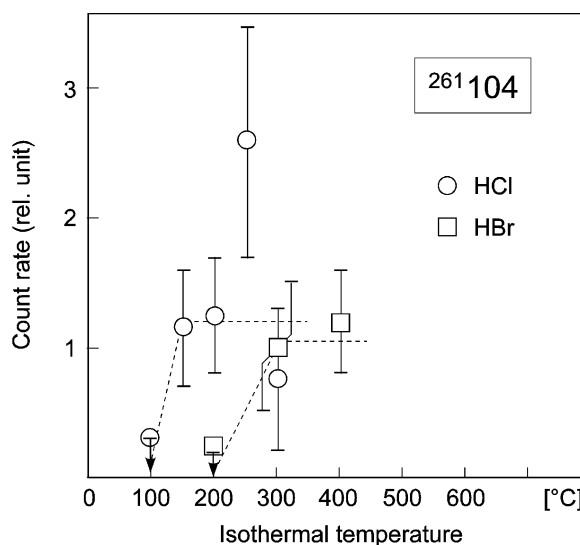


Fig. 2: Chromatographic curves for the α -event group between 8.3 to 8.4 MeV assigned to $^{261}104$ and its daughter nuclide ^{257}No .

In Fig. 2 the measured yields of the event group between 8.3 to 8.4 MeV is shown as a function of the OLGA temperature for HCl and Hbr. We observe that element 104 forms volatile molecules with HCl above about 150 EC. With HBr the retention temperature at which maximum yield is found is shifted to about 300 EC.

This shift is indicative of a lower volatility of element 104 bromide if compared to element 104 chloride. Most likely, the compounds formed in the OLGA systems under our experimental conditions are 104Cl_4 and 104Br_4 , respectively.

Simultaneously measured Hf produced in the reaction with Gd indicated a lower volatility of both the chloride and the bromide if compared to the corresponding 104 chloride and bromide, respectively. Having in mind that ZrCl_4 and ZrBr_4 are slightly less volatile than the corresponding Hf compounds we have the volatility sequence element 104 > Hf > Zr, for both the chlorides and the bromides, respectively.

The high volatility of element 104 chloride is in line with estimates using relativistic models /2/.

Acknowledgments

We highly appreciate the excellent beam of ^{18}O delivered to the experiment with the 4m cyclotron at FLNR. The warm hospitality for some of us during the stay at Dubna is highly appreciated. This project was supported by INTAS under contract 94-424.

References

- /1/ D. Piguet et al., PSI Annual Report 1994, Annex IIIA, p. 68, PSI (1995)
- /2/ A. Türler, Radiochim. Acta **72**, 7 (1996).

FIRST THERMOCHEMICAL PROPERTY OF SEABORGIUM DETERMINED

S. Hübener, M. Grantz, St. Taut, A. Vahle for a

LBL Berkeley - University Bern - FLNR Dubna - GSI Darmstadt - TU Dresden - Chalmers University of Technology Göteborg - GH Kassel - ITS and LLNL Livermore - University Mainz - University Oslo - FZ Rossendorf - JAERI Tokai - PSI Villigen collaboration

Using the PSI On-Line Gas Chromatography Apparatus OLGA III the nuclides ^{265}Sg and ^{266}Sg were unambiguously identified and their half-lives determined. As predicted by relativistic calculations and by extrapolations of chemical properties, it was demonstrated that Sg oxychlorides are indeed less volatile than their lighter homologue Mo- and equally or less volatile than W-oxychlorides.

After a first successful experiment /1/, in which we chemically separated Sg in the form of volatile oxychlorides and unambiguously identified the nuclides ^{265}Sg and ^{266}Sg using OLGA III, a second series of experiments was performed. It was our goal to confirm the results of the first experiment and to determine the volatility of Sg-oxychlorides in respect to their lighter homologue group 6 oxychlorides.

In relativistic calculations /2/ it was shown that SgO_2Cl_2 should be the most stable oxychloride compound of Sg, and the least volatile MO_2Cl_2 compound. From extrapolations of thermochemical properties it was concluded that SgO_2Cl_2 , as a macroscopic compound, has a higher sublimation enthalpy than WO_2Cl_2 or MoO_2Cl_2 and also SgOCl_4 . With the aid of an empirical correlation between sublimation enthalpy and adsorption enthalpy on quartz surfaces $\Delta H_a^{0(T)}(\text{SgO}_2\text{Cl}_2) = -106 \text{ kJ/mol}$ was predicted /3/.

First, the volatility of WO_2Cl_2 was carefully measured under conditions which were identical to the actual Sg experiment. Short-lived W-isotopes were produced in the 119 MeV ^{22}Ne on ^{152}Gd reaction at the GSI UNILAC accelerator.

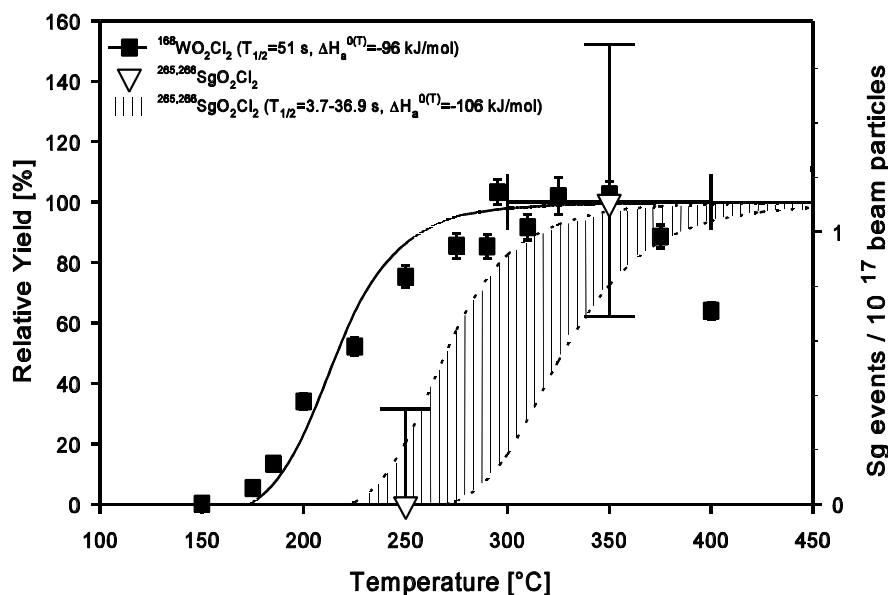


Fig.1: Relative yield of WO_2Cl_2 and SgO_2Cl_2 as a function of isothermal temperature and the predicted yield of $^{265,266}\text{SgO}_2\text{Cl}_2$ for $\Delta H_a^{0(T)}(\text{SgO}_2\text{Cl}_2) = -106 \text{ kJ/mol}$ and a half-life interval from 3.7 to 36.9 s.

The Sg experiment was performed with a mixed $^{248}\text{Cm}/^{152}\text{Gd}$ target ($750 \mu\text{g}/\text{cm}^2$ ^{248}Cm , $150 \mu\text{g}/\text{cm}^2$ ^{152}Gd) at a ^{22}Ne beam energy of 123 MeV. The same quartz glass column as in the preceding W experiment was used. Spontaneous fission decays and α -decays were registered with the GSI Rotating Wheel Multidetector Analyzer ROMA. Simultaneously, the yield of short-lived W was monitored with a HPGe detector, in order to ensure that the chemical separation was proceeding with high chemical yield.

The yield curve measured for $^{168}\text{WO}_2\text{Cl}_2$ ($t_{1/2} = 51 \text{ s}$) is shown in Fig. 1. With the Monte Carlo method an adsorption enthalpy $\Delta H_a^{0(T)}(\text{WO}_2\text{Cl}_2) = -96 \text{ kJ/mol}$ was determined in good agreement with a previous measurement /1/. In addition, the shape of the calculated yield curve corresponds very well to the experimental data.

At 350°C isothermal temperature and with a beam dose of $2.31 \cdot 10^{17}$ two decay chains attributed to ^{265}Sg and one decay chain attributed to ^{266}Sg were observed, confirming earlier results where

Sg decays were observed at 300°C and 400°C isothermal temperature. At the lower isothermal temperature of 250°C a beam dose of 5.22×10^{17} was accumulated without observing decays of $^{265,266}\text{Sg}$. Nevertheless, ^{168}W was still detected at about 75% of its yield at 350°C and was used to monitor system performance.

Tab. 1: $^{265,266}\text{Sg}$ events observed in the 1996 experiments.

E_1 [MeV]	$^a t_1$ [s]	E_2 [MeV]	$^a t_2$ [s]	Mode	Decay Assignment	Isothermal Temperature
8.87	7.0	8.20	15.2	MD	$^{265}\text{Sg} \rightarrow ^{261}\text{Rf}$ or ^{257}No	350°C
8.68	1.4	8.35	150.2	MD	$^{265}\text{Sg} \rightarrow ^{261}\text{Rf}$ or ^{257}No	350°C
8.74	15.1	SF	1.7		$^{266}\text{Sg} \rightarrow ^{262}\text{Rf}$	350°C
8.65	3.5	SF	2.4		$^{266}\text{Sg} \rightarrow ^{262}\text{Rf}$	119 MeV, direct catch, tape system

In Tab. 1 all event chains attributed to the decay of ^{265}Sg and ^{266}Sg are summarized. Together with the decay chains observed in the 1995 experiments /1/, new more accurate half-lives and production cross sections can be calculated for ^{265}Sg and ^{266}Sg (122 ± 2 MeV, 68% c.i.):

$$^{265}\text{Sg}: \quad t_{1/2} = 5.4 (+4.4/-1.7) \text{ s} \quad \text{and} \quad F = 395 (+250/-180) \text{ pb}, \quad \text{and for}$$

$$^{266}\text{Sg}: \quad t_{1/2} = 15.6 (+21.3/-5.7) \text{ s} \quad \text{and} \quad F = 22 (+20/-13) \text{ pb}.$$

In Fig. 1 all seven Sg events which were measured at 300°C to 400°C isothermal temperature were summarized to one data point. Furthermore, the right hand scale of Fig. 1 was chosen in such a manner that the mean number of detected Sg events per 10^{17} beam particles corresponded to 100% relative yield. The error limits on the Sg data point in relative yield correspond therefore to the 68% error of 7 detected events. At 250°C isothermal temperature 0 events were observed. The upper error limit of 0 events at a 68% confidence level corresponds to 1.84 events /4/. Also shown are the expected yield curve intervals for $^{265}\text{SgO}_2\text{Cl}_2$ and $^{266}\text{SgO}_2\text{Cl}_2$ calculated for $\Delta H_a^{(T)}(\text{SgO}_2\text{Cl}_2) = -106$ kJ/mol and half-lives (including error limits) from this report. The predicted volatility of SgO_2Cl_2 is in full agreement with the available experimental data. In order to compare the volatility of SgO_2Cl_2 with its lighter homologues the limits of possible adsorption enthalpies have to be determined. They are given by a relative yield # 32% at 250°C and a lower half-life limit of 3.7 s and a relative yield of # 62% and an upper half-life limit of 36.9 s. The corresponding interval of adsorption enthalpy is:

$$- 95 \text{ kJ/mol} \leq \Delta H_a^{(T)}(\text{SgO}_2\text{Cl}_2) \leq - 130 \text{ kJ/mol}.$$

Therefore, the relative volatility of group 6 oxychlorides is $\text{MoO}_2\text{Cl}_2 > \text{WO}_2\text{Cl}_2 \geq \text{SgO}_2\text{Cl}_2$. The error limits on the adsorption enthalpy depend not only on the statistics of the experimental data but also on the error limits of the half-lives. More accurate half-life measurements will significantly reduce the current interval of possible adsorption enthalpy values. Nevertheless, we have determined the first thermochemical property of a compound of the heaviest element currently accessible by chemical means.

References

- /1/ A. Türler et al., PSI Annual Report 1995 / Annex IIIA, 65 (1996).
- /2/ V. Pershina et al., J. Phys. Chem. **100**, 8748 (1996).
- /3/ B. Eichler et al., PSI Annual Report 1993 / Annex IIIA, 95 (1994).
- /4/ K.H. Schmidt et al., Z. Phys. **A316**, 19 (1984).

II. PUBLICATIONS, PATENTS, LECTURES AND POSTERS

PUBLICATIONS

Allen, P.G., D.K. Shuh, J.J. Bucher, N.M. Edelstein, T. Reich, M.A. Denecke, H. Nitsche
EXAFS determination of uranium structures: the uranyl ion complexed with tartaric, citric, and malic acids
Inorganic Chemistry **35**, 784 (1996)

Allen, P.G., G. Bernhard, J.J. Bucher, S.B. Clark, M.A. Denecke, N.M. Edelstein, G. Geipel, C.A. Langton, H. Moll, H. Nitsche, T. Reich, D.K. Shuh
Studies of Actinides by X-ray Absorption Spectroscopy
Stanford Synchrotron Radiation Laboratory 1995 Activity Report, p. 179 (1996)

Allen, P.G., J.J. Bucher, N.M. Edelstein, D.K. Shuh, T. Reich, M. Denecke, H. Nitsche
Applications of Synchrotron Radiation to Chemical Issues in the Environmental Sciences
in: K.L. D'Amico, L.J. Terminello, D.K. Shuh (Eds.); *Synchrotron Radiation Techniques in Industrial, Chemical, and Materials Science*; Plenum Press, New York (1996), pp. 169-185

Al Mahamid, I., K.A. Becraft, N.L. Hakem, R.C. Gatti, H. Nitsche
Stability of various plutonium valence states in the presence of NTA and EDTA
Radiochimica Acta **74**, 129 (1996)

Bernhard, G., G. Geipel, V. Brendler, H. Nitsche
Speciation of uranium in seepage waters from a mine tailing pile studied by time-resolved laser-induced fluorescence spectroscopy (TRLFS)
Radiochimica Acta **74**, 87-91 (1996)

Brendler, V., W. Voigt
Isopiestic measurements at high temperatures. III. The ternary systems $\text{KCl-MgCl}_2\text{-H}_2\text{O}$ at 155°C
Journal of Solution Chemistry **25** (1), 83-93 (1996)

Brendler, V., G. Geipel, G. Bernhard, H. Nitsche
Complexation in the system $\text{UO}_2^{2+}/\text{PO}_4^{3-}/\text{OH}^-(\text{aq})$: potentiometric and spectroscopic investigations at very low ionic strengths
Radiochimica Acta **74**, 75-80 (1996)

Denecke, M.A., H. Moll, S. Pompe, D. Rettig, H. Friedrich, G. Bernhard, T. Reich, H. Nitsche
Determination of the Arsenic Oxidation State in Environmentally Relevant Waters by XANES Spectroscopy
HASYLAB Annual Report 1995, **2**, 593 (1996)

Denecke, M.A., S. Pompe, H. Moll, K.H. Heise, T. Reich, G. Bernhard, H. Nitsche
EXAFS Studies on Anhydrous Complexes of Uranyl and Ortho-Substituted Benzoic Acids
HASYLAB Annual Report 1995, **2**, 629 (1996)

Eichler, B., S. Hübener, N. Erdmann, K. Eberhardt, H. Funk, G. Herrmann, S. Köhler, N. Trautmann, G. Passler, F.-J. Urban
Eine Atomstrahlquelle für Actinoide - Konzeption, Aufbau und Wirkungsweise
PSI Bericht Nr. 96-03, Januar 1996

Geipel, G., G. Bernhard, V. Brendler, H. Nitsche
Sorption of uranium(VI) on rock material of a mine tailing pile: solution speciation by fluorescence spectroscopy
Radiochimica Acta **74**, 235-238 (1996)

Hudson, E.A., P.G. Allen, L.J. Terminello, M.A. Denecke, T. Reich
Polarized X-ray Absorption Spectroscopy of the Uranyl Ion: Comparison of Experiment and Theory
Physical Review B **54**, 156 (1996)

Kubatova, A., M. Matucha, M. Bubner
Application of ^{13}C -labeled polychlorinated biphenyl congener 153 as internal standard in the gas chromatographic-mass spectrometric analysis of polychlorinated biphenyls
J. Chromatogr. A **750**, 245 (1996)

- Moll, H., G. Geipel, W. Matz, G. Bernhard, H. Nitsche
Solubility and speciation of $(\text{UO}_2)_2\text{SiO}_4 \cdot 2\text{H}_2\text{O}$ in aqueous systems
Radiochimica Acta **74**, 3 (1996)
- Morss, L.R., M.A.J. Schmidt, K.L. Nash, P.G. Allen, J.J. Bucher, N.M. Edelstein, D.K. Shuh, M.A. Denecke, H. Nitsche, T. Reich
EXAFS studies of lanthanide coordination in crystalline phosphates and amorphous phytates in: K.L. D'Amico, L.J. Terminello, D.K. Shuh (Eds.); *Synchrotron Radiation Techniques in Industrial, Chemical, and Materials Science*; Plenum Press, New York (1996), pp. 229-235
- Nebelung, C., S. Hübener, G. Bernhard
Methodenentwicklung zur Freimessung von Bauschutt auf alpha-aktive Nuklide (Th, U, Np, Pu, Am)
Schlußbericht BMBF-Fördervorhaben 02 S 7442 2
- Nefedov, V.I., Yu.A. Teterin, T. Reich, H. Nitsche
Determination of Interatomic Distances in Uranyl Compounds on the Basis of $\text{U6p}_{3/2}$ -Level Splitting
Doklady Akademii Nauk **348**, 634 (1996) (in Russian)
- Nitsche, H., R.J. Silva
Investigation of the carbonate complexation of Pu(IV) in aqueous solution
Radiochimica Acta **72**, 65 (1996)
- Novak, C.F., H. Nitsche, H.B. Silber, K.E. Roberts, P.C. Torretto, T. Prussin, K. Becraft, S.A. Carpenter, D.E. Hobart, I. Al Mahamid
Neptunium(V) and neptunium(VI) solubilities in synthetic brines of interest to the Waste Isolation Pilot Plant (WIPP)
Radiochimica Acta **74**, 31 (1996)
- Pompe, S., M.A. Denecke, H. Moll, M. Bubner, H. Funke, T. Reich, K.H. Heise, G. Bernhard, H. Nitsche
Investigation of the Interaction of Humic Acids with Uranyl Ions by Extended X-ray Absorption Fine Structure Spectroscopy (EXAFS)
HASYLAB Annual Report 1995, **2**, 595 (1996)
- Pompe, S., M. Bubner, M.A. Denecke, T. Reich, A. Brachmann, G. Geipel, R. Nicolai, K.H. Heise, H. Nitsche
A comparison of natural humic acids with synthetic humic acid model substances: characterization and interaction with uranium(VI)
Radiochimica Acta **74**, 135-140 (1996)
- Pompe, S., K.H. Heise, H. Nitsche
Capillary electrophoresis for a "finger-print" characterization of fulvic and humic acids
J. Chromatogr. A **723**, 215 (1996)
- Reich, T., M.A. Denecke, S. Pompe, H. Nitsche, P.G. Allen, J.J. Bucher, N.M. Edelstein, D.K. Shuh
Characterization of Uranyl Ions with Humic Acids by X-ray Absorption Spectroscopy in: K.L. D'Amico, L.J. Terminello, D.K. Shuh (Eds.); *Synchrotron Radiation Techniques in Industrial, Chemical, and Materials Science*; Plenum Press, New York (1996), pp. 215-228
- Reich, T., H. Moll, M.A. Denecke, G. Geipel, G. Bernhard, H. Nitsche, P.G. Allen, J.J. Bucher, N. Kaltsoyannis, N.M. Edelstein, D.K. Shuh
Characterization of hydrous uranyl silicate by EXAFS
Radiochimica Acta **74**, 219 (1996)
- Schumann, D., S. Fischer, R. Dressler, S. Taut, H. Nitsche, N. Trautmann, M. Schädel, W. Bröchle, B. Schausten, A.F. Novgorodov, R. Misak, B. Eichler, H. Gäggler, D. Jost, A. Türler, H. Bruchertseifer
Sorption of subgroup IV, V, and VI elements on ion exchangers from HCl/HF solutions: model experiments for chemical studies of the elements 105 and 106 in aqueous solution
Radiochimica Acta **72**, 137 (1996)

Schumann, D., M. Andrassy, H. Bruchertseifer, W. Bröchle, R. Misiak, H. Nitsche, A.F. Novgorodov, M. Schädel, B. Schausten
Sorption Behaviour of W, Hf, Lu, U and Th Radionuclides on Ion Exchange Resins
GSI Scientific Report 1995, GSI 96-1, S. 174

Schädel, M., J. Alstad, M. Andrassy, W. Bröchle, R. Dressler, K. Eberhardt, B. Eichler, B. Fricke, H.W. Gäggeler, M. Gärtner, R. Günther, K.E. Gregorich, R. Heimann, D.C. Hoffman, S. Hübener, E. Jäger, D.T. Jost, B. Kadkhodayan, J.V. Kratz, D.M. Lee, R. Malmbeck, M. Mendel, R. Misiak, A. Nähler, Y. Nagame, J.P. Omtvedt, Y. Oura, W. Paulus, V. Pershina, F. Rocker, B. Schausten, E. Schimpf, D. Schumann, A. Seibert, G. Skarnemark, E. Sylwester, S. Taut, S. Timokhin, U. Tharun, P. Thörle, N. Trautmann, A. Türler, N. Wiehl, B. Wierczinski, G. Wirth, A. Yakushev, S. Zauner
Chemistry with Element 106, Seaborgium - The Isotopes ²⁶⁵Sg and ²⁶⁶Sg
GSI Scientific Report 1995, GSI 96-1, S. 10

Taut, S., S. Hübener, H. Nitsche, B. Eichler, H.W. Gäggeler, M. Schädel, E. Jäger, W. Bröchle
Thermochromatography of Heavy Actinides at High Temperatures
GSI Scientific Report 1995, GSI 96-1, S. 175

Teterin, Yu.A., V.I. Nefedov, K.E. Ivanov, A.S. Baev, G. Geipel, T. Reich, H. Nitsche
X-ray Photoelectron Spectroscopy Investigation of the Interaction of UO₂(ClO₄)₂ with Diabase
Doklady Akademii Nauk **350**, 503 (1996) (in Russian)

Teterin, Yu.A., V.I. Nefedov, K.E. Ivanov, A.S. Baev, G. Geipel, T. Reich, H. Nitsche
X-ray Photoelectron Spectroscopy Investigation of the Interaction of UO₂(ClO₄)₂ with Calcite and Diabase Minerals
Zhurnal Neorganicheskoi Khimii **41**, 1884 (1996) (in Russian)

Türler, A., B. Eichler, D.T. Jost, D. Piquet, H.W. Gäggeler, K.E. Gregorich, B. Kadkhodayan, S.A. Kreek, D.M. Lee, M. Mohar, E. Sylwester, D.C. Hoffman, S. Hübener
On-line Gas Phase Chromatography with Chlorides of Niobium and Hahnium (Element 105)
Radiochimica Acta **73**, 55-66 (1996)

Türler, A., B. Eichler, D.T. Jost, R. Dressler, D. Piquet, H.W. Gäggeler, S. Hübener, M. Boettger, M. Grantz
Studies of Mo-Oxichlorides as Homologues of Element 106
Labor für Radio- und Umweltchemie der Universität Bern und des Paul Scherrer Instituts Annual Report 1995, 28.02.1996

Uhlirva, H., M. Matucha, M. Kretschmar, M. Bubner
Aufnahme und Verteilung von Trichloressigsäure in Trieben Norwegischer Fichte
Z. Umweltchem. Ökotox. **8** (3), 138 (1996)

Vahle, A., S. Hübener, R. Dressler, B. Eichler, A. Türler
Monte Carlo Simulation of Reaction Gas Chromatography of Group 6 Elements
GSI Scientific Report 1995, GSI 96-1, S. 176

Yarzhemsky, V.G., T. Reich, L.V. Chernysheva, P. Streubel, R. Szargan
Lineshape Asymmetry Parameters in X-ray Photoelectron Spectra
Journal of Electron Spectroscopy and Related Phenomena **77**, 15 (1996)

Zänker, H., W. Richter, G. Hüttig, H. Nitsche, W. Wiesener, A. Mende;
Charakterisierung der Submicron-Partikel in einem umweltrelevanten Wasser: Stauwasser in einer Kommunal Mülldeponie über einem Schlammteich (Tailing) der Uranerzaufbereitung in Freital/Sachsen
FZR Bericht FZR-155, Oktober 1996

PATENTS

Förster, E., K.H. Heise, H. Nitsche
Verfahren zur elektrochemischen Mineralisierung von insbesondere C-14-markierten organischen Abfällen
Patent registered by Deutsches Patentamt; Az. 196 46 049.2 (08.11.1996)

PH.D. THESIS

Vahle, A.

Hochtemperaturgaschromatographie mit Spuren Mengen der Homologen des Elementes 106 im O_2 - $H_2O_{(g)}/SiO_{2(s)}$ -System
TU Dresden, Germany, 1996

LECTURES

Allen, P.G., D.K. Shuh, J.J. Bucher, N.M. Edelstein, C.A. Palmer, T. Reich, M.A. Denecke, H. Nitsche

Chemical Speciation Studies of Radionuclides by EXAFS
9th International Conference on X-ray Absorption Fine Structure
Grenoble, France, 26.-30.08.1996

Baraniak, L., M. Thieme, H. Funke, G. Schuster
Stofftransportvorgänge des Radiums in gelaugten und ungelagerten Sedimenten im Bereich der Lagerstätte Königstein
WISMUT GmbH
Chemnitz, Germany, 30.01.1996

Bernhard, G., G. Geipel, V. Brendler, H. Nitsche
Bestimmung der Speziation des Urans in bergbautypischen Wässern
Workshop: Sanierung der Hinterlassenschaften des Uranbergbaus, Teil 1, SMU
Dresden, Germany, 11.11.1996

Bernhard, G.
Herstellung von Molybdän-99/Technetium-99m - Basis der Nuklearmedizin
TU München, Institut für Radiochemie
München, Germany, 26.11.1996

Bonsdorf, G., M.A. Denecke, K. Schäfer, S. Christen, H. Langbein, W. Gunßer
X-ray Absorption Spectroscopic and Mössbauer Studies of Redox and Cation-Ordering Processes in Manganese Ferrite
International Symposium on the Reactivity of Solids
Hamburg, Germany, 09.-12.09.1996

Brendler, V., G. Bernhard, G. Geipel, H. Nitsche
Erarbeitung und Bewertung physiko-chemischer Modelle
Workshop: Sanierung der Hinterlassenschaften des Uranbergbaus, Teil 1, SMU
Dresden, Germany, 11.11.1996

Geipel, G., G. Bernhard, H. Nitsche
Karbonatkomplexierung vom Uranium unter den natürlichen Bedingungen der Bergbaufolgelandschaften
Freiberger Isotopenkolloquium, TU Bergakademie Freiberg
Freiberg, Germany, 30.09.-02.10.1996

Geipel, G., V. Brendler, A. Brachmann, G. Bernhard, H. Nitsche
Laserinduzierte spektroskopische Untersuchungen an bergbaulich beeinflussten Wässern Sachsens
Seminarvortrag, Institut für Nukleare Entsorgung im Forschungszentrum Karlsruhe
Karlsruhe, Germany, 17.12.1996

Geipel, G., T. Reich, V. Brendler, G. Bernhard, H. Nitsche
Laser and X-Ray Absorption Studies to Characterize Uranium Interfacial Phenomena
International Workshop on Interfacial Effects in Quantum Engineering Systems
Mito, Japan, 21.-23.08.1996

Hübener, S.
Thermochromatography of nobelium in metal columns
Seminar of the Flerov Laboratory for Nuclear Reactions, JINR
Dubna, Russia, 14.02.1996

Nebelung, C., H. Nitsche, S. Hübener, G. Bernhard
Stand des Projektvorhabens BMBF-02 S 7442 2 und Ziele des Neuantrages
5.Sitzung des Arbeitskreises „Freimessung von Anlagenteilen und Bauschutt aus dem Abbau
kerntechnischer Anlagen des Brennstoffkreislaufes“, TU München
München, Germany, 15.03.1996

Nebelung, C., H. Nitsche
Direktmessung alpha-aktiver Nuklide
6. Sitzung Arbeitskreis “Freimessung von Anlagenteilen und Bauschutt aus dem Abbau kern-
technischer Anlagen des Brennstoffkreislaufes”
Rossendorf, Germany, 06.11.1996

Nebelung, C., H. Nitsche, S. Hübener, G. Bernhard
Entwicklung einer einfachen " -Meßmethode
Seminar Freigabemessung, Ministerium für Umwelt und Verkehr Baden-Württemberg
Stuttgart, Germany, 19.11.1996

Nitsche, H.
Huminsäure-Modellsubstanzen: Charakterisierung und Komplexierungsverhalten von Uran
TU München, Institut für Hydrogeologie, Hydrochemie und Umweltanalytik
München, Germany, Januar 1996

Nitsche, H.
Forschungsarbeiten zum Umweltausbreitungsverhalten von Radionukliden
Friedrich-Schiller-Universität Jena, Biologisch-Pharmazeutische Fakultät
Jena, Germany, February 1996

Nitsche, H., R.J. Silva
Actinide environmental radiochemistry
211th ACS National Meeting; Symposium honoring the Centennial of the Discovery of Radioac-
tivity
New Orleans, USA, March 1996

Nitsche, H.
Speciation measurements in environmentally relevant systems
VTT Technical Research Center
Espoo, Finland, May 1996

Nitsche, H.
Uranium speciation in seepage and flood waters of uranium mines and mine tailing piles
University of Helsinki, Institute of Radiochemistry
Helsinki, Finland, May 1996

Nitsche, H.
Moderne Methoden zur Radionuklid-/Metallspeziation: Anwendungen in Chemie und Biologie
Technische Universität Dresden, Institut für Pflanzen- und Holzchemie
Dresden, Germany, May 1996

Nitsche, H.
Modern techniques for radionuclide and metal speciation: X-ray absorption spectroscopy and
time-resolved fluorescence spectroscopy
Chalmers University of Technology
Gothenburg, Sweden, June 1996

Nitsche, H.
The Institute of Radiochemistry at the Forschungszentrum Rossendorf e.V.: A research profile
V.G. Khlopin Radium Institute
St. Petersburg, Russia, June 1996

Nitsche, H.
Research at the Institute of Radiochemistry at the Forschungszentrum Rossendorf e.V.
St. Petersburg State University, Institute of Radiochemistry
St. Petersburg, Russia, June 1996

Nitsche, H.
XAS studies of model and environmental radionuclide systems: present and future
9th International Conference on X-ray Absorption Fine Structure
Grenoble, France, 26.-30.08.1996

Nitsche, H., V. Brendler, G. Geipel, T. Reich, G. Bernhard
Speciation in model systems and environmental samples - modern techniques
212th ACS National Meeting
Orlando, USA, 25.-29.08.1996

Nitsche, H.
From concentration to molecular structure: selected examples of non-nuclear methods in radiochemistry
4th International Conference on Nuclear and Radiochemistry
Saint Malo, France, 08.-13.09.1996

Nitsche, H.
Uranium mining in East Germany: research opportunities for waste treatment and remediation
Paul Scherrer Institute
Villingen, Switzerland, September 1996

Nitsche, H.
Grundlagenforschung zur Remediation radioaktiv kontaminierter Gebiete
Universität Leipzig, Fakultät für Physik und Geowissenschaften
Leipzig, Germany, Oktober 1996

Nitsche, H.
X-ray absorption spectroscopy (XAS) and laser fluorescence studies for environmental uranium research
European Commission, Institute for Transuranium Research
Karlsruhe, Germany, November 1996

Reich, T., E.A. Hudson, M.A. Denecke, P.G. Allen, H. Nitsche
Structural Analysis of Uranium(VI) Complexes by X-ray Absorption Spectroscopy
1st Russian-German Seminar on X-ray Photoelectron Spectroscopy and X-ray Spectroscopy
Voronezh, Russia, 27.05.-01.06.1996

Reich, T.
Structural Analysis of Uranium(VI) Complexes by X-ray Absorption Spectroscopy
Seminar at Department of Geological and Environmental Sciences, Stanford University
Stanford, CA, USA, 17.06.1996

Reich, T.
Structural Analysis of Uranium(VI) Complexes by X-ray Absorption Spectroscopy
Actinide Chemistry Group Seminar, Lawrence Berkeley National Laboratory
Berkeley, CA, USA, 21.06.1996

Reich, T., H. Nitsche
X-ray Absorption Spectroscopy in Environmental Radiochemistry at FZR
1996 Stanford Synchrotron Radiation Laboratory User's Conference
Stanford, CA, USA, 24.-25.10.1996

Türler, A., W. Bröchle, R. Dressler, B. Eichler, H.W. Gäggeler, M. Gärtner, K.E. Gregorich, D.C. Hoffman, S. Hübener, E. Jäger, D.T. Jost, A.B. Yakushev, M. Schädel, E. Schimpf, S.N. Timokhin
On-Line Gas Chemistry of Seaborgium (Element 106) Oxichlorides
4th International Conference on Nuclear and Radiochemistry
Saint Malo, France, 08.-13.09.1996

POSTERS

- Arnold, T., T. Zorn, G. Bernhard, H. Nitsche
Sorption of Uranium(VI) onto Phyllite
Euresco conference on "Geochemistry of Crustal Fluids"
Seefeld, Austria, 06.-11.12.1996
- Baraniak, L., M. Thieme, H. Funke, G. Bernhard, K. Nindel, J. Schreyer, H. Nitsche
Radium Sorption on Sandy and Clayey Sediments of the Upper Saxon Elbe River Valley
4th International Conference on Nuclear and Radiochemistry
Saint Malo, France, 08.-13.09.1996
- Bernhard, G., G. Geipel, V. Brendler, A. Brachmann, H. Nitsche
Speciation of Uranium in Natural Waters of a Uranium Mining Area
4th International Conference on Nuclear and Radiochemistry
Saint Malo, France, 08.-13.09.1996
- Bernhard, G., G. Geipel, V. Brendler, A. Brachmann, H. Nitsche
Speziation von Uranium in bergbaulich beeinflussten Wässern Sachsens
GDCh, Umwelttagung 1996
Ulm, Germany, 07.-10.10.1996
- Brendler, V., G. Geipel, G. Bernhard, H. Nitsche
Modern methods for the determination of thermodynamic properties of aqueous complexes:
application to the system uranyl-phosphate-water
Euresco conference on "Geochemistry of Crustal Fluids"
Seefeld, Austria, 06.-11.12.1996
- Bubner, M., C. Bock, M. Kolb, E. van Raaij, G. Bruhn, K.H. Heise, H. Nitsche, H. Harms, U.
Förstner
Abbau polychlorierter Biphenyle (PCB) in Pflanzen und bei Kompostierungsprozessen - Unter-
suchungen mit [¹⁴C]PCB Nr. 77
GDCh, Umwelttagung 1996
Ulm, Germany, 07.-10.10.1996
- Denecke, M.A., T. Reich, S. Pompe, M. Bubner, K.H. Heise, H. Nitsche, P.G. Allen, J.J. Bucher,
N.M. Edelstein, D.K Shuh
Differentiating between monodentate and bidentate carboxylate ligands coordinated to uranyl
ions using EXAFS
9th International Conference on X-ray Absorption Fine Structure
Grenoble, France, 26.-30.08.1996
- Denecke, M.A., H. Moll, S. Pompe, D. Rettig, H. Friedrich, G. Bernhard, T. Reich, H. Nitsche
Determination of the Arsenic Oxidation State in Environmentally Relevant Waters by XANES
Spectroscopy
HASLAB-Nutzertreffen
Hamburg, Germany, 26.01.1996
- Denecke, M.A., S. Pompe, H. Moll, K.H. Heise, T. Reich, G. Bernhard, H. Nitsche
EXAFS Studies on Anhydrous Complexes of Uranyl and ortho-Substituted Benzoic Acids
HASLAB-Nutzertreffen
Hamburg, Germany, 26.01.1996
- Denecke, M.A., S. Pompe, H. Moll, M. Bubner, T. Reich, K.H. Heise, G. Bernhard, H. Nitsche
EXAFS Untersuchungen an Uranyl-Huminsäure-Komplexen
GDCh, Umwelttagung 1996
Ulm, Germany, 07.-10.10.1996
- Denecke, M.A., H. Friedrich, T. Reich, G. Bernhard, D. Rettig, T. Zorn, H. Nitsche
Bestimmung des Oxidationszustandes von Arsen im Tailingwasser einer Uranerzaufbereitungs-
anlage
GDCh, Umwelttagung 1996
Ulm, Germany, 07.-10.10.1996

Gärtner, M., M. Boettger, B. Eichler, H.W. Gäggeler, M. Grantz, S. Hübener, D.T. Jost, A. Türler, A.B. Yakushev
 On-line gas chromatography of Mo, W and U (Oxi)chlorides
 4th International Conference on Nuclear and Radiochemistry
 Saint Malo, France, 08.-13.09.1996

Geipel, G., L. Baraniak, H. Funke, V. Brendler, G. Bernhard, H. Nitsche
 Bestimmung und Bewertung des Schadstoffaustrags aus Hinterlassenschaften des Uranbergbaus
 Wissenschaftsvereinigung Blaue Liste, Globaler und regionaler Wandel, Umweltforschung der WBL
 Potsdam, Germany, 06.11.1996

Geipel, G., L. Baraniak, H. Funke, V. Brendler, G. Bernhard, H. Nitsche
 Bestimmung und Bewertung des Schadstoffaustrags aus Hinterlassenschaften des Uranbergbaus
 BMBF, Technologie Dialog Umwelt
 Halle, Germany, 06.-12.12.1996

Hallmeier, K.H., T. Reich, C. Hennig, F. Thiel, L. Beyer, J. Cassabó, R. Szargan
 X-ray Absorption Study of Copper(II) Binuclear Complexes with 3,5-Bis(2-Pyridyl)-Pyrazolates
 9th International Conference on X-ray Absorption Fine Structure
 Grenoble, France, 26.-30.08.1996

Hübener, S., H. Funke, A. Vahle, R. Dressler, B. Eichler, A. Türler
 Evaluation of Thermo-chromatographic Surface Reaction Studies of Group 6 Elements
 4th International Conference on Nuclear and Radiochemistry
 Saint Malo, France, 08.-13.09.1996

Jankowsky, R., S. Kirsch, B. Noll, H. Spies, B. Johannsen, T. Reich, M.A. Denecke, S. Pompe, H. Moll, G. Bernhard, H. Nitsche
 Structural Investigations of Rhenium Complexes by EXAFS
 HASYLAB-Nutzertreffen
 Hamburg, Germany, 26.01.1996

Jost, D.T., G. Buklanov, R. Dressler, B. Eichler, H.W. Gäggeler, M. Gärtner, M. Grantz, S. Hübener, V. Lebedev, D. Piguet, S. Timoklin, A. Türler, M.V. Vedeneev, A. Yakushev, I. Zvara
 Isothermal gas chromatography of short lived HF isotopes and element 104 in chlorinating, oxygen containing carrier gas
 4th International Conference on Nuclear and Radiochemistry
 Saint Malo, France, 08.-13.09.1996

Pompe, S., M.A. Denecke, H. Moll, M. Bubner, T. Reich, H. Funke, K.H. Heise, G. Bernhard, H. Nitsche
 EXAFS Investigations on Uranyl Humates and Model Compounds
 HASYLAB-Nutzertreffen
 Hamburg, Germany, 26.01.1996

Pompe, S., M.A. Denecke, H. Moll, H. Funke, T. Reich, K.H. Heise, G. Bernhard, H. Nitsche
 Investigation of the Interaction of Humic Acid with Uranyl Ions by Extended X-Ray Absorption Fine Structure Spectroscopy (EXAFS)
 HASYLAB-Nutzertreffen
 Hamburg, Germany, 26.01.1996

Moll, H., G. Geipel, T. Reich, V. Brendler, G. Bernhard, H. Nitsche
 Interaction of Uranium(VI) with Silicon Species in Aqueous Solutions
 4th International Conference on Nuclear and Radiochemistry
 Saint Malo, France, 08.-13.09.1996

Reich, T., P.A. Heimann, W.R.A. Huff, B.L. Petersen, Z. Hussain, D.A. Shirley
 Near-Threshold Behavior of the K-Shell Satellites in N₂
 17th International Conference X-ray and Inner-Shell Processes
 Hamburg, Germany, 09.-13.09.1996

- Reich, T., M.A. Denecke, V. Brendler, H. Nitsche, P.G. Allen, J.J. Bucher, N.M. Edelstein, D.K. Shuh
EXAFS Study of Uranium(VI) Complexes with Aliphatic Carboxylic Acids in Aqueous Solution
9th International Conference on X-ray Absorption Fine Structure
Grenoble, France, 26.-30.08.1996
- Reich, T., G. Geipel, Yu.A. Teterin, V.I. Nefedov, K.E. Ivanov, A.S. Baev, M.A. Denecke, G. Bernhard, H. Nitsche, P.G. Allen, J.J. Bucher, N.M. Edelstein, D.K. Shuh
XPS and EXAFS Studies of the Interaction of Uranium(VI) with Calcite and Diabase
4th International Conference on Nuclear and Radiochemistry
Saint Malo, France, 08.-13.09.1996
- Reich, T., M.A. Denecke, S. Pompe, A. Otto, V. Brendler, K.H. Heise, H. Nitsche, P.G. Allen, J.J. Bucher, N.M. Edelstein, D.K. Shuh
Structural Analysis of the Interaction of Uranium(VI) with Humic Acid and Simple Carboxylic Acids using EXAFS
4th International Conference on Nuclear and Radiochemistry
Saint Malo, France, 08.-13.09.1996
- Schumann, D., R. Dressler, St. Taut, S. Fischer, H. Nitsche, N. Trautmann, M. Schädel, W. Brühle, B. Schausten, A.F. Novgorodov, R. Misiak, B. Eichler, H.W. Gäggeler, D.T. Jost, A. Türler, H. Bruchertseifer
Model Experiments for Chemical Studies of the Elements 105 and 106 in Aqueous Solution
4th International Conference on Nuclear and Radiochemistry
Saint Malo, France, 08.-13.09.1996
- Taut, St., S. Hübener, B. Eichler, H.W. Gäggeler, M. Schädel, S. Timokhin, I. Zvara, H. Nitsche
Thermochromatography of Heavy Actinides on Metal Surfaces at High Temperature
4th International Conference on Nuclear and Radiochemistry
Saint Malo, France, 08.-13.09.1996
- Teterin, Yu.A., K.E. Ivanov, A.S. Baev, V.I. Nefedov, G. Geipel, T. Reich, H. Nitsche
X-ray Photoelectron Study of the Interaction of $\text{UO}_2(\text{ClO}_4)_2$ with Calcite and Diabase Minerals in Water Solutions
1st Russian-German Seminar on X-ray Photoelectron Spectroscopy and X-ray Spectroscopy
Voronezh, Russia, 27.05.-01.06.1996
- Vahle, A., S. Hübener, B. Eichler, D. T. Jost, D. Piguet, A. Türler
Gas Chromatography Studies of Group 6 Elements in the $\text{O}_2\text{-H}_2\text{O}_{(g)}/\text{SiO}_{2(s)}$ -System
4th International Conference on Nuclear and Radiochemistry
Saint Malo, France, 08.-13.09.1996
- Yakushev, A.B., G.V. Buklanov, B. Eichler, H.W. Gäggeler, M. Grantz, S. Hübener, D.T. Jost, V. Lebedev, D. Piguet, S. Timokhin, A. Türler, M.V. Vedenev, I. Zvara
OLGA experiments with $^{261}\text{104}$ under chlorinating and brominating conditions
4th International Conference on Nuclear and Radiochemistry
Saint Malo, France, 08.-13.09.1996
- Yarzhemsky, V.G., T. Reich, P. Streubel, R. Szargan
Lineshape Asymmetry Parameters in X-ray Photoelectron Spectra
17th International Conference X-ray and Inner-Shell Processes
Hamburg, Germany, 09.-13.09.1996

III. SEMINARS

INSTITUTE SEMINARS

Dr. Norman Edelstein

Lawrence Berkeley National Laboratory, Berkeley (USA)
Speciation of Radionuclides by X-ray Absorption Spectroscopy
09.04.1996

Dipl. Min. Stephan Krämer

California Institute of Technology, Environmental Engineering Science, Pasadena, (USA)
Kinetik der ligandenkontrollierten Auflösung von Oxidphasen
16.04.1996

Dr. Barbara Hard

Umwelt-Forschungszentrum Leipzig GmbH, Sektion "Umweltmikrobiologie"
Entwicklung eines mikrobiologischen Verfahrens zur Reinigung radioaktiv belasteter Uran-
bergwerkswässer aus Ronneburg/Thüringen
10.05.1996

Dr. Thomas Fanghänel

Forschungszentrum Karlsruhe, Institut für Nukleare Entsorgungstechnik
Aquatische Chemie von Actiniden in konzentrierten Salzlösungen
21.05.1996

Prof. Dr. Vladimir Balek

Nuclear Research Institute Rez, Czech Republic
Radiometrische Emaniermethode zur Charakterisierung von Festkörperoberflächen
11.06.1996

Dr. Sonja Selenska-Pobell

Universität Bayreuth, Lehrstuhl für Genetik / TU Dresden, Institut für Mikrobiologie
Die Rolle von Bakterien in Uran-Abfallhalden
12.06.1996

Priv. Doz. Dr. Klaus Albert

Universität Tübingen
Grundlagen und Anwendungen der Festkörper-NMR-Spektroskopie zur Untersuchung um-
weltrelevanter Proben
19.06.1996

Dr. Alexej A. Bessonov

Russian Academy of Science, Institute of Physical Chemistry; Moscow, Russia
Electron Absorption Spectra and Structure Peculiarities of Solid Neptunium(V) Compounds
27.06.1996

Prof. Dr. Hans Bergmann

Friedrich-Schiller-Universität Jena, Institut für Ernährung und Umwelt
Spurenelementstatus ökochemischer Reaktionen in Pflanzen in Abhängigkeit von bioche-
mischen Faktoren und der Bodenfeuchte
02.07.1996

Dr. Alexej A. Bessonov

Russian Academy of Science, Institute of Physical Chemistry; Moscow, Russia
On Hydration Number of Actinide Dioxo Cations
10.07.1996

Prof. Dr. Shinya Nagasaki

University of Tokyo, Japan
Colloid Chemistry and Migration in Geologic Formation - Recent Research Activities in the
University of Tokyo
13.08.1996

Dr. Evgeni Kalinin

St. Petersburg State University, Dept. of Radiochemistry; St. Petersburg, Russia
Tritium and Chemistry of Intermediate Reactive Particles
21.08.1996

Dr. Patrick G. Allen
Glenn T. Seaborg Institute for Transactinium Science, LLNL Livermore, USA
XAFS Speciation Studies of Radionuclides
02.09.1996

Prof. Dr. Gregory R. Choppin
The Florida State University, Department of Chemistry, Tallahassee, USA
Present and Future Technologies for Actinide Separation
19.09.1996

Prof. Dr. Gregory R. Choppin
The Florida State University, Department of Chemistry, Tallahassee, USA
100th Anniversary of the Discovery of Radioactivity
20.09.1996 (FZR Center Seminar)

Prof. Dr. Carolyn J. Anderson
Washington University, Med.Center, Mallinckrodt Institute of Radiology, St. Louis, USA
Copper-64-labeled Proteins and Peptides for PET Imaging and Therapy
09.10.1996

Prof. Dr. Vala Ragnarsdottir
University of Bristol, Department of Geology; Bristol, Great Britain
The Structure and Coordination of Aqueous and Mineral Surface Complexes
15.10.1996

BS Chris Muskett
University of Bristol, Department of Geology; Bristol, Great Britain
Adsorption of Uranium onto Ironhydroxides and Phyllosilicates
15.10.1996

Prof. Dr. Alexander S. Shulakow
St. Petersburg State University, Institute of Physics; St. Petersburg, Russia
XUV Emission Spectroscopy as a Tool for the Study of Chemical Phase Composition of Thin Layers
17.10.1996

Prof. Dr. Hansruedi von Gunten
Labor für Radio- und Umweltchemie der Universität Bern und des Paul-Scherrer-Instituts,
Villigen, Schweiz
Ungleichgewichte in den natürlichen Zerfallsreihen - Anwendungen in der Geochemie
22.10.1996

Prof. Dr. Hansruedi von Gunten
Labor für Radio- und Umweltchemie der Universität Bern und des Paul-Scherrer-Instituts,
Villigen, Schweiz
Altersbestimmung mit nuklearen Methoden - Ein Überblick und neuere Anwendungen
24.10.1996 (FZR Center Seminar)

Prof. Dr. Svetlana Tretjakova
VIK Dubna, Russia
Solid State Nuclear Detectors for Radiochemistry
21.11.1996

Dr. Andrey V. Legin
St. Petersburg State University, Dept. of Radiochemistry; St. Petersburg, Russia
Solid State Chemical Sensors and Sensor Systems for Analysis of Complex Liquid Media
04.12.1996

INTERNAL SEMINARS (open to the public)

Dr. Harald Zänker
Einführung in die Photonenkorrelationspektroskopie
30.04.1996

Dr. Harald Zänker

Kolloidchemische Untersuchungen an Kieselsäure und Uran-Silikat-Komplex in saurer Lösung (I)

18.06.1996

Dr. Harald Zänker

Kolloidchemische Untersuchungen an Kieselsäure und Uran-Silikat-Komplex in saurer Lösung (II)

27.06.1996

Dipl.-Chem. A. Roßberg

Untersuchungen zur Charakterisierung von titan- und chromhaltigen Ni/Al₂O₃- Katalysatoren (Diplomarbeit TH Merseburg)

30.09.1996

Dr. Eckhart Förster

Das C-14-Konvertierungsprojekt - bisherige Ergebnisse und Ausblick

15.10.1996

Dr. Melissa A. Denecke

EXAFS-Ergebnisse von festen Uranylcarboxylaten

04.11.1996

Dipl.-Chem.. R. Jankowsky (FWB)

Strukturuntersuchungen an Aminosäure - und Oligopeptiden von Rhenium und Technetium

04.11.1996

Dipl.-Chem.. A. Roßberg

EXAFS-Ergebnisse zur Sorption von U(VI) an Kohlen

05.12.1996

Dr. G. Bonsdorf (TU Dresden)

XANES- und Mößbauer-Spektroskopie zur Untersuchung von Redox- und Kationenordnungsprozessen in Manganferrit

05.12.1996

Dr. Tobias Reich

EXAFS-Ergebnisse zur Uranabsorption an Calcit, Diabas und Silicagel

17.12.1996

WORKSHOPS

Tagung Arbeitskreis "Freimessung von Anlagenteilen und Bauschutt aus dem Abbau kerntechnischer Anlagen des Brennstoffkreislaufs "

FZR, Institut für Radiochemie; VKTA Rossendorf

TU München, Institut für Radiochemie

FZ Karlsruhe (INR, PTE, HDB, KGV, HS-US)

WAK-LA Karlsruhe

BfS-Salzgitter

GRS Köln

LfU Baden-Württemberg

Bayrisches Landesamt für Umweltschutz

Wismut GmbH, Chemnitz

Rosendorf, 06.11.1996

C. Nebelung (FZR)

Direktmessung alpha-aktiver Nuklide

K. Fleischer (VKTA)

Eindringverhalten radioaktiver Kontamination in ungeschützte Betonoberflächen

S. Niese, B. Gleisberg, W. Boden (VKTA)

Low-level Aktivitätsbestimmung von Leitnukliden im Eindampfdruckstand im KKW Lubmin

R. Berg (WAK)
Stand der Anlagencharakterisierung der WAK

C. Schultheiss (FZK/ INR)
Verfahren zur direkten Beschichtung von Probenträgern für die Alpha-Spektrometrie

S. Nikles, U. Gerstmann (TU München)
Stand der Arbeiten zur Freimessung

Methods and Applications of Low-Level Radioactivity Measurements

Forschungszentrum Rossendorf (FZR)
Verein für Kernverfahrenstechnik und Analytik Rossendorf (VTKA)
Rossendorf, 07.-08.11.1996

Einfluß von Huminsäuren auf das Migrationsverhalten radioaktiver und nichtradioaktiver Stoffe

Forschungszentrum Rossendorf, Institut für Radiochemie
Universität Mainz, Institut für Kernchemie
Universität des Saarlandes, Institut für Anorg. u. Analyt. Chemie und Radiochemie
Forschungszentrum Karlsruhe, Institut für Nukleare Entsorgung
Rossendorf, 14.-15.11.1996

S. Pompe (Rossendorf)
Darstellung und Charakterisierung von synthetischen Huminsäuren als Funktionalitätsmodelle natürlicher Huminsäuren

A. Brachmann (Rossendorf)
Bestimmung von Komplexbildungskonstanten des Urans mit Funktionalitätsmodellen und natürlichen Huminsäuren mittels TRLFS

T. Reich (Rossendorf)
EXAFS-Messungen an Komplexen von Uranyl mit Funktionalitätsmodellen und natürlichen Huminsäuren

A. Mansel (Mainz)
Komplexierung von La(III), Sm(III) und Am(III) in Huminsäurelösungen

A. Seibert (Mainz)
Komplexierung von Np(V) in geringer Konzentration mit Huminsäure

U. Keuth (Saarbrücken)
Fraktionierung von Huminsäuren durch Isotachophorese und Kapillar-Zonenelektrophorese

H. Schank (Saarbrücken)
Bestimmung von Schwermetallen in Gegenwart von Huminsäuren mit Hilfe elektrochemischer Verfahren

Chr. Marquard (Karlsruhe)
Komplexierung von Np(V) mit Huminsäuren

R. Artinger (Karlsruhe)
Stand der experimentellen Arbeiten zur Migration von Aktiniden in Säulenexperimenten

H. Geckeis (Karlsruhe)
Einfluß von Huminsäuren auf die Sorption von Aktinidionen an Mineraloberflächen

IV. PERSONNEL

PERSONNEL

Director

Prof. Dr. H. Nitsche

Administrative Staff

H. Pospischil

K. Wünsche

Scientific Staff

Dr. T. Arnold*
Dr. L. Baraniak
PD Dr. G. Bernhard
Dr. V. Brendler⁺
Dr. M. Böttger*
Dr. M. Bubner
Dr. M. Denecke⁺

Dr. H.-J. Engelmann
Dr. E. Förster*
Dr. H. Funke
Dr. G. Geipel
Dr. K.H. Heise
Dr. S. Hübener
Dr. P. Merker

DC C. Nebelung
Dr. P. Panak*
Dr. T. Reich
Dr. D. Rettig
Dr. S. Taut*
Dr. H. Zänker

Technical Staff

B. Eisold
J. Falkenberg
DI(FH) H. Friedrich
Ch. Fröhlich
DI(FH) G. Grambole
G. Heinz

H. Heyne
B. Hiller
DI(FH) G. Hüttig
DI(FH) R. Jander
P. Kluge
DI(FH) M. Meyer

Ch. Müller
H. Neubert
DC(FH) A. Otto*
A. Rumpel
R. Ruske
DI(FH) K. Wolf*

Graduate Students

DMin. A. Brachmann
DP M. Grantz
DC B. Mack

DC H. Moll
DC S. Pompe
DC A. Roßberg

DC M. Schmidt
DC A. Vahle
DC T. Zorn

⁺ post doc

* term contract

V. ACKNOWLEDGMENTS

ACKNOWLEDGMENT OF FINANCIAL SUPPORT

The Institute is part of the Forschungszentrum Rossendorf e.V., which is financed in equal parts by the Federal Republic of Germany and the Free State of Saxony.

Three projects were supported by the Bundesministerium für Bildung, Wissenschaft, Forschung und Technologie (BMBF):

- Stilllegung und Rückbau: Direktmessung α -aktiver Nuklide in Bauschutt zur Freigabeentscheidung.
Contract No. BMBF 02 S 7655 A8
- Chemistry of element 106.
Contract No. BMBF 06 DR 666 I (4)/1
- Influence of humic acids on migration behavior of radioactive and non-radioactive heavy elements under natural conditions.
Contract No. BMBF 02 E 88150

Three projects were supported by Commission of the European Communities:

- Effects of Humic Substances on the Migration of Radionuclides: Complexation and Transport of Actinides.
Contract No. F14W-CT96-0027
- Joint European Thermodynamic Database for Environmental Modeling (JETDEM).
In collaboration with:
FZK Karlsruhe, Germany; RCM Environmental Ltd., United Kingdom; Kungliga Tekniska Hogskolan, Department of Chemistry, Sweden; University of Aberdeen, Department of Chemistry, United Kingdom; Quantisci, Spain; Uppsala University, Institute of Earth Sciences, Sweden
Contract No. F14W-CT96-0029
- Restoration Strategies for Radioactive Contaminated Sites and their Close Surroundings (RESTRAT).
In collaboration with:
SCK-CEN Mol, Belgium; Studsvik Ecosafe AB, Sweden; Riso National Laboratory, Denmark; Westlakes Research Institutes, Great Britain
Contract No. F14P-CT95-0021

The Sächsisches Staatsministerium für Wissenschaft und Kunst provided support for the following projects:

- Mine-water Induced Wood Decomposition and Influence of the Degradation Products on Radionuclide Speciation, Sorption and Migration.
Contract No. SMWK 4.7541.83-FZR/402
- Influence of Natural Water-borne Organic Substances on the Valency of Radionuclides and Toxic Heavy Metals.
Contract No. SMWK 4.7541.88-FZR/512
- Soil-Plant Transfer Factors for Uranium.
Contract No. SMWK 4.7531.50-03-VKTA/601
- Chemical conversion of ^{14}C -labeled products to [^{14}C]Barium carbonate for long-time disposal.
Contract No. SMWK 4.7581.312/20

- Förderung von Maßnahmen und Projekten der Entwicklungshilfe für die Staaten Mittel-, Ost- und Südeuropas sowie die neuen unabhängigen Staaten (NUS).
Contract No. SMWK 26-3551.10/96-85 Reg. Präsidium

One project was supported by Deutsche Forschungsgemeinschaft (DFG):

- Properties of heavy actinides.
Contract No. DFG Hu 642/1-1

Five projects were supported by the following sponsors:

- Migration of ^{226}Ra in sediments of the Königstein uranium mine.
was supported in part by a contract with the WISMUT GmbH.
- INTAS: Gas-phase chemistry studies of elements 104 and 106.
In collaboration with:
University of Berne, Switzerland,
Joint Institute of Nuclear Research, Russia
Contract No. INTAS 94-424.
- Development of experimental arrangements and methods for on-line high temperature gas chromatography of the heaviest elements.
In cooperation with GSI.
GSI DRINK.
- EXAFS-Untersuchungen umweltrelevanter Uranylkomplexverbindungen und deren Sorbante.
Hamburger Synchrotronstrahlungslabor HASYLAB am Deutschen Elektronen-Synchrotron DESY;
Contract No. II-94-06
- Complexation and Sorption Phenomena of Uranium in Environmentally-Relevant Systems.
Stanford Synchrotron Radiation Laboratory SSRL; U.S. Department of Energy
Contract No. 2362 MP